Novel Feedback and Signalling Mechanisms for Interference Management and Efficient Modulation

Rami Abu-alhiga

Abstract

In order to meet the ever-growing demand for mobile data, a number of different technologies have been adopted by the fourth generation standardization bodies. These include multiple access schemes such as spatial division multiple access (SDMA), and efficient modulation techniques such as orthogonal frequency division multiplexing (OFDM)-based modulation. The specific objectives of this theses are to develop an effective feedback method for *interference management* in smart antenna SDMA systems and to design an efficient OFDM-based modulation technique, where an *additional dimension* is added to the conventional two-dimensional modulation techniques such as quadrature amplitude modulation (QAM).

In SDMA time division duplex (TDD) systems, where channel reciprocity is maintained, uplink (UL) channel sounding method is considered as one of the most promising feedback methods due to its bandwidth and delay efficiency. Conventional channel sounding (CCS) only conveys the channel state information (CSI) of each active user to the base station (BS). Due to the limitation in system performance because of co-channel interference (CCI) from adjacent cells in interference-limited scenarios, CSI is only a suboptimal metric for multiuser spatial multiplexing optimization. The first major contribution of this theses is a novel interference feedback method proposed to provide the BS with implicit knowledge about the interference level received by each mobile station (MS). More specifically, it is proposed to *weight* the conventional channel sounding pilots by the level of the experienced interference at the user's side. Interference-weighted channel sounding (IWCS) acts as a spectrally efficient feedback technique that provides the BS with implicit knowledge about CCI experienced by each MS, and significantly improves the downlink (DL) sum capacity for both greedy and fair scheduling policies. For the sake of completeness, a novel procedure is developed to make the IWCS pilots usable for UL optimization. It is proposed to *divide* the optimization metric obtained from the IWCS pilots by the interference experienced at the BS's antennas. The resultant new metric, the channel gain divided by the multiplication of DL and UL interference, provides link-protection awareness and is used to optimize both UL and DL. Using maximum capacity scheduling criterion, the link-protection aware metric results in a gain in the median system sum capacity of 26.7% and 12.5% in DL and UL respectively compared to the case when conventional channel sounding techniques are used. Moreover, heuristic algorithm has been proposed in order to facilitate a practical optimization and to reduce the computational complexity.
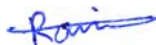
The second major contribution of this theses is an innovative transmission approach, referred to as *subcarrier-index* modulation (SIM), which is proposed to be integrated with OFDM. The key idea of SIM is to employ the subcarrier-index to convey information to the receiver. Furthermore, a closed-form analytical bit error ratio (BER) of SIM OFDM in Rayleigh channel is derived. Simulation results show BER performance gain of 4 dB over 4-QAM OFDM for both coded and uncoded data without power saving policy. Alternatively, power saving policy maintains an average gain of 1 dB while only using half OFDM symbol transmit power.

Declaration of originality

I hereby declare that the research recorded in this thesis and the thesis itself was composed and originated entirely by myself in the in the School of Engineering and Science at Jacobs University and in the School of Engineering at The University of Edinburgh.

MATLAB codes used to perform the simulations were written by myself with the following exceptions:

- The code used to uniformly users of the multicell layout in Chapter 4 was modified from routine written by Zubin Barucha

- The channel model used in the simulations performed in Chapter 5 was written by Van Duc Nguyen and Birendra Ghimire.

Rami Abu-alhiga

Acknowledgements

First and foremost, I would like to thank Allah, praised and exalted is He, for giving me patience and helping me finish this thesis.

I would like to take this opportunity to acknowledge the excellent support provided by my supervisor Harald Haas throughout my doctoral studies. He ensured a great start for my doctoral studies with stimulating discussions to narrow down my research focus. He sharpened my focus and helped me improve methodological and theoretical basis of the research. His critical remarks and continuous feedbacks over multiple drafts of papers and thesis were immensely useful. He really made me work hard to produce high quality pieces of work. Teaching opportunities with him on courses on digital communications were hugely beneficial for me to develop my teaching skills further.

Also, I am very thankful for the financial and logistical support provided to me by the University of Edinburgh, and the School of Engineering in particular. Without this support I could not have embarked on my studies. The colleagues at the Institute for Digital Communication provided regular pleasant breaks from hectic work of PhD. Sharing joys and sorrows of PhD process with Zubin, Sinan, Mostafa, Birendra, Nikola, Mohammad and many others were a great source of support.

Last but not the least; my wife Nahed, daughters Muna and Tuqa, sons Hani and Ala' deserve special thanking. I am deeply thankful for the love, excellent support, patience and encouragement of them. They put up with me over three years and supported in all possible ways to let me concentrate on my studies. The inspirational support of my mother Muna was always with me; she wanted me to be a successful person and I wish I could fulfil her dreams.

Contents

List of figures

List of tables

Acronyms and abbreviations

1G	First generation
2-D	Two-dimensional
2G	Second generation
3G	Third generation
3GPP	Third generation partnership project
4G	Forth generation
ACK/NACK	Acknowledgement/negative acknowledgement
AIM	Antenna-index modulation
AMC	Adaptive modulation and coding
AMPS	Advanced mobile phone service
AoA	Angle of arrival
APM	Amplitude/phase modulation
ASK	Amplitude shift keying
AWGN	Additive white Gaussian noise
BD	Block diagonalization
BER	Bit error ratio
BPSK	Binary phase shift keying
bps	bit per second
BS	Base station
BW	Bandwidth
CCI	Co-channel interference
CCS	Conventional channel sounding
cdf	Cumulative distribution function

CDS	Channel dependent scheduling
CDMA	Code division multiple access
CFR	Channel frequency response
CoI	Cell of interest
CoV	Coefficient of variation
CSI	Channel state information
CTF	Channel transfer function
D/A	Digital-to-analogue
DAB	Digital audio broadcasting
D-BLAST	Diagonal Bell laboratories layered space-time
DFT	Discrete Fourier transform
DL	Downlink
DoF	Degree of freedom
DPC	Dirty-paper coding
DVB	Digital video broadcasting
EGC	Equal gain combining
ES	Exhaustive search
EUTRA	Enhanced universal terrestrial radio access
FCC	Federal communications commission
FDD	Frequency division duplex
FDM	Frequency division multiplexing
FDMA	Frequency division multiple access
FEC	Forward error correction
FFT	Fast Fourier transform
GCL	Generalized chirp-like
GPRS	General packet radio service
GSM	Global system for mobile communication
HA	Heuristic algorithm
HSDPA	High speed downlink packet access
HSUPA	High speed uplink packet access
HSPA	High speed packet access
ICI	Inter-carrier interference
IEEE	Institute of electrical and electronics engineers

IFFT	Inverse Fast Fourier transform
i.i.d.	Independent and identically distributed
IMT-2000	International mobile telecommunication
IP	Internet protocol
IS-95	Interim standard
ISI	Inter-symbol interference
ITU	International telecommunication union
IWCS	Interference-weighted channel sounding
LOS	Line of sight
LTE	Long term evolution
M-ASK	M-ary amplitude shift keying
MC	Maximum capacity
MCS	Modulation and coding scheme
MIMO	Multiple-input multiple-output
MISO	Multiple-input single-output
MMSE	Minimum mean square error
MRC	Maximum ratio combining
MS	Mobile station
MU-MIMO	Multiuser multiple-input multiple-output
NLOS	Non line of sight
NTT	Nippon telephone and teleghraph
OA	Omnidirectional antenna
OFDM	Orthogonal frequency division multiplexing
OOK	On-off keying
P2P	Point-to-point
PACE	Pilot aided channel estimation
PAPR	Peak to average power ratio
PDC	Personal digital cellular
PF	Proportional fair
PRP	Power reallocation policy
PSP	Power saving policy
QAM	Quadrature amplitude modulation
QoS	Quality of service

S/P	Serial to parallel
SA	Smart antenna
SB	Score-based
SC-FDMA	Single-carrier frequency division multiple access
SDMA	Space division multiple access
SER	Symbol error ratio
SINR	Signal-to-interference-plus-noise-ratio
SISO	Single Input Single Output
SIMO	Single-input multiple-output
SIM	Subcarrier index modulation
SNR	Signal-to-noise ratio
SP	Sample-space population
SM	Spatial modulation
SMS	Short message service
TACS	Total access communication system
TDD	Time division duplex
TDMA	Time division multiple acces
TSIM	Time-slot index modulation
TTI	Transmission time interval
UL	Uplink
UMTS	Universal mobile telecommunications system
UTRA	Universal terrestrial radio access
V-BLAST	Vertical Bell laboratories layered space-time
VOIP	Voice over IP
WAP	Wireless application protocol
WIMAX	Worldwide interoperability for microwave acces
WLAN	Wireless local area network
ZF	Zero forcing

Nomenclature

$*$	Convolution operation
$(\cdot)^{-1}$	Inverse of a matrix or a vector
$(\cdot)^{*}$	Complex conjugate
$(\cdot)^{H}$	Complex conjugate transpose of a matrix, or the Hermitian
$(\cdot)^{T}$	Transpose of a matrix
$\det(\cdot)$	Determinant of a matrix
$\mathrm{E}(\cdot)$	Expected value
$\mathrm{tr}(\cdot)$	Trace of a matrix
α	Amplitude of fading coefficient
A	Antenna-dependant constant
B	Input bit-stream of conventional OFDM
B_{OOK}	Input bit-substream of OOK modulator in SIM OFDM
B_{QAM}	Input bit-substream of QAM modulator in SIM OFDM
C	Instantaneous channel capacity (in bps/Hz)
C_u	Instantaneous MIMO channel capacity of user u (in bps/Hz)
$\overline{C}$	Ergodic channel capacity (in bps/Hz)
$\overline{C}_{FS}$	Ergodic capacity of frequency selective MIMO channel (in bps/Hz)
C^{MC}	Instantaneous cell capacity using MC scheduler (in bps/Hz)
C^{PF}	Instantaneous cell capacity using PF scheduler (in bps/Hz)
C^{SB}	Instantaneous cell capacity using SB scheduler (in bps/Hz)
C_v	Instantaneous channel capacity of the vth group of users (in bps/Hz)
d	Link distance
d_0	Reference distance

$d_{\mathrm{QAM}}^{\mathrm{PRP}}$	Euclidean distance of SIM OFDM QAM with PRP
$d_{\mathrm{OOK}}^{\mathrm{PRP}}$	Euclidean distance of SIM OFDM OOK with PRP
$d_{\mathrm{QAM}}^{\mathrm{PSP}}$	Euclidean distance of SIM OFDM QAM with PSP
$d_{\mathrm{OOK}}^{\mathrm{PSP}}$	Euclidean distance of SIM OFDM OOK with PSP
$d_{\mathrm{QAM}}^{\mathrm{OFDM}}$	Euclidean distance of conventional OFDM QAM
ϵ	Ratio of active subcarriers
$\overline{E}_s$	Average constellation symbol energy
f_c	Carrier frequency (in Hz)
g	Link gain (in dB)
$\mathrm{G_H}$	Group of high-order modulations
$\mathrm{G_L}$	Group of low-order modulations
$\overline{\gamma}_s$	Average SNR per constellation symbol
$\overline{\gamma}_s^{\mathrm{QAM-PRP}}$	Effective average SNR of QAM detection per active subcarrier under PRP
$\overline{\gamma}_s^{\mathrm{QAM-PSP}}$	Effective average SNR of QAM detection per active subcarrier under PSP
$\overline{\gamma}_s^{\mathrm{OOK-PRP}}$	Effective average SNR of OOK detection per active subcarrier under PRP
$\overline{\gamma}_s^{\mathrm{OOK-PSP}}$	Effective average SNR of OOK detection per active subcarrier under PSP
$\overline{\gamma}_{\mathrm{sc}}^{\mathrm{PRP}}$	Average SNR per active subcarrier under PRP
$\overline{\gamma}_{\mathrm{sc}}^{\mathrm{PSP}}$	Average SNR per active subcarrier under PSP
$\mathbf{H}$	MIMO channel matrix
$\mathbf{H}_u$	MIMO channel matrix of user u
$\mathbf{H}_u^{(j)}$	j^{th} row of MIMO channel matrix of user u
$\mathbf{H}_{\mathrm{S}}$	Network MIMO channel
$h_{\nu,\kappa}$	Channel coefficient between receive antenna ν and transmit antenna κ
$h_u^{j,i}$	UL channel coefficient between the jth smart (directional) antenna at the base station and the ith omnidirectional antenna at user u
I_j^{UL}	UL intercell CCI experienced by the jth smart antenna at the base station
I_u^{DL}	DL intercell CCI experienced by user u
$\mathbf{I}_n$	Identity matrix of size $n \times n$
K	Number of users in single-cell DL MU-MIMO system
L	Number of multipaths
λ	Wavelength
λ_i	Eigenvalues
λ_{u_i}	Eigenvalues of user u

$\mathbf{\Lambda}$	Diagonal matrix of the eigenvalues
$\mathbf{n}$	receive AWGN vector
$\mathbf{\tilde{n}}$	SVD-based shaped receive AWGN vector
n_{sc}	per-subcarrier receive AWGN
N_0	AWGN power spectral density
N_{BS}	Number of smart antennas at the base station
N_{ex}	Number of excess subcarriers
N_{FFT}	FFT size
N_{maj}	Number of bits of the majority bit-value
N_{MS}	Number of omnidirectional antennas at each mobile station
$N_{\mathrm{ones}}^{B_{\mathrm{OOK}}}$	Number of logical ones in B_{OOK} bit-substream
N_R	Number of receive antennas
N_s	Number of flat fading sub-channels in frequency selective MIMO Channel
N_T	Number of transmit antennas
N_{U}	Number of active users requesting access to network
$N_{\mathrm{zeroes}}^{B_{\mathrm{OOK}}}$	Number of logical zeroes in B_{OOK} bit-substream
M	QAM constellation size
M_{H}	Constellation size of high-order modulation
M_{L}	Constellation size of low-order modulation
P_i	Optimal power allocation of ith spatial stream (in Watts)
P_r	Power of received signal (in Watts)
P_t	Power of transmitted MIMO signal (in Watts)
P_{Tx}	Power of transmitted OFDM symbol (in Watts)
P_{e}	Total BER of SIM OFDM
P_{s}	SER of M-ASK detection
P_{q}	BER of estimating B_{QAM}
P_{sc}	BER of estimating B_{OOK}
$P_{\mathrm{sc}}^{\mathrm{PRP}}$	BER of estimating B_{OOK} with PRP
$P_{\mathrm{sc}}^{\mathrm{PSP}}$	BER of estimating B_{OOK} with PSP
$P_{\mathrm{q}}^{\mathrm{PRP}}$	BER of estimating B_{QAM} with PRP
$P_{\mathrm{q}}^{\mathrm{PSP}}$	BER of estimating B_{QAM} with PSP
$\mathbf{O}_u^{\mathrm{DL-BM}}$	Matrix containing the coefficients of perfectly estimated DL-BM of user u
$\mathbf{O}_u^{\mathrm{DL-IAM}}$	Matrix containing the coefficients of perfectly estimated DL-IAM of user u

$\mathbf{O}_u^{\mathrm{DL-LGAM}}$	Matrix containing the coefficients of perfectly estimated DL-LGAM of user u
$\mathbf{O}_u^{\mathrm{LPAM}}$	Matrix containing the coefficients of perfectly estimated DL-LPAM of user u
$\mathbf{O}_u^{\mathrm{UL-IAM}}$	Matrix containing the coefficients of perfectly estimated UL-IAM of user u
r	Rank of a matrix
$\mathbf{R_{xx}}$	Covariance matrix of $\mathbf{x}$
σ^2	Variance of Gaussian distributed random variable
σ_{S}	Standard deviation of log-normal shadowing
s_k	Number of data stream intended to user k during DL
S_v	Rank of capacity realization of the vth group of users
SP	Number of possible groups of scheduled users in the sample-space population
t	Time instant
T_s	Transmitted symbol duration
T_{delay}	Maximum propagation delay
$T^{\mathrm{SIM\,OFDM}}$	SIM OFDM spectral efficiency
T^{OFDM}	OFDM spectral efficiency
$\mathbf{T}$	Block diagonalization precoding Matrix
μ	Path loss exponent
$\mathbf{U}$	Left-hand side SVD-based unitary matrix
$\mathbf{V}$	Right-hand side SVD-based unitary matrix
W	Size of the observation window for SB scheduler
$\overline{\mathbf{W}}$	Linear mapping matrix of conventional OFDM modulator
$\mathbf{x}$	Transmit data vector
$\tilde{\mathbf{x}}$	Precoded transmit data vector
$\mathbf{y}$	Receive data vector
$\tilde{\mathbf{y}}$	SVD-based shaped receive data vector
ξ	Log-normal distributed random variable modeling shadowing effects

Chapter 1

Introduction

1.1 Outline of research areas

The specific objectives of this thesis are to develop an effective feedback method for interference management in smart antenna (SA)-based multiple-input multiple-output (MIMO) systems, also known as space division multiple access (SDMA), and to design an efficient modulation technique in the multicarrier frequency domain. More specifically, the research described in this thesis is concentrated on the following areas:

The first objective of this thesis is to develop a bandwidth-efficient and delay-efficient feedback mechanism for intercell interference limited closed-loop cellular SDMA systems. It is assumed in this thesis that the considered SDMA system utilizes a block diagonalization (BD) beamforming algorithm to eliminate intracell co-channel interference (CCI) (which is caused by the same-cell transmitters). Therefore, intercell CCI (which is caused by the other-cell transmitters) experienced by any entity dominates both intracell CCI and thermal noise. The proposed feedback mechanism is particularly attractive for time division duplex (TDD) mode where channel knowledge is made available at the transmitter by exploiting channel reciprocity. In the considered SDMA system, the base stations (BS) and the mobile stations (MS) are equipped with excess number of SAs and relatively limited number of omnidirectional antennas (OAs), respectively. Such configuration gives access to two types of diversity, namely SA selection and multiuser diversity, to be jointly exploited in order to improve the opportunistic spatial multiplexing gain. It is worth mentioning that time and frequency diversity techniques are beyond

1

the scope of this thesis.

The second objective of this thesis is to enhance the reliability, power efficiency, and spectral efficiency of conventional orthogonal frequency division multiplexing (OFDM) transmission by exploiting the orthogonality of the subcarriers in radically novel approach. The proposed transmission approach, referred to as subcarrier-index modulation (SIM), is integrated with OFDM. The key idea of SIM is to use the subcarrier-index as a source of information. The performance of the proposed SIM OFDM system is compared against a noise limited conventional OFDM system where perfect frequency synchronization is assumed.

1.2   History

The most important events in the history of wireless communications can be traced back to experiments and inventions carried out during the 19th century by scientists like Michael Faraday and James Maxwell [1, 2]. They predicted the existence of the electromagnetic waves, and their theory was the technological basis of the practical wireless apparatus developed between 1880 and 1950 by scientists such as Guglielmo Marconi, Nikola Tesla, Heinrich Hertz, and many others [2–5]. By the middle of the 20th century, Shannon laid the theoretical foundations of digital communications in a paper entitled "A Mathematical Theory of Communication", his famous work on information theory [6]. Shannon's work and works of others such as Harry Nyquist [7] have significantly contributed to the intensive development of wireless communications. A very modern direction of wireless communication is mobile communications or cellular systems.

Due to the wire-free advantage, mobile wireless communication devices have become an essential part of almost all aspects of human lifestyle. However, the radio spectrum is a scarce medium shared among various, and potentially competing technologies. Consequently, regulatory bodies such as international telecommunication union (ITU) plays an important role in the evolution of radio technologies via partitioning the spectrum into parts of different bandwidths to be allocated to particular types of service and technologies. This is facilitated by the formation of the standardization groups of radio technologies. Both of regularity bodies and standardization groups aim at providing specifications for air-interfaces to ensure interoperability among devices from various vendors, and to pursuit efficient utilization of the available spectrum [8].

In 1983, the cellular concept, invented by Bell laboratories, was commercially introduced through the first generation (1G) analog cellular systems based on the advanced mobile phone service (AMPS) standard. Meanwhile, similar standards such as Nippon telephone and telegraph (NTT) and total access communication system (TACS) were developed around the world [9, 10]. Since the 1G systems were independently developed within national boundaries, they lacked interoperability and, hence, global roaming was not possible [11].

Unlike 1G analog systems, second generation (2G) systems are designed to utilize digital modulation transmission. Global system for mobile communication (GSM), north America interim standard (IS)-95 system, and personal digital cellular (PDC) system are popular examples of 2G voice-dominated systems. Due to the collaborative effort in which GSM was developed, GSM supported roaming, and was considered as a widely accepted standard [12]. In spite of the widespread acceptance of 2G systems, they were dominantly designed for voice applications. Over the last decade, data applications have grown rapidly from short message services (SMS), wireless application protocol (WAP) browsers, and positioning applications to a dramatic growth of multimedia and web-based applications enabled by third generation (3G) systems [13].

According to the ITU definitions, 3G technologies that meet the ITU requirements are members of the international mobile telecommunication (IMT)-2000 family. From standardization point of view, there are three main organizations developing the standards meeting IMT-2000 requirements: third generation partnership project (3GPP), the institute of electrical and electronics engineers (IEEE), and 3GPP2.

In order to provide the user with advanced communication services targeted by 3G systems, the mobile phone of 2G systems has rapidly evolved into an integrated mobile device that encompasses almost the same computation capability of personal computers. Nowadays, some wireless technologies enable users to access a considerable amount of information and media on an anywhere-anytime basis. For instance, the IEEE 802.11 standard provides local access to Internet. Alternatively, wider areas are covered by other systems such as GSM networks and their enhanced packet-switched versions, *i.e.* general packet radio service (GPRS). For instance, the initial version of 3G networks developed by 3GPP has provided users with wireless access to internet at speeds up to 1.8 M bps [13]. In summary, such movement from the 2G to 3G systems is mainly motivated by the introduction of data services. Therefore, cellular standards are continuously evolving to meet the ever growing demand for wideband capabilities,

reliable high data rates, and enhanced coverage [13].

Currently, 3GPP is the dominant standards development group for mobile radio systems which are serving approximately 90% of the global mobile subscribers. Generally, 3GPP standards are structured as releases. Consequently, discussion within 3GPP refers to the functionality in one release or another. Release 98 and earlier releases specify 2G GSM-based networks. Release 99 specifies the first universal mobile telecommunications system (UMTS) 3G networks incorporating a code division multiple access (CDMA) air-interface [14]. Release 4 adds features including an all internet protocol (IP) core network. The specifications have been extended with high speed downlink and uplink packet access (HSDPA and HSUPA), also known collectively as HSPA, in release 5 and 6, respectively [15]. HSPA has been further enhanced in release 7, for the first time in cellular networks, with the introduction MIMO technology [16]. Long term evolution (LTE) is presented in release 8 which aims at better utilization of the scarce spectrum while supporting high mobility in various propagation environments [13].

In continuing the technology progression from GSM and UMTS families within 3GPP, the LTE of UMTS (release 8) is just one of the latest steps in an advancing series of wireless communication technologies [17]. However, being defined as 3G technology LTE does not meet the requirements for the fourth generation (4G) technologies defined by ITU. Therefore, a work on LTE-advanced within 3GPP has recently started. LTE-advanced is envisaged to meet the goals and attributes of the systems beyond 3G (IMT-advanced). In other words, LTE-advanced can be seen as completing the trend of expansion of service provision beyond voice calls towards a multimedia air-interface [18]. It should be noted that there is an other technology which is developed to meet the requirement for 4G. This technology is mobile Worldwide interoperability for microwave access (WiMAX) [19] which can be considered as the major 4G technology competing with LTE-advanced [20].

In light of the above, the emphasis and the contributions of this thesis are on mechanisms to be applied on the latest enhancement of LTE standard (LTE-advanced). In particular, this thesis focuses on the key physical layer technologies to improved spectrum utilization promised by LTE-advanced, as is detailed in the subsequent chapters.

The remainder of this chapter is organized as follows: Section 1.3 formulates the targeted problems and the motivation of the proposed solutions. Also, it gives the specific contributions associated with each objective of this thesis. The thesis assumptions and the overall thesis layout are given in section 1.4 and section 1.5, respectively.

1.3 Motivation and contributions

LTE-advanced systems are faced with a number of distinctive attributes and challenges which include limited radio resources, increased user demand for higher data rates, asymmetric traffic, and interference-limited transmission. Driven by the ever-growing demand for higher data rates to effectively use the mobile Internet, future applications are expected to generate a significant amount of both downlink (DL) and uplink (UL) traffic which requires continuous connectivity with quite diverse quality of service (QoS) requirements. Given limited radio resources and various propagation environments, voice over IP (VOIP) applications, such as Skype, and self-generated multimedia content platforms, such as YouTube, Facebook, and Flickr, are popular examples that impose major challenge on the design of LTE-advanced wireless systems. One of the latest studies from ABI Research, a market intelligence company specializing in global connectivity and emerging technology, shows that in 2008 the mobile data traffic around the world reached 1.3 Exabytes (10^{18}). By 2014, the study expected the amount to reach 19.2 Exabytes. Furthermore, it has been shown that video streaming is one of the dominating application areas which will grow splendidly [21].

In order to meet such diverse requirements, especially, the ever-growing demand for mobile data, a number of different technologies have been adopted by LTE-advanced. These include advanced multiple access schemes such as SDMA, and efficient modulation techniques such as OFDM-based modulation technologies (e.g. single carrier frequency division multiple access (SC-FDMA) which can be viewed as a linearly pre-coded OFDM scheme) [22, 23]. Therefore, there is a broad agreement recently among LTE standardization groups that closed-loop multi-carrier opportunistic SDMA will be the key to achieve the promised data rates of 1 Gbps and more [24].

It is well known that CCI, caused by frequency reuse, is considered as one of the major impairments that limits the performance of current and 4G wireless systems [25]. To outmaneuver such obstacle, various techniques such as joint detection, interference cancelation, and interference management have been proposed. One of the most promising technologies is to utilize the adaptability of SAs (also known as directional antennas or antenna arrays). Spatial signal pre-processing along with SAs can provide much more efficient reuse of the available spectrum and, hence, an improvement in the overall system capacity. This gain is achievable by adaptively utilizing directional transmission and reception at the BS in order to enhance coverage and/or mitigate CCI.

Recently, MIMO communication is widely recognized as the key technology for achieving high data rates and for providing significant capacity improvements [26, 27]. Unlike the traditional resource allocation in single-input single-output (SISO) fading channels, which is performed in time and frequency domains, the resources in MIMO systems are usually allocated among the antennas (the spatial domain). From closed-loop MIMO point of view, channel aware adaptive resource allocation has been shown to maintain higher system capacity compared to fixed resource allocation [28–30]. In particular, adaptive resource allocation is becoming more critical with scarce resources and ever-increased demand for high data rates.

It has been presented in closed-loop MIMO literature that the optimal power allocation among multiple transmit antennas is water-filling algorithm [26]. However, to enable optimal power allocation, perfect channel state information (CSI) at the transmitter is required. Some other work focused on transmit beamforming and precoding with limited feedback [31–35], where the transmitter uses a quantized CSI feedback to adjust the power and phases of the transmitted signals.

To further reduce the amount of feedback and complexity, per-antenna rate and power control strategies have been proposed [36–40]. By adapting the rate and power for each antenna separately, the performance (error probability [41] or throughput [42–45]) can be improved greatly at a slight cost of complexity. Additionally, antenna selection is proposed to reduce the number of the spatial streams and the receiver complexity as well. Various criteria for receive antenna selection or transmit antenna selection are presented, aiming at minimizing the error probability [42, 43, 46–49] or maximizing the capacity bounds [38, 46]. It has been shown that only a small performance loss is experienced when the transmitter/receiver selects a good subset of the available antennas based on the instantaneous CSI. However, it has been found that in spatially correlated scenarios, proper transmit antenna selection cannot just be used to decrease the number of spatial streams, but as an effective means to achieve performance gains by exploiting multiple antenna diversity [47]. When the channel links exhibit spatial correlation (due to the lack of spacing between antennas or the existence of small angular spread), the degrees of freedom (DoF) of the channel are usually less than the number of transmit antennas. Therefore, by the use of transmit antenna selection, the resources are allocated only to the uncorrelated spatial streams so that an enhanced capacity gain can be achieved.

Most of the above work focused on the point-to-point (P2P) link in single user scenario. In a multiuser MIMO (MU-MIMO) context, MIMO communication can offer enormous capacity

growth by exploiting spatial multiplexing and multiuser scheduling. Therefore, opportunistic approaches have recently attracted considerable attention [50, 51]. So far, opportunistic resource allocation in a MU-MIMO scenario is still an open issue. Wong *et al.* and Dai *et al.* [52, 53] consider a multiuser MIMO system and focused on multiuser precoding and turbo space-time multiuser detection, respectively. More recent work has addressed the issue of cross-layer resource allocation in DL MU-MIMO systems [54]. In broadcast MU-MIMO channels, dirty-paper coding (DPC) [55] can achieve the maximum throughput (the capacity region) [56–58]. In particular, DPC can accomplish this by using successive interference precancelation through employing complex encoding and decoding. Unfortunately, DPC is classified as a non-linear technique that has very high complexity and is impractical to implement. Due to the fact that DPC is computationally expensive for practical implementations, its contribution is primarily to determine the achievable capacity region of MU-MIMO channel under a per-cell equal power constraint. Therefore, many alternative practical precoding approaches have been proposed to offer a trade-off between complexity and performance [59–64]. These alternatives considered different criteria and methods such as minimum mean squared error (MMSE) [65, 66], channel decomposition, and zero forcing (ZF) [52, 67–69].

One of the most attractive approaches is the BD algorithm which supports orthogonal multiple spatial stream transmission. In BD algorithm, the precoding matrix of each user is designed to lie in the null space of all remaining channels of other in-cell users, and hence the intracell multiuser CCI is pre-eliminated [63, 68, 69]. In particular, SA-based SDMA, implementing BD algorithm, can multiplex users in the same radio frequency spectrum (*i.e.* same time-frequency resource) within a cell by allocating the channel to spatially separable users. This can be done while maintaining tolerable, almost negligible, intracell CCI enabled by BD signal pre-processing capabilities. Moreover, channel aware adaptive SDMA scheme can be achieved through joint exploitation of the spatial DoF represented by the excess number of SAs at the BS along with multiuser diversity. Generally, the radio channel encountered by an array of antenna elements is referred to as beam. In other words, SA technology along with BD algorithm can enable the BS to adaptively steer multiple orthogonal beams to a group of spatially dispersed MSs [51], as depicted in Fig. 1.1.

The joint beam selection and user scheduling for orthogonal SDMA-TDD system is a key problem addressed in the fourth chapter of this thesis. As mentioned earlier, the availability of CSI of all in-cell users at the BS is crucial in MU-MIMO communication scenario to optimally
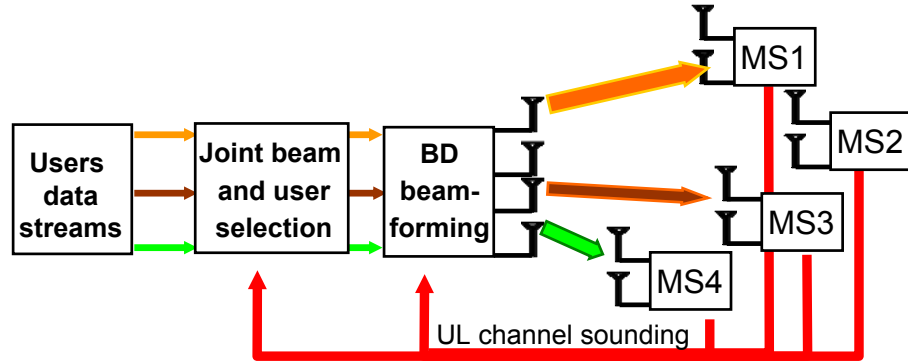
Figure 1.1: *A block diagram of SA-based MU-MIMO transmission implementing BD beamforming*

incorporate different precoding techniques such as BD, adaptive beamforming, or antenna selection, in order to increase the overall system spectral efficiency. Basically, there are two methods for providing a BS with CSI of all associated MSs, namely limited (quantized) feedback and analog feedback. Limited feedback (also know as direct feedback) involves the MS to measure the DL channel and to transmit a feedback messages of quantized CSI reports to the BS during the UL transmission. Alternatively, the second method, referred to as UL channel sounding according to LTE terminology, involves the BS to estimate the DL channel based on channel response estimates obtained from reference signals (pilots) received from the MS during UL transmission. Channel sounding offers advantages in terms of overhead, complexity, estimation reliability, and delay. Clearly, TDD systems offer a straightforward way for the BS to acquire the CSI enabled through channel reciprocity [70, 71]. The advantages of UL channel sounding are discussed in the next chapter and a more detailed treatment can be found, for instance, in the technical documents of the evolved universal terrestrial radio access (EUTRA) study item launched in the LTE concept, and particularly in [71, 72].

In light of the above, the benchmark system considered in this thesis for the system level analysis of the feedback methodology is a closed-loop SDMA TDD system. In the benchmark system, a BD technique is utilized to optimize the MU-MIMO spatial resources allocation problem based on perfect instantaneous CSI of each in-cell active user obtained from UL channel sounding pilots. The main goal of the benchmark system is to adaptively communicate with a group of users over disjoint spatial streams while optimizing the gains of the MU-MIMO channels. The optimization aims at enhancing the overall system capacity using fixed and uniformly distributed transmit power.

Most of the ZF-based precoding algorithms (e.g. BD) have been designed to *only* mitigate intra-cell CCI from different users in the same cell without considering CCI coming from transmitters in other cells. In a cellular environment, especially when full frequency reuse is considered, intercell (also known as other-cell) CCI becomes a key challenge which cannot be eliminated by BD-like algorithms. Moreover, it has been shown that intercell CCI can significantly degrade the performance of SDMA systems [73]. More specifically, if the BS schedules a group of users only based on the available CSI, the scheduling decision might be *optimum* for a noise limited system, but high intercell CCI at the respective MSs might render the scheduling decision greatly suboptimum. Therefore, the signal-to-interference-plus-noise ratio (SINR) would be a more appropriate metric in multicell interference limited scenarios, but this metric cannot directly be obtained from conventional channel sounding (CCS). Thus, the key challenge here is to provide knowledge of intercell CCI observed by each user to the BS in addition to CSI. If, furthermore, intercell CCI observed by each SA at the BS itself is taken into account, the beam selection and user scheduling process can be jointly improved for both DL and UL [74].

The contribution associated with the feedback-based interference management for SDMA can be split into three key items:

- A novel interference feedback mechanism is proposed. The proposed mechanism implicitly provides the BS with knowledge about the level of intercell CCI received by each active MS. It is proposed to weight the UL channel sounding pilots by the level of the received intercell CCI at each MS. The weighted uplink channel sounding pilots act as a bandwidth-efficient and delay-efficient means for the instantaneous provision of knowledge of both CSI and intercell CCI level experienced at each active user to the BS. Such modification will compensate for the missing interference knowledge at the BS when UL channel sounding is used. In other words, the interference-weighted channel sounding (IWCS) pilots can be used to timely and implicitly signal the level of other-cell intercell CCI experienced at each MS to the BS.

- A novel procedure is developed to make the IWCS pilots usable for UL optimization. It is proposed to divide the metric obtained from the IWCS pilots by the intercell CCI experienced at the BS. The resultant new metric, which is implicitly dependent on downlink (DL) and UL intercell CCI, provides link-protection awareness and is used to jointly improve spectral efficiency in UL as well in DL. Particularly, the optimization metric enabled by this enhancement provides the scheduler with knowledge of the potential in-

terference caused by a candidate in-cell transmitters to already established links in the neighboring cells.

- Finally, in order to facilitate a practical implementation, a heuristic algorithm (HA) has been proposed to reduce the computational complexity involved in the addressed optimization problem.

In the context of research aimed at finding new degrees of freedom for better spectral efficiency, many techniques such as spatial modulation (SM), and space shift keying (SSK) [75–78] have been recently developed to meet the continuous demand for increased data rates. Such ever-growing demand has been the main motivation for developing an efficient OFDM-based modulation technique in this thesis (the second major contribution of this thesis).

Among the many transmitter and receiver concepts proposed so far in MIMO literature, SM [75] is a new and recently proposed wireless transmission technique for single user MIMO (SU-MIMO) wireless systems. SM has been shown to be a promising low-complexity alternative to several popular MIMO schemes which can be integrated with OFDM [79]. The fundamental and distinguishable property that makes SM different from other MIMO techniques is the utilization of the spatial constellation pattern of the transmit-antennas as a source of information. In other words, SM can be considered as a multiple antenna transmission technique where the information bits are mapped into a constellation point in the 2-D signal domain, and a constellation point in the spatial domain such that the antenna index is employed to convey information. More specifically, at each transmission instant, only one transmit antenna is activated while the other antennas transmit zero power. At the receiver side, maximum receive ratio combining is used to estimate the active antenna index, and then the transmitted symbol is estimated [75].

Inspired by the underlying idea of SM, this thesis exploits the subcarrier orthogonality of SU-SISO OFDM wireless systems in an innovative fashion to add a new dimension to the complex 2-D signal plan. The new dimension devised in this thesis is referred to as subcarrier-index dimension.

It is well known that OFDM is a multicarrier modulation method in which a number of orthogonal subcarriers is transmitted simultaneously [80]. Recent years have witnessed real time deployment of OFDM for wireless communication systems such as digital audio broadcasting (DAB) [81], digital video broadcasting (DVB) [82], and wireless local area network (WLAN) [80]. Such deployment has provided an experimental proof for some of the key benefits of

OFDM, which include:

- Compared to frequency division multiplexing (FDM), OFDM is capable of converting a wideband frequency selective channel into multiple flat fading channels in a more efficient way in terms of spectral utilization [83].

- Unlike single carrier transmission, OFDM exploits the robustness of multicarrier transmission against time dispersive channels to mitigate inter-symbol interference (ISI) by inserting a guard interval at the beginning of each symbol [84].

- Simple receiver structure is enabled by frequency domain equalizers [84].

As with all benefits, however, there is a price to pay. One of the key disadvantages of OFDM is that the peak to average power ratio (PAPR) of an OFDM signal is relatively high. Consequently, a highly linear radio frequency (RF) power amplifier is needed, resulting in increasing the cost of the transmitter of OFDM [85]. However, this problem is minor for the DL since BS can implement expensive power amplifiers. By contrast, solving this problem at the MS side is infeasible due to power consumption and manufacturing cost limitations. Therefore, LTE has adopted SC-FDMA for UL due to its significantly lower PAPR. Also, OFDM systems use multiple subcarriers of different frequencies. The subcarriers are packed tightly into an operating channel, and small shifts in subcarrier frequency may cause interference between subcarriers, a phenomenon called inter-carrier interference (ICI). Frequency shifts may occur because of the Doppler effect or because there is slight difference between the transmitter and the receiver clock frequencies (synchronization problem).

In conventional OFDM systems, modulation techniques such as BPSK (binary phase shift keying), and multilevel quadrature amplitude modulation (M-QAM) map a fixed number of information bits into signal constellation symbol. Each signal constellation symbol represents a point in the two-dimensional (2-D) baseband signal space [86, 87].

The SIM transmission technique proposed in this thesis employs the subcarrier-index to convey information in an on-off keying (OOK) fashion. SIM OFDM aims at providing either BER performance enhancement or power-efficiency improvement over conventional OFDM by incorporating different power allocation policies.

The contribution associated with the SIM OFDM technique can be summarized as follows:

- The SIM is proposed as a novel power-efficient and spectral-efficient modulation scheme which exploits the orthogonality of OFDM subcarriers in a different approach for information transmission. In particular, this technique always provides error probability performance improvement, but power efficiency can be traded-off against error probability performance compared to conventional OFDM. Moreover, the subcarrier-index detection involves negligible complexity at the receiver.

- The simplicity of extending the subcarrier-index concept as a potential source of information to other dimensions such as time and space opens an entirely new way to enhance spectral and/or power efficiency at negligible implementation cost.

- Finally, in order to support the link level simulation results, a closed form expression of the error probability of SIM OFDM using different power allocation policies is derived.

1.4   Thesis assumptions

On the one hand, the key assumptions associated with system level analysis of the IWCS pilots performance can be summarized as follows:

- The considered closed-loop SDMA system enjoys a perfect knowledge of the MIMO channel coefficients of each active user. Hence, channel-dependent matrix transformations at both BS and MS is exploited to decompose the channel matrix into a collection of uncoupled parallel SISO channels.

- The considered problem of jointly adapting the MU-MIMO link parameters for a set of flat fading co-channel interfering MIMO links exploits two Dofs: transmit antenna selection, and user selection in cross-layer fashion.

- The time and frequency DoFs (e.g. frequency channel dependent scheduling and frequency domain link adaptation) are not considered in this study.

- This thesis assumes that BD algorithm completely eliminates intracell CCI and, hence, the system is limited by intercell CCI only which also dominates thermal noise.

- According to the definition of UL channel sounding mechanism adopted by LTE, channel sounding pilots are different from the demodulation pilots dedicated for coherent data detection. This implies that modifying the UL channel sounding pilots does not hinder

channel estimation processes related to coherent data detection. In particular, the only purpose of the proposed modification on the UL channel sounding pilots is to add interference awareness to the channel sounding methodology. Also according to the LTE technical documents related to the UL channel sounding pilots, the predetermined sounding waveforms are transmitted using orthogonal signals among all active users in all cells using the same frequency band. In particular, the sounding pilot sequences are chosen to be orthogonal in frequency domain among all of the users' antennas [88, 89]. In summary, the above properties enable the BS to estimate the UL wideband channel for each antenna of each active user without any intracell or intercell CCI between the channel sounding pilots. Moreover, error in channel estimation due to the presence of noise is beyond the scope of this thesis, hence, perfect channel estimation is considered as outlined in the first assumption.

On the other hand, the key assumptions associated with link level analysis of the SIM OFDM performance can be summarized as follows:

- The considered conventional OFDM system is assumed to be perfectly synchronized in time and frequency domains.

- To simplify the analytical derivation of the error probability of SIM OFDM, the two associated estimation processes are assumed to be independent.

1.5   Organization of the thesis

The rest of this thesis is organized as follows:

- Chapter 2 provides the required background for this thesis. This includes the cellular concept and related preliminaries such as frequency reuse and duplexing, the characteristics of the wireless channel and the resultant different types of diversities, and a brief overview of feedback methodologies.

- Chapter 3 presents an overview of the definition of a MIMO channel, the MIMO capacity, and MU-MIMO beamforming algorithms, particularly, the BD algorithm. It also describes the basic concept of cross-layer approach for multiuser scheduling in SDMA systems.

- Chapter 4 starts with brief signal model of CCS transmission followed by the introduction of the first major contribution of this thesis which is the novel interference-weighting method that enables UL CCS pilots to convey an implicit knowledge of the experienced interference at the user side to the BS along with CSI. Then, it discusses the channel diagonalization-based optimization methodology employing the interference-aware-metric provided by IWCS pilots. In order to extend the usability of IWCS mechanism to UL optimization, another contribution is presented in which the IWCS estimated metrics are further modified by accounting for the experienced interference at the BS. The resultant metric adds a link-protection awareness to the scheduler so the potential caused interference towards already exiting links in adjacent cells is mitigated. A summary of all optimization metrics provided by both CCS and IWCS is presented to lead to the comparative analysis results. Moreover, the involved computational complexity with such optimization problem is mathematically modeled and two HAs are proposed to reduce it at the cost of negligible loss in overall performance.

  Chapter 4 also outlines the simulation platform and discusses the results obtained via system level Monte Carlo simulations. In this chapter, a comparison is performed between the achievable cell and user capacities for different optimization metrics. The results have been obtained using both exhaustive search and HA approaches. Finally, different forms of fairness related results are analyzed and discussed.

- Chapter 5 briefly reviews conventional OFDM transmission and proposes the SIM concept to be integrated with conventional OFDM. Also it presents some of SIM OFDM attributes such as signalling, spectral efficiency, and power control. A closed form of error probability of SIM OFDM under different power control schemes is derived in this chapter. Finally, SIM concept is generalized via examples associated with other dimensions such as time and space.

  Furthermore, Chapter 5 describes the link level simulation model used to assess the performance of SIM OFDM. It specifically presents a comparative analysis of SIM OFDM and conventional OFDM in terms of bit error probability performance for coded and uncoded data under different power allocation policies. The obtained results are verified by aid of the closed form analytical model derived in this chapter.

- Finally, Chapter 6 draws conclusions of this thesis and poses relevant future questions for research.

Chapter 2

Key principles of multiple access and feedback methodologies

In this chapter, fundamental concepts related to wireless communications, multiple access schemes, and feedback methodologies are presented.

2.1 Cellular preliminaries

2.1.1 Cellular concept

Cellular systems are a type of infrastructure-based network where a given region is divided into cells to efficiently use the available spectrum. The fundamental assumption behind the cellular concept is frequency reuse, which relies on the power drop-off with propagation distance. Hence, the same frequency spectrum can be reused at spatially-separated locations (cells). Specifically, the available spectrum of the cellular network is divided into radio channels using one of the multiple access schemes discussed in section 2.1.6.

Unfortunately, reusing all radio channels (frequency reuse of 1) in each cell will give rise to excessive intercell interference (e.g. CCI). In order to maintain tolerable intercell interference among adjacent cells, a frequency reuse factor greater than 1 is used in 2G cellular systems. As is shown in Fig. 2.1, the cells are grouped into clusters (7 cell/cluster all of the same borderline style as in this example). The available bandwidth is divided into smaller bands (as many bands

as cells in a cluster) of non-overlapping adjacent frequency channels (represented in Fig. 2.1 by different numbers). The bands are then allocated to the cells of a cluster in such a way that cells using the same chunk of channels are sufficiently spaced so that the level of intercell CCI is tolerable.
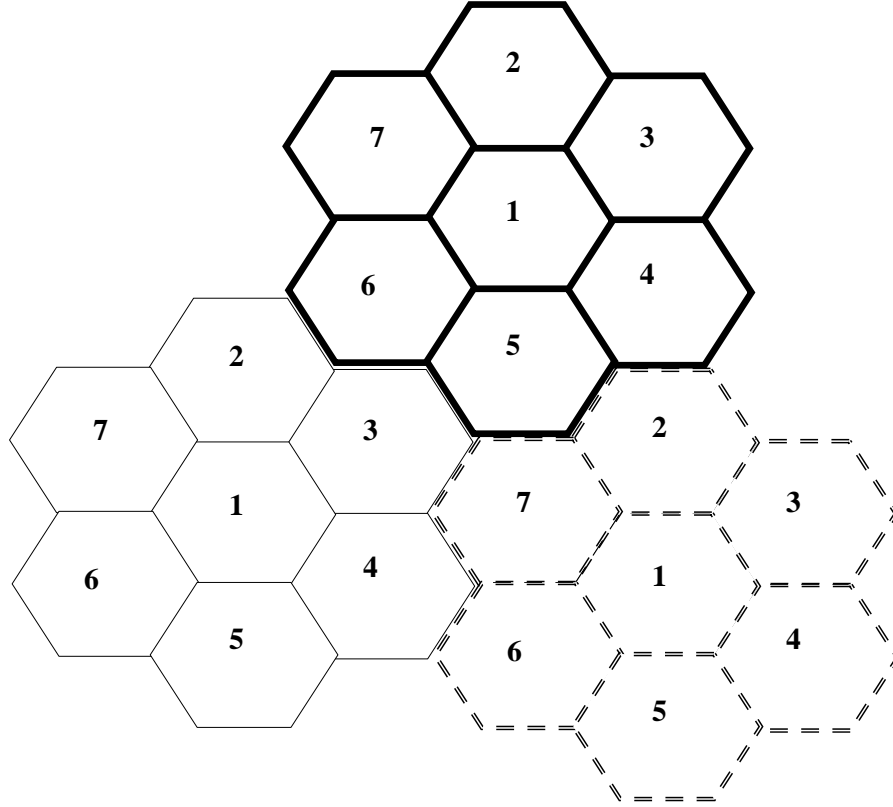
Figure 2.1: *Typical cellular network with frequency reuse factor of 7*

Having a frequency reuse factor greater than 1 apparently limits the overall network capacity in terms of channels/cell which dictates the number of served users per coverage area. Therefore, different versions of the fractional/soft frequency reuse (FFR) concept are recently proposed to improve the overall network capacity [90–93]. According to [90] and [91], the FFR concept suggests that the available bandwidth is partitioned into two parts. The first part serves the users located in the cell-center, while the second part is allocated to the cell-edge users. Afterwards, the cell-edge bandwidth is divided into three bands and the cell-edge area is divided into three sectors. These three sectors are allocated orthogonal frequency bands, hence, the cell-edge region uses a frequency reuse factor of three. Meanwhile the cell-centre region benefits from a frequency reuse of one, see Fig. 2.2. It should be noted that the FFR concept is not limited to

OFDMA networks but it is also applicable to GSM and CDMA networks.
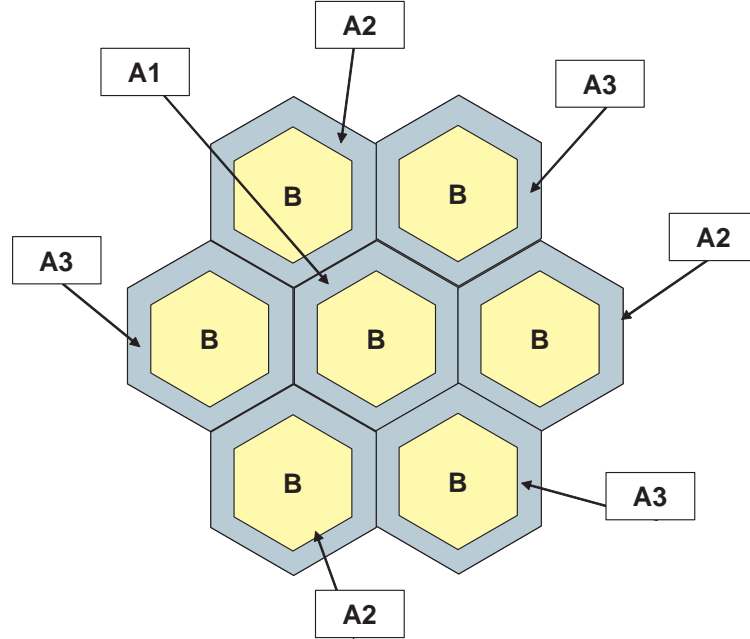
Figure 2.2: *Fractional/soft frequency reuse concept with a frequency reuse factor of 3 at the cell-edge*

In any cellular network, there are two types of radio channels: control channels that convey control messages, and data channels to carry information. The outgoing transmission from a BS to a MS is typically referred to as downlink, while the incoming transmission from a MS to a BS is correspondingly referred to as uplink. Basically, DL and UL transmissions are separated using duplexing techniques, see Fig. 2.3. Unlike unidirectional communication which is referred to as '*simplex*', '*duplex*' refers to bidirectional communication between two entities. Simultaneous bidirectional transmission is referred to as full duplex such as normal telephone conversation. In contrast, bidirectional transmission occurring at mutually exclusive times is known as half duplex such as walkie-talkie systems. There are two prevalent duplexing techniques, namely TDD and frequency division duplex (FDD). Inherently, TDD is a half duplex scheme while FDD can support both full duplex and half duplex e.g. GSM, see Fig. 2.4.

In TDD, DL and UL transmissions share the same frequency band but occupy two transmit time intervals (TTI) separated by guard time interval to switch the communication mode from reception to transmission or vice versa. Conversely, FDD allocates DL and UL two non-overlapping frequency bands. A guard frequency band is used for the separation to mitigate self-interference
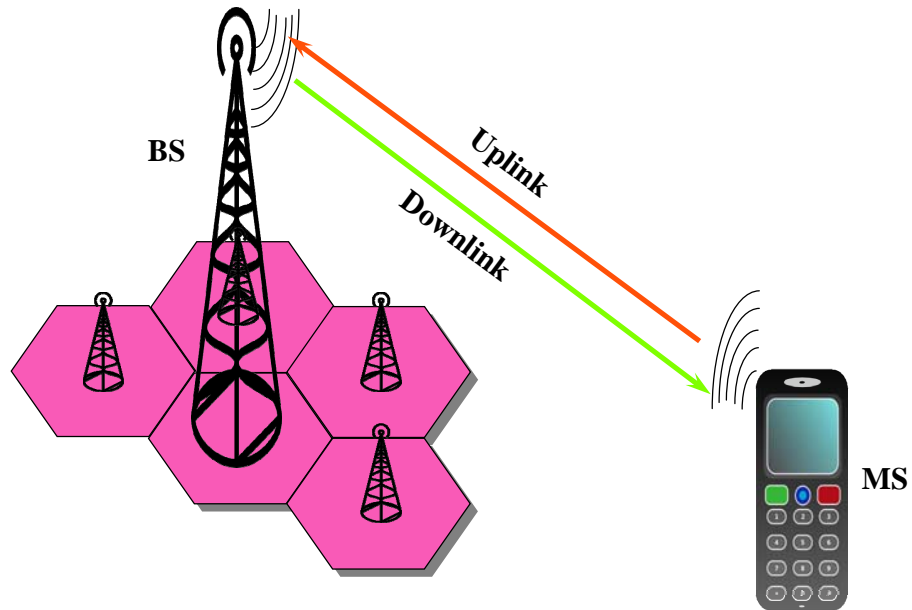
Figure 2.3: *Duplexing in cellular systems*

or inter-band leakage during simultaneous transmission on both DL and UL. These bands are usually of the same width, which is advantageous for symmetric traffic such as voice services. Therefore, FDD has been primarily used in 2G systems to meet the requirements of traditional voice services, *i.e.* GSM.
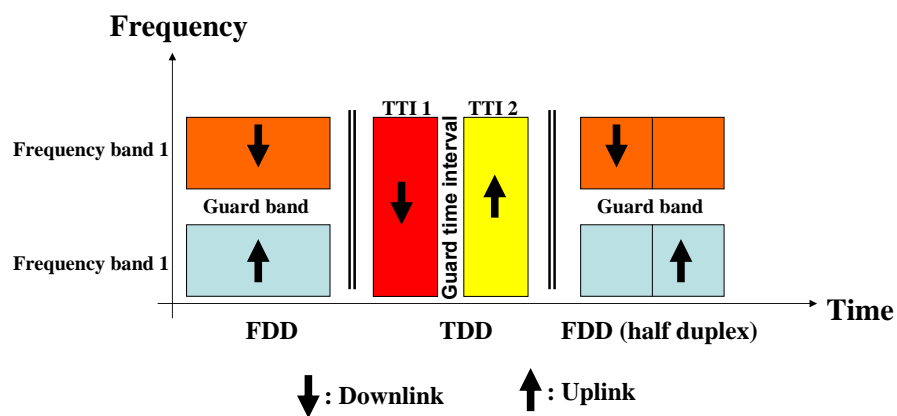
Figure 2.4: *FDD vs. TDD*

2.1.2 Radio channel characteristics

One basic feature of radio channels is that the transmitted signal is attenuated between a transmit and a receive antenna as a function of the propagation distance. This distance-dependent attenuation is known as free space path loss.

Path loss: is the attenuation in the signal power caused by the distance between the transmitter and the receiver. In line-of-sight (LOS) free space propagation scenario, the power of received signal is inversely proportional to the second power of the distance. However, in practical scenarios with the presence of obstructions, the attenuation power exponent may vary with typical values in the order of between 3 to 5. The path loss is usually modeled as follows:

$$P_r = P_t \left(\frac{d_0}{d} \right)^{\mu} \tag{2.1}$$

where P_r and P_t are the received and the transmitted signal, respectively, d is the distance between the transmitter and the receiver, d_0 denotes a reference distance, and μ is the path loss exponent.

Another important feature of radio channels is that outgoing signal propagates over a variety of paths towards the receiver. These paths arise mainly from three physical mechanisms [94]:

- Reflection: propagating signals impinge on objects with smooth surface larger than its wavelength such as ceiling, buildings, and walls.

- Scattering: scattering occurs when the propagation environment has many objects with dimensions smaller than the signal wavelength such as rough surfaces, foliage, and lamp posts.

- Diffraction: sharp edges obstructing the propagation environment cause the traveling signal to bend.

These phenomena cause multiple replicas of the signal arriving along a number of different paths at the receiver. Such complex interaction with the environment is known as multipath propagation. Multipath propagation can add attenuation, distortion, and delays to the received signal. A simplified illustration of the multipath environment is depicted in Fig. 2.5.

For mobile receivers, the coherent summation of the multipath received signals can be constructive or destructive. Since the multipath versions of the signal experience different delays, the

amplitude and the phase of the coherent summation of the received signals are time-varying. For the case when the power of the resulting signal is significantly reduced, this phenomenon is called multipath fading. Consequently, the radio channel exhibits multipath fading in the time domain which severely affect the reception quality.

Generally, fading can be attributed and broadly classified into two main classes:

- **Long-term fading**: or slow fading, caused by blocking results from terrain contours such as mountains, hills, and buildings. Such blocking is also known as shadowing which is slowly time-varying and can be modeled with log-normal distribution.

  The path loss along with the shadowing effect can be mathematically expressed in decibels as follows:

  $$g = A + 10\mu \log_{10}(d/d_0) + \xi, \tag{2.2}$$

  where A is an antenna-dependent constant; and ξ is a zero mean Gaussian distributed random variable with standard deviation σ_S in dB.

- **Short-term fading**: also known as small-scale fading which is due to the different multipath signals being added up with random phases, constructively or destructively, at the receiver. This causes a rapid fluctuations in the received signal level. The multipath channel, as a time-variant finite impulse response system, can be modeled using the simplified tapped delay line multipath channel model described in [95–97]. An arbitrary power delay profile with maximum propagation delay T_{delay}, the total time interval during which reflections with significant energy arrive, is assumed. The number of temporal taps is $L = \left(\frac{T_{\text{delay}}}{\tau}\right) + 1$, where τ is the tap-delay. For a particular link, the impulse response of the channel between receive antenna ν and transmit antenna κ at time t to an impulse input applied at $t - \tau$ can be written as

  $$h_{\nu,\kappa}(t,\tau) = \sum_{l}^{L} \rho_l(t) \exp(-j\, 2\pi\, f_c \tau_l(t)) \delta(\tau - \tau_l(t)) \tag{2.3}$$

  where l refers to the lth temporal tap of the channel, and $\delta(t)$ is the Dirac delta function. Since the total number of the multipaths is usually large, $h_{\nu,\kappa}(t,\tau)$ can be modeled as a complex-valued Gaussian random process according to the central limit theorem [86]. In the case of flat fading, all frequency components of the transmitted signal undergo almost the same random attenuation and phase shift, the channel impulse response is expressed

as

$$h_{\nu,\kappa}(t,\tau) = \alpha(t)\exp(j\psi(t))\delta(\tau) \qquad (2.4)$$

On the other hand, when the propagation delay is larger than the symbol duration, the frequency components of the trasmitted signal will go through different attenuations and phases. This is called frequency-selective fading and the channel can be expressed as

$$h_{\nu,\kappa}(t,\tau) = \sum_l^L \alpha_l(t)\exp(j\psi_l(t))\delta(\tau - \tau_l(t)) \qquad (2.5)$$

where $\alpha_l(t)$ is the channel gain and $\psi_l(t)$ is the channel phase shift. The channel gain $\alpha_l(t)$ can be statistically modeled with a Rayleigh distribution for non-line-of-sight (NLOS) propagation, and with a Rician distribution for the LOS case.
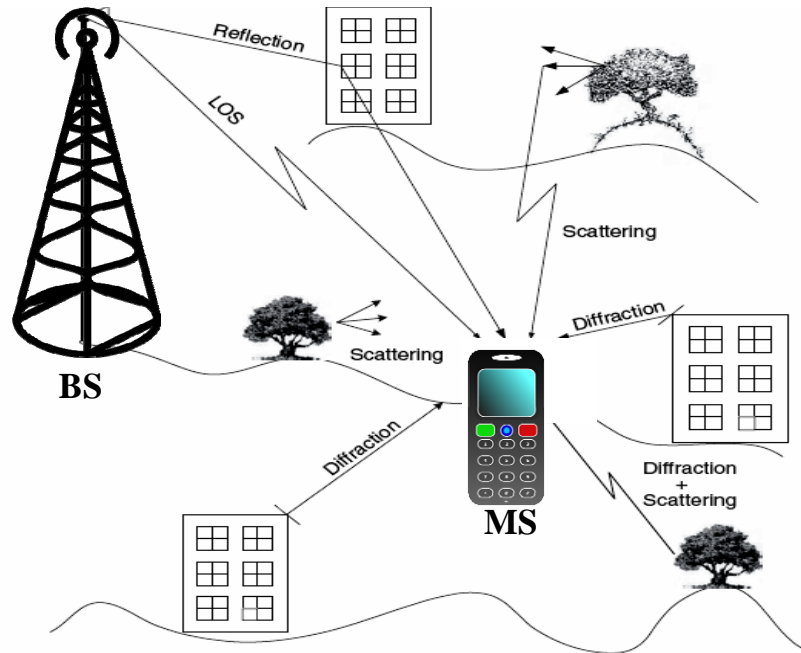
Figure 2.5: *Multipath propagation caused by various natural and man-made objects located between and around the transmitter and the receiver*

2.1.3   Radio channel diversity

Multipath fading can be combated by combining two or more versions of the received signal to enhance the reception. The basic idea is that while some of the received copies of the

transmitted signal may suffer fading, others may not. This basic effect is known as diversity which results from the spreading of the signal in different dimensions, *i.e.* time, frequency, and space. Generally, combining techniques can be classified into three categories: selection diversity, equal gain combining (EGC), and maximum ratio combining (MRC) [98]. In selection diversity, the signal with the highest received level is selected by the receiver. In EGC, all received copies are coherently added with equal amplitude and phase. In MRC, the amplitudes are weighted proportionally to the received signal-to-noise ratio (SNR) prior to summing the signals, while the phases are kept equal. The improvement in system performance due to implementing diversity techniques is termed as diversity gain.

Generally, multipath propagation and movement of the MS creates dispersion in the channel across a number of domains. Such channel dispersion is a result of the received signal energy being spread in the frequency, time, and space. These three primary types of diversity are briefly described as follows:

Frequency diversity: delay spread

Multipath propagation results in delay differences among the received versions of the transmitted symbol over different paths. The span of these differences in delay is known as delay spread, which causes inter-symbol interference (ISI). For the case of short symbol duration compared to the channel propagation delay, the amplitude of the channel frequency response will vary over the duration of the symbol resulting in frequency selective fading.

Coherence bandwidth and delay spread are parameters which describe the time dispersive nature of the channel and can be considered as a Fourier transform pair. The coherence bandwidth B_c can be defined as the bandwidth over which the frequency correlation function is above 0.9. For such definition the coherence bandwidth is

$$B_c \approx \frac{1}{50\sigma_{\mathrm{rms}}} \tag{2.6}$$

where the σ_{rms} is root mean squared delay spread and can be defined as the second central moment of the power delay profile as follows

$$\sigma_{\mathrm{rms}} = \sqrt{\frac{\sum_l^L \alpha_l^2 \tau_l^2}{\sum_l^L \alpha_l^2} - \left(\frac{\sum_l^L \alpha_l^2 \tau_l}{\sum_l^L \alpha_l^2}\right)^2} \tag{2.7}$$

In summary, frequency selectivity can be characterized in terms of coherence bandwidth, which represents the maximum frequency interval over which the channel frequency response remains approximately of a constant gain and linear phase (flat fading channel).

When the signal bandwidth is wider than the coherence bandwidth the channel becomes frequency-selective [99].

Time diversity: Doppler spread

The movement of the MS or surrounding scatterers gives rise to Doppler spread, which shifts the frequency of the received signal from the transmitted frequency due to its relative motion. Multipath propagation of the signal causes the relative speed of the MS with respect to different copies of the received signal to differ, which results in different Doppler shifts. The width of these shifts is referred to as the maximum Doppler spread, which is inversely proportional to the coherence time of the channel. That is

$$T_c \approx \frac{1}{f_d} \tag{2.8}$$

where f_d is the maximum Doppler spread, and the coherence time T_c represents the time interval over which the channel does not change significantly. The channels with short coherence time are considered as fast fading channels (time selective fading) [86]. Fig. 2.6 illustrates a simple classification of small-scale fading according to both delay spread and Doppler spread.

Space diversity: angular spread

Angular spread refers to the spread of the arrival and departure angles of multipath communication link. Specifically, the amplitude of the signal received over multiple paths depends on the spatial position of the antenna, which results in spacial selective fading. Spacial selective fading can be characterized by the coherence distance, which represents the maximum distance between two adjacent antennas for which the channel response is strongly correlated. According to the central limit theorem, each elements of the MIMO channel matrix associated with two MIMO transceivers located in rich scattering environment can be modeled as a complex Gaussian random variable. Moreover, the MIMO channel is considered as spatially uncorrelated if the antenna spacing is greater than half the wavelength of the transmitted signal [86]. This MIMO channel can be modeled as a Rayleigh MIMO fading channel, which has been

Small-Scale Fading
(Based on multipath time delay spread)

Flat Fading	**Freauency Selective Fading**
1. BW of signal < BW of channel	1. BW of signal > BW of channel
2. Delay spread < symbol period	2. Delay spread > symbol period

Small-Scale Fading
(Based on Doppler spread)

Fast Fading	**Slow Fading**
1. High Doppler spread	1. Low Doppler spread
2. Coherence time < symbol period	2. Coherence time > symbol period
3. Channel variations faster than baseband signal variations	3. Channel variations slower than baseband signal variations

Figure 2.6: *Types of small-scale fading based on delay spread and Doppler spread [10]*

intensively used for link level and system level evaluation in the MIMO related research and, hence, it is adopted in feedback-based interference management objective of this thesis. The interested reader can refer to [100] for other physical and statistical models.

In summary, frequency diversity implies that the signal is modulated using several carrier frequencies (multicarrier transmission) separated by at least the coherence bandwidth of the fading channel, so that each signal will fade almost independently of the others. With time diversity, the signal is transmitted during different time slots separated by at least the coherence time of the fading channel. Finally, space diversity involves either transmitting the signal from several antennas or receiving it using several antennas or both. Specifically, each antenna is separated in space so that signals departing/reaching different antennas will independently fade. This can offer a DoF for selection or can be combined to improve the received power.

2.1.4 TDD *vs.* FDD

This section compares these two duplexing schemes with respect to their bandwidth efficiency, experienced interference, suitability for data applications and delay.

- **Bandwidth efficiency**: An FDD system uses different bands for the UL and the DL and therefore a guard frequency band is needed to mitigate inter band interference. The size of the guard frequency band scales with the system bandwidth. Consequently, for wideband systems a significant amount of the available bandwidth is consumed by the guard frequency band. In contrast to FDD, TDD does not require a guard frequency band since it uses a single band for transmission in both DL and UL separated by a switching time interval. The duration of the switching time interval is independent of the system bandwidth and is only dictated by the hardware circuitry of the communicating entities. Therefore, TDD is the more bandwidth-efficient scheme.

- **Feedback mechanism**: In TDD, DL and UL share the same frequency band and, therefore, they are reciprocal. Hence, on the one hand, TDD has the advantage of using knowledge gained at the BS about the channel during UL mode to infer the channel of the subsequent DL TTI (UL CCS). On the other hand, FDD uses different bands for DL and UL and therefore generally cannot use UL information for DL. Clearly, FDD requires an explicit transmission (direct feedback) of the DL channel state information CSI on UL.

- **Latency**: In FDD, direct feedback tends to have much higher latency between the time of the channel estimation and the time of the subsequent DL transmission. The resulting outdated CSI can have serious consequences on the performance of closed-loop transmission algorithms in fast time-varying channels.

- **Hardware complexity**: Since FDD facilitates continuous and simultaneous transmission in UL and DL, special filters (duplexers) along with mechanical and electrical shielding are required to mitigate the inter-band interference. In TDD, duplexers and isolation technology are unnecessary since UL and DL transmission are never simultaneous. Consequently, FDD involves higher complexity and expensive hardware as compared to TDD.

- **Flexibility**: Unlike symmetric voice traffic, data traffic is inherently asymmetric, where DL traffic surpasses UL traffic by an approximate ratio of 4:1 in business applications

and even higher in residential scenarios [13]. Due to the fact that FDD utilizes frequency bands with equal fixed bandwidth, FDD is inadequate for packet-based services. Furthermore, these bandwidths are regulated by authorities like federal communications commission (FCC) or limited by the hardware functionality. In contrast, TDD can adaptively allocate resources to support symmetric and asymmetric traffic or even a mix of both. This can be maintained by adjusting the location of the guard time interval within the frame according to the traffic asymmetry ratio. In other words, TDD can borrow time from UL to increase DL as necessary, or vice versa.

- **Induced CCI**: Both FDD and TDD experience other-entity interference (BS-to-MS and MS-to-BS interference). However, TDD also suffers from same-entity interference (BS-to-BS and MS-to-MS interference), as depicted in Fig. 2.7.
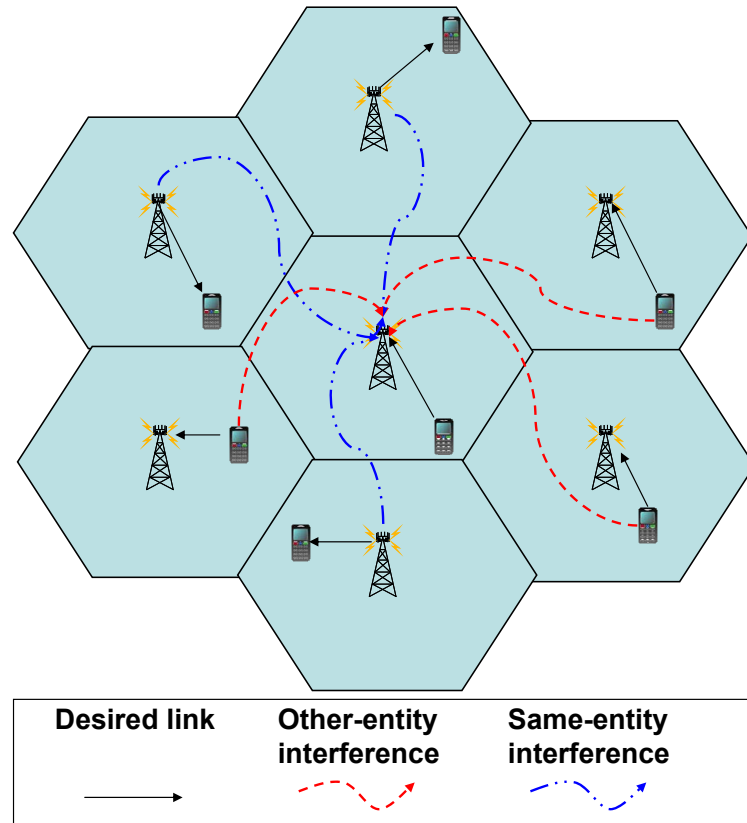
Figure 2.7: *Intercell CCI scenarios in TDD cellular network*

In summary, TDD is a more desirable duplexing technology that allows 4G system to cope with the convergence of voice, video and data services, while maintaining the needs of each

individual user. From closed-loop system point of view, due to the TDD channel reciprocity, TDD can support more advanced pre-transmission signal processing techniques than FDD. To be specific, TDD avoids the feedback limitation resulting from quantized CSI as in the FDD case.

2.1.5 Reciprocity of TDD radio channel

In a TDD system, the UL and DL share the same frequency band, and therefore the two links can be modeled as reciprocals and consequently simple transposes of each other. Hence, the TDD system has the advantage of using knowledge gained about the channel on the UL to infer the channel on the DL [25]. Hence, channel estimation can be performed in arbitrary direction of the link, and it gives the same results without regard to estimation errors. For example in the case of UL CCS, the MS transmits orthogonal pilots during UL to be used by the BS to estimate the channel coefficients in order to decode the UL data. Due to reciprocity, the same information on the channel coefficients can be used by the BS to accordingly adapt the DL traffic to enhance the MS reception. Later in section 2.2, the UL CCS feedback method is discussed in more detail.

2.1.6 Spectrum sharing schemes

The wireless system capacity, which determines the upper bound for the system throughput, is often most limited by the frequency spectrum. Capacity improvements generally focus on efficient bandwidth utilization through resource reuse [101]. As outlined earlier, reuse refers to the ability to use some system resources to increase the number of physical channels that occupy the same spectrum [102]. System capacity can be increased if the number of channels per BS is increased provided that CCI is tolerable. As illustrated in Fig. 2.7, CCI occurs when two transmitters simultaneously transmit on the same frequency channel. If the desired and the interference signal levels at a receiver are approximately similar, the receiver cannot distinguish between the two signals, giving arise to CCI. On the other hand, CCI is negligible if the interference signal level is significantly lower than the desired one. In multiuser communication systems, the way of coordinating the transmission associated with multiple users sharing the same cell resources is referred to as multiple access strategies. In particular, these strategies discipline how a group of users is awarded access to shared system resources. There are four common multiple access strategies: FDMA, time division multiple access (TDMA), SDMA,
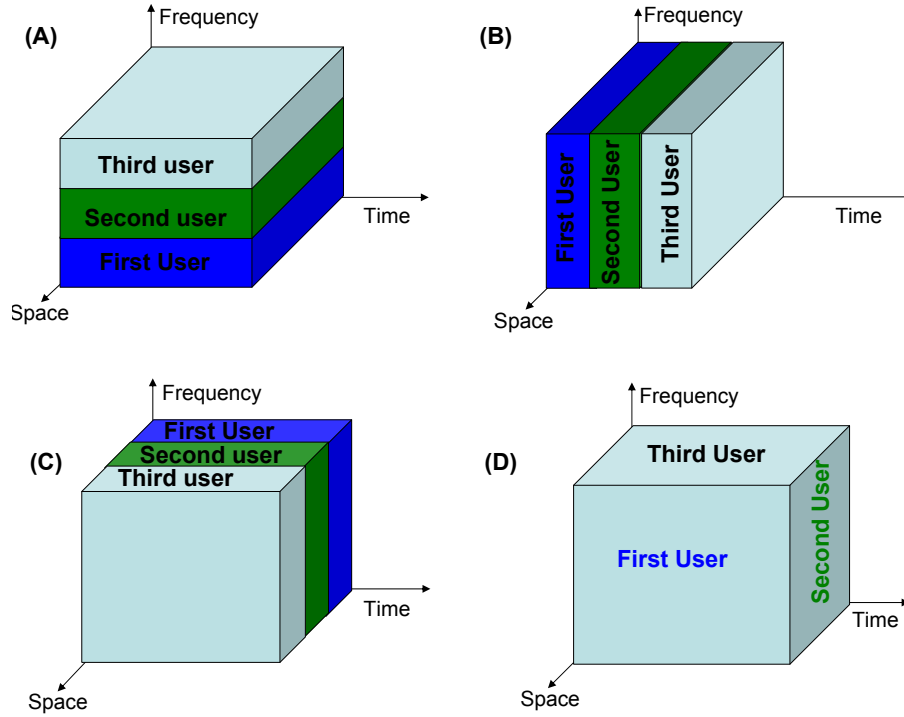
Figure 2.8: *Multiple access schemes: (A) FDMA, (B) TDMA, (C) SDMA, and (D) CDMA.*

and CDMA, which are summarized below. Fig. 2.8 illustrates how the resources are allocated across multiple users according to each multiple access strategy.

Time division multiple access

According to TDMA, multiple users who require access to the network can transmit on the same frequency band if their transmissions are non-overlapping in time as shown in Fig. 2.8. More specifically, a single user is permitted to transmit during a particular time-slot while all other active users are assigned to different slots. One of the key advantages of TDMA is the possibility of allocating time-slots based on demand. However, TDMA has some drawbacks such as synchronization [103].

Frequency division multiple access

In contrast to TDMA, FDMA divides the available spectrum into several smaller frequency bands that can be simultaneously allocated to different users. Basically, each user is assigned a particular frequency band and may therefore transmit continuously. Consequently, time syn-

chronization is avoided but, however, frequency synchronization is needed.

An OFDM-based multiple access scheme known as OFDMA is a bandwidth-efficient special case of FDMA where the bandwidth is divided into multiple narrowband channels of orthogonal subcarriers [11].

Code division multiple access

The motivation of proposing CDMA is to award network access to all active users simultaneously over the whole available bandwidth. This is achieved by coding transmission of each active user in such away that it becomes orthogonal to other transmissions belonging to the other users. The basic principle of CDMA is illustrated in Fig. 2.8. Basically, the coding can be considered as modulation with a relatively high bandwidth sequence known as the spreading signal. In order to create orthogonality among the active users, CDMA allocates a pseudo noise sequence to each active user that is approximately orthogonal to the spreading sequences of different users, or to time-shifts of its own [104]. Therefore, the multiuser interference that each user experiences will be similar to Gaussian noise, which makes CDMA an interference-limited system [105]. Thus, power control is needed to keep the received power level constant over the users, which is known as the near-far effect [106, 107].

Space division multiple access

In SDMA, frequencies can also be reused within the same cell by using SAs or beamforming. In this case, to avoid intra cell CCI the antennas should have low side-lobe levels and low front-to-back ratios [108]. By exploiting the properties of SAs, which will be discussed later in this chapter, transmit beamforming can be used to focus the transmit power in some directions over others. This property is exploited in SDMA systems to directionally transmit several simultaneous transmissions in different directions. In order to do this, a knowledge of the directions of each user, also known as angel of arrival (AoA) needs to be available at the transmitter. This knowledge may be estimated from the channel covariance matrix of each user, especially, for small angular spread transmission.

In summary, SDMA divides the cell into sectors and only a single user is granted the same time-frequency resource in each sector. From implementation point of view, the beam formed with transmit beamforming will never be completely concentrated in the direction of the desired

receiver. There will always be some energy leakage that creates interference to users within the same cell. It is important to remind that this thesis assumes that this kind of SDMA-specific intracell CCI is complectly eliminated by means of BD-algorithm as outlined in the previous chapter.

Within the 3GPP evolution track, these multiple access schemes have been used by successive generations. 2G GSM family was based on a hybridization of TDMA and FDMA [109–111]. 3G UMTS family marked the adoption of CDMA by the 3GPP evolution track, which is known as WCDMA [112–115]. Finally, LTE-advanced (classified as 4G) has adopted a combined version of OFDMA-SDMA for DL and SC-FDMA-SDMA for UL [116–118].

2.2 Overview of feedback methodologies

Basically, there are two methods for providing a BS with the CSI of all MSs, namely direct feedback and UL channel sounding. This section highlights the motivation behind choosing UL channel sounding in this thesis for the case of TDD by conducting a brief comparison between both feedback methods.

2.2.1 Direct feedback

According to LTE terminology this feedback method is termed as codebook-based feedback. In this method, the MS determines the best entry in a predefined codebook of precoding (beam-forming) vectors/matrices and transmits a feedback indication to the BS conveying the index value. In codebook feedback, the MS uses downlink channel estimates to determine the best codebook weight or weights for BS to use as a precoding vector/matrix. The MS creates a feedback indication that includes the codebook index and then sends the feedback indication to BS. This method can be considered as a candidate option for FDD systems which require an explicit transfer of the DL CSI during the UL transmission due to the absence of the channel reciprocity feature.

2.2.2 Uplink channel sounding

In UL channel sounding, the MS transmits a sounding waveform on the UL and the BS estimates the UL channel of the MS from the received sounding waveform. The sounding pilot

sequences are chosen to be orthogonal between all of the users' antennas and also are designed to have a low peak to average power ratio (PAPR) in the time domain, [88, 89]. The details of UL channel sounding are given in 3GPP technical documents such as [71, 119]. However, a brief treatment of the uplink channel sounding signal model is given below.

According to LTE technical documents related to uplink channel sounding, the BS instructs the MS where and how to sound (*i.e.*, send a known pilot sequence) on the uplink. The information obtained from uplink channel sounding at the BS is used for determining downlink beamforming weights, for MIMO channel dependent scheduling on the uplink, as well as for MIMO channel dependent scheduling on the downlink [119]. According to the structure discussed in [71, 119], channel sounding pilots enable the BS to estimate the UL wideband channel for each antenna of each active user without any intracell or intercell CCI between the channel sounding pilots. Moreover, error in channel estimation due to the presence of noise is beyond the scope of this thesis, hence, perfect channel estimation has been considered as one of the assumptions of this thesis.

2.2.3 Comparison of feedback methodologies

In a TDD system, there are several compelling reasons for employing UL channel sounding rather than codebook-based feedback:

- First, channel sounding has the ability to leverage UL data transmissions without additional overhead provided that the occupied frequency bandwidth of the UL transmissions encompasses the occupied bandwidth of the subsequent downlink transmission.

- Second, any codebook-based feedback scheme must account for the number of SAs at the BS. In a codebook-based feedback scheme, the MS must be able to estimate the DL channel no matter how many SAs are at the BS. Thus, the complexity of the MS, and the information to be fed back increase with the number of antennas at BS. In contrast, channel sounding schemes are independent of the number of BS antennas. In other words, the problem of channel estimation is much more difficult in a codebook-based feedback scheme than in a channel sounding scheme. More specifically, in codebook-based feedback, the air-interface must enable the MS to estimate the channel between its antennas and a relatively larger number of SAs at the BS. Such estimation imposes a heavy processing load on a MS in a direct feedback scheme, while in a channel sounding scheme

the estimation process takes place at the BS side [120]. For instant, consider the case where the BS has eight transmit antennas and the MS has a two receive antennas. In a channel sounding scheme, the BS must estimate the channel between its eight antennas and the two transmit antennas. In contrast, in a codebook-based feedback scheme, the air interface must enable the MS to estimate the channel between its two antennas and the eight transmit antennas (an eight-source channel estimation problem, which is much more difficult).

- Third, in TDD systems, codebook-based feedback schemes tend to have much higher latency between the time of the channel estimation and the time of the subsequent DL transmission. The resulting outdated CSI can have serious consequences on the performance of closed-loop transmission schemes in mobile time-varying channels. In particular, the delay caused by the quantization and coding of the CSI may cause the CSI to become invalid for use at the transmitter especially in fast variant channel propagation scenarios.

  By contrast, channel sounding reference signals can be transmitted at the end of the UL, then be used by the transmission algorithm in the subsequent DL. In other words, the CSI of UL can be used by the transmission algorithm in the first few symbol intervals of the subsequent DL. In contrast, in a codebook-based feedback scheme, the channel is measured in a DL portion and then feedback information is quantized to be fed back on the next UL through some dedicated physical feedback channel for use on the next DL. It is worth mentioning that the physical feedback channel needs to consist of some reference signals to facilitate the coherent detection of the feedback information at the BS.

2.3 Summary

This chapter has briefly reviewed the fundamentals of cellular networks such as cellular concept, frequency reuse, and duplexing. The characteristics of SISO wireless channel and the associated DoFs were introduced. A comparison between TDD and FDD was presented with special focus on TDD reciprocity. Also, the basic principles of the common multiple access schemes were reviewed. It was emphasized that SDMA is a suitable candidate for 4G systems due to its robustness to intracell CCI, ability to enhance coverage, as well as because SDMA multiplies the system capacity. Furthermore, two basic feedback methodologies, namely code-

book based feedback and UL channel sounding, were discussed. It was pointed out that UL channel sounding is superior compared to codebook-based feedback in terms of overhead, latency, and complexity.

The next chapter will concentrate on the characteristics of MIMO channel, MIMO capacity, and the basic concepts of SA-based SDMA systems implementing precoding techniques.

Chapter 3

Overview of multiuser MIMO systems

3.1 MIMO fundamentals

For a long time in wireless systems, multiple antenna systems was acknowledged for their potential to enhance communications [121]. In the last two decades, most of the scientific research was conducted in attempt to comprehend their fundamental capabilities. Historically, the invention of so-called MIMO systems was recognized as a key milestone in the mid 1990s [122].

3.1.1 Multiple antenna configuration modes

Depending on the availability of multiple antennas at the transmitter and/or the receiver, multiple antennas communication can be classified into three basic modes in addition to the SISO mode, see Fig. 3.1. Implementing multiple antennas at only one side of the communication link forms two types of space diversity: receive and transmit diversity which are referred to as SIMO (single-input multiple-output) and MISO (multiple-input single-output) modes, respectively. For the SIMO mode, having N_R antennas at the receiver provides fundamentally two different gains: power gain and diversity gain. Power gain is obtained from the increment in the total received signal power due to multiple antennas at the receiver. Generally, power gain scales linearly with N_R. Diversity gain is achievable due to the fact that the probability of having unfavorable channel conditions decreases by averaging over multiple independent spatial streams. For the MISO mode, transmit antenna selection or precoding techniques can be used

to enhance the reception based on having the CSI at the transmitter. Additionally, some techniques such as space-time coding make it possible to achieve both power gain and full diversity gain [99]. Finally, having both multiple transmit and receive antennas creates a full MIMO link which also includes SIMO and MISO as special cases.
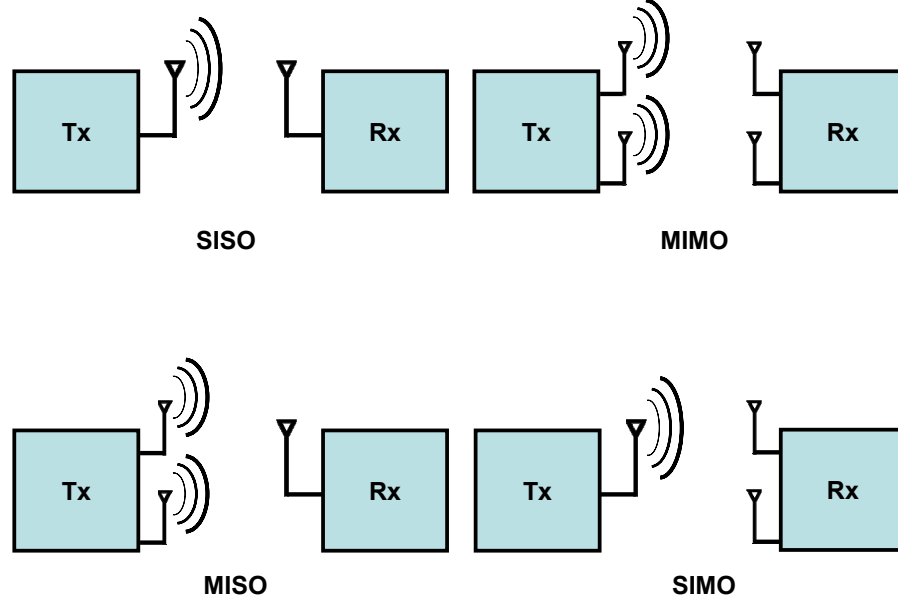
Figure 3.1: *Multiple antennas communication modes*

3.1.2   Multiple antenna benefits

MIMO deployment can significantly increase data rates through spatial multiplexing where parallel data streams are transmitted over the MIMO channel. Therefore, MIMO communication provides another gain, in addition to power and diversity gains, known as multiplexing gain as in diagonal Bell labs layered space time (D-BLAST) systems. In summary, the different modes of MIMO communication can improve the reliability of the system and/or the system capacity.

Beamforming

Beamforming enables adaptive steering of a directional antenna gain by concentrating the transmission into a desirable direction or pattern. This increases the power of the received signal and reduces interference towards other coexisting links. Hence, the potential improvement in the SINR can facilitate wider transmission range or higher order modulation and coding schemes

(MCS). Furthermore, beamforming is the key enabling technology for SDMA that provides simultaneous access to several users to use the same frequency within the same cell and, thus, the overall system capacity is multiplied [123, 124].

Diversity

Spatial diversity provided by the multiple antennas, such as the Alamouti scheme [125], can be used to increase the robustness of a transmission against channel impairments and multipath fading. Therefore, the coverage can be extended and/or the error probability can be reduced.

Multiplexing

Simultaneous multiple data streams can be transmitted over full rank MIMO channel, provided that the number of receiving antennas is at least equal to the number of transmit antennas. Therefore, spatial multiplexing multiplies the capacity of a SISO link.

Hybrid

Combining some or all of the above benefits results in hybrid scheme as SA-based SDMA systems implementing vertical Bell labs layered space time (V-BLAST) algorithm where beamforming and multiplexing gains are combined. Another example is D-BLAST which achieves multiplexing gain while exploiting the spatial diversity.

3.2 MIMO single user system model

Fig. 3.2 shows a single users MIMO system with N_T transmit antennas and N_R receive antennas, hence, $N_R \times N_T$ transmission links. At the transmitter side, let $\mathbf{x}$ be the $(N_T \times 1)$-dimensional transmitted signal vector at time instant t. At the receiver side, let $\mathbf{y}$ and $\mathbf{n}$ be the $(N_R \times 1)$-dimensional received signal and the received noise vectors at time instant t, respectively. The input-output representation of this MIMO system is given by

$$\mathbf{y(t)} = \mathbf{Hx(t)} + \mathbf{n}(t) \tag{3.1}$$
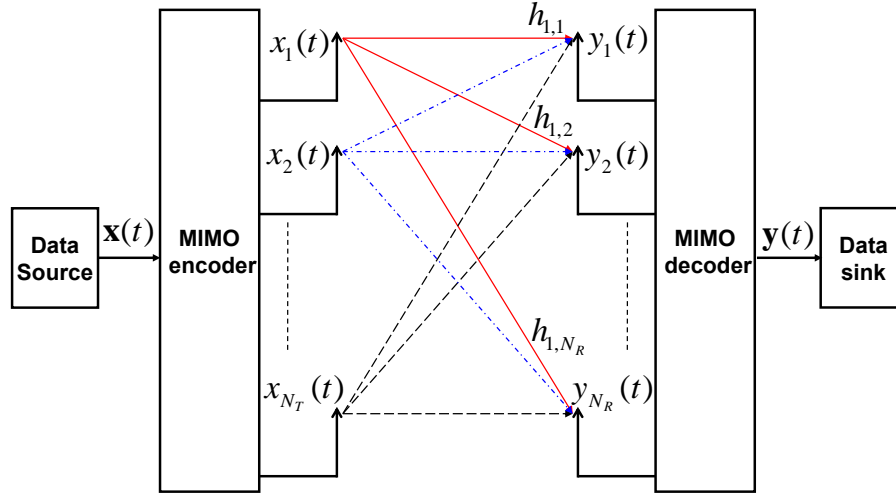
Figure 3.2: *Schematic illustration of basic MIMO system*

where $\mathbf{H}$ is a time-invariant channel matrix of size $N_R \times N_T$. The received signal at each receive antenna can be represented as the summation of the signals transmitted by all antennas multiplied by the channel response of the respective link and added to the noise at the receiving antenna as follows:

$$y_\nu = \sum_{\kappa=1}^{N_T} h_{\nu,\kappa} x_\kappa + n_\nu \qquad (3.2)$$

For the case of uniform power allocation among all transmit antennas, the signal power from each transmit antenna is generally fixed to P_t/N_T, where $P_t = \sum_{\kappa=1}^{N_T} \|x_\kappa\|^2$. The components of the received noise vector $\mathbf{n}$ are statistically independent zero-mean complex Gaussian variables with variance σ^2.

3.3 MIMO channel model

According to the maximum propagation delay compared to the transmitted symbol duration, MIMO channel can be modeled as flat fading channel or frequency selective fading channel, see Fig. 3.3

3.3.1 Flat fading MIMO channel

A flat fading channel forces all frequency components of the transmitted signal to be similarly attenuated. Since all the multipath versions of the signal arrive within a symbol duration at the
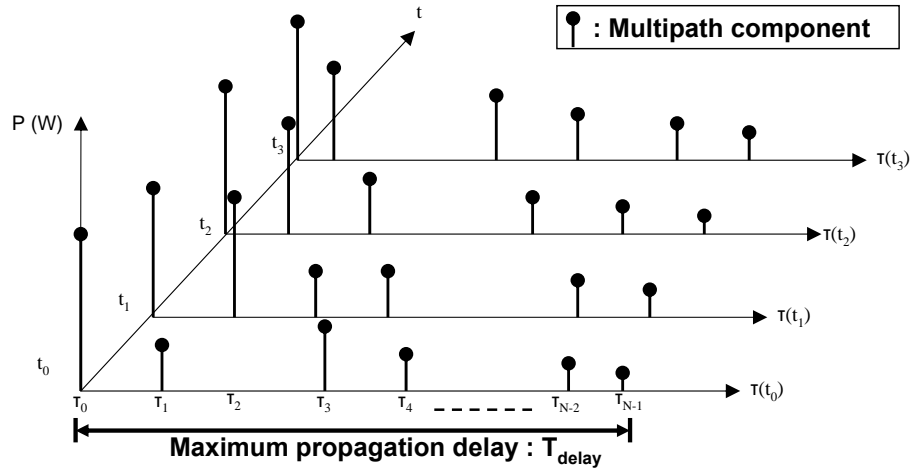
Figure 3.3: *Frequency flat fading vs. frequency selective fading*

receiver, the channel matrix is modeled as $N_R \times N_T$ matrix with single channel component for each link.

$$\begin{bmatrix} y_1(t) \\ y_2(t) \\ \vdots \\ y_{N_R}(t) \end{bmatrix} = \underbrace{\begin{bmatrix} h_{11} & h_{12} & \ldots & h_{1N_T} \\ h_{21} & h_{22} & \ldots & h_{2N_T} \\ \vdots & \vdots & \vdots & \vdots \\ h_{N_R1} & h_{N_R2} & \ldots & h_{N_RN_T} \end{bmatrix}}_{\text{flat fading channel}} \begin{bmatrix} x_1(t) \\ x_2(t) \\ \vdots \\ x_{N_T}(t) \end{bmatrix} + \begin{bmatrix} n_1(t) \\ n_2(t) \\ \vdots \\ n_{N_R}(t) \end{bmatrix} \quad (3.3)$$

3.3.2 Frequency selective fading MIMO channel

As the name suggests, different frequency components of a signal transmitted over frequency selective fading channel are differently attenuated and phase-shifted. Due to the fact that the multipath delay is longer than the transmitted symbol duration, the channel of any link is modeled as an impulse response $h(\tau)$ whose length is equal to L, where L is the number of multi-

paths.

$$
\begin{bmatrix} y_1(t) \\ y_2(t) \\ \vdots \\ y_{N_R}(t) \end{bmatrix} = \sum_{l=0}^{L-1} \underbrace{\begin{bmatrix} h_{1,1}(\tau_l) & \dots & h_{1,N_T}(\tau_l) \\ h_{2,1}(\tau_l) & \dots & h_{2,N_T} \\ \vdots & \vdots & \vdots \\ h_{N_R,1}(\tau_l) & \dots & h_{N_R,N_T}(\tau_l) \end{bmatrix}}_{\text{frequency selective fading channel}} \begin{bmatrix} x_1(t-\tau_l) \\ x_2(t-\tau_l) \\ \vdots \\ x_{N_T}(t-\tau_l) \end{bmatrix} + \begin{bmatrix} n_1(t) \\ n_2(t) \\ \vdots \\ n_{N_R}(t) \end{bmatrix}
$$

(3.4)

the signal received by ν^{th} receive antenna is obtained as

$$
y_\nu(t) = \sum_{\kappa=1}^{N_T} x_\kappa(t) * h_{\nu,\kappa}(\tau) + n_\nu(t)
$$

(3.5)

where $*$ donates convolution

$$
\begin{aligned}
x_\kappa(t) &= [x_\kappa(t-\tau_0) \ x_\kappa(t-\tau_1) \dots x_\kappa(t-\tau_{L-1})] \\
h_{\nu,\kappa}(\tau) &= [h_{\nu,\kappa}(\tau_0) \ h_{\nu,\kappa}(\tau_1) \dots h_{\nu,\kappa}(\tau_{L-1})]
\end{aligned}
$$

and $*$ donates convolution.

3.4 MIMO channel capacity

The channel capacity is defined as the maximum data rate that can be transmitted over the channel with an arbitrary small error probability [121]. Channel capacity is an important metric for channel characterization which depends on what is known about CSI at the transmitter and/or receiver. In this section, expressions for channel capacities depending on the frequency selectivity of the channel are given for deterministic and stochastic channel models. Since the focus of this thesis is on flat fading MIMO channels, the capacity is discussed in details for frequency flat fading and very briefly for frequency selective fading.

3.4.1 Frequency flat MIMO channel

Deterministic channel with CSI at the receiver

The input-output relationship for a MIMO system in flat fading channel is expressed as

$$
\mathbf{y} = \sqrt{\frac{P_t}{N_T}} \mathbf{H} \mathbf{x} + \mathbf{n} \tag{3.6}
$$

where $\mathbf{y}$ is the $(N_R \times 1)$-dimensional received signal vector and $\mathbf{x}$ is the $N_T \times 1$ transmitted signal vector. The AWGN has noise power spectral density N_0 with covariance matrix $\mathrm{E}\left[\mathbf{n}\mathbf{n}^H\right] = \sigma^2 \mathbf{I}_{N_R}$. The covariance matrix of $\mathbf{x}$ is $\mathbf{R_{xx}} = \mathrm{E}\left[\mathbf{x}\mathbf{x}^H\right]$, and P_t is the total average power available at the transmitter over a symbol period. The signals have equal power at all transmit antennas. Assuming $\mathbf{x}$ to have zero mean, $\mathbf{R_{xx}}$ must satisfy $\mathrm{tr}(\mathrm{E}\left[\mathbf{x}\mathbf{x}^H\right]) = N_T$ in order to constrain the total average transmit power (The total transmit power is given by $\mathrm{tr}(\mathrm{E}\left[\mathbf{x}\mathbf{x}^H\right])$ which is equal to N_T and the transmitted signals are multiplied by a factor $\sqrt{P_t/N_T}$. Thus the total transmit power P_t is kept fixed.

It is assumed that the channel matrix $\mathbf{H}$ is fixed and deterministic. From [99], the capacity of the MIMO channel is given as

$$
C = \max_{\mathrm{tr}(\mathbf{R_{xx}})=N_T} \log_2 \det\left(\mathbf{I}_{N_R} + \frac{P_t}{N_T N_0} \mathbf{H}\mathbf{R_{xx}}\mathbf{H}^H\right) \ \ \mathrm{bps/Hz} \tag{3.7}
$$

where the capacity C is the maximum achievable data rate per unit bandwidth.

When the transmitted signal vector $\mathbf{x}$ is assumed to have zero mean and is statistically independent and identical *i.e.*, $\mathbf{R_{xx}} = \mathbf{I}_{N_T}$ and the channel knowledge (e.g. CSI) is unavailable at the transmitter. Using singular value decomposition (SVD), the channel matrix can be diagonalized as in this form

$$
\mathbf{H}\mathbf{H}^H = \mathbf{U}\mathbf{\Lambda}\mathbf{V}^H \tag{3.8}
$$

where $\mathbf{U}$ and $\mathbf{V}$ are unitary matrices. Λ is a $N_R \times N_T$ diagonal matrix of the eigenvalues λ_i of $\mathbf{H}\mathbf{H}^H$ with $\lambda_i \geq 0$ and $\lambda_i \geq \lambda_{i+1}$. By substituting (3.8) in (3.7), (3.7) can be reformulated as follows

$$
C = \log_2 \det(\mathbf{I}_{N_R} + \frac{P_t}{N_T N_0}\mathbf{H}\mathbf{H}^H) = \log_2 \det(\mathbf{I}_{N_R} + \frac{P_t}{N_T N_0}\mathbf{U}\mathbf{\Lambda}\mathbf{V}^H) \tag{3.9}
$$

or equivalently

$$C = \sum_{i=1}^{r} \log_2(1 + \frac{P_t}{N_T N_0}\lambda_i) = \sum_{i=1}^{r} \log_2(1 + \frac{\rho\lambda_i}{N_T}); \text{ where } \rho = \frac{P_t}{N_0} \qquad (3.10)$$

where r is the rank of the channel. From this expression, the capacity of a MIMO channel is also interpreted as the sum of capacities of r SISO channels each weighted with power gain λ_i ($i = 1 \ldots r$). Transmission using multiple antennas virtually creates a multiple scalar spatial data pipes (spatial streams) between the transmitter and receiver.

From a linear algebra point of view, the number of eigenvalues which is also the rank of matrix $\mathbf{H}$ cannot exceed the number of columns or rows of the matrix [99]. Therefore, the rank of matrix is constrained by $r_{\leq}\min(N_R, N_T)$ with equality if the matrix is full rank (which is referred to as a rich scattering environment) and, hence, all rows and columns are independent. In summary, the MIMO channel capacity depends on two factors: the rank of the MIMO channel and the covariance of the transmitted signal.

Deterministic channel with CSI at both transmitter and receiver

It is well known that the single user MIMO capacity is maximized when the channel is diagonalized by the SVD procedure and the power is distributed by the water-filling algorithm [99]. As previously highlighted, the MIMO channel provides a multiplexing gain which results from the fact that the MIMO channel can be decomposed into a number of r parallel independent channels. By multiplexing independent data onto these independent channels, an r-fold increment in data rate is obtained compared to SISO transmission. Assuming a perfect knowledge of the MIMO channel $\mathbf{H}$ at both the transmitter and receiver, an SVD-based transmit precoding and receiver shaping can be used to linearly transform the input and the output of the channels as follows:

$$\tilde{\mathbf{x}} = \mathbf{V}^H\mathbf{x} \qquad (3.11)$$
$$\tilde{\mathbf{y}} = \mathbf{U}^H\mathbf{y}$$
$$\tilde{\mathbf{n}} = \mathbf{U}^H\mathbf{n}$$

Note that $\mathbf{U}$ and $\mathbf{V}$ are unitary matrices so the transformation does not change neither the distribution of $\mathbf{n}$ nor the energy content of $\mathbf{x}$.

The input-output relationship of the channel can be formulated as follows

$$\tilde{\mathbf{y}} = \mathbf{\Lambda}\tilde{\mathbf{x}} + \tilde{\mathbf{n}} \tag{3.12}$$

or as a parallel SISO scalar channels:

$$\tilde{y}_i = \sqrt{\lambda_i}\tilde{x}_i + \tilde{n}_i, i = 1, 2, ..., r \tag{3.13}$$

where λ_i is the ith singular value of $\mathbf{HH}^H$. This SVD-based procedure is shown in Fig.3.4 Now, the availability of CSI at the transmitter allows for optimal power allocation across the
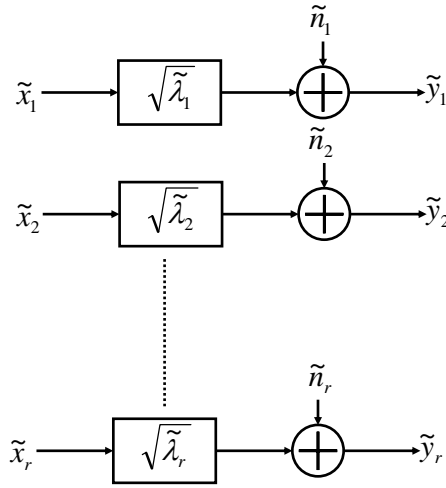
Figure 3.4: *Converting a MIMO channel into a parallel channels using SVD*

independent spatial channels and, hence the capacity in (3.10) can be rewritten as follows:

$$C = \sum_{i=1}^{r} \log_2(1 + \rho_i\lambda_i); \ \ \text{where } \rho = \frac{P_i}{N_0} \tag{3.14}$$

where $\sum_{i=1}^{r} P_i = P_t$, and P_i is the optimal power allocation of the ith spatial stream.

3.4.2 Ergodic capacity of flat MIMO random channel

The previous treatment of MIMO channel capacity applies for the case of a deterministic channel realization. However, in reality, the MIMO channel changes randomly over time, hence, ergodic capacity is used for the purpose of temporal capacity characterization. This section defines and discusses the ergodic capacity of random MIMO channels.

The elements of $\mathbf{H}$, $h_{\nu,\kappa}$ ($\nu = 1 \ldots N_R, \kappa = 1 \ldots N_T$) are random variable and are normalized so that $\mathrm{E}\left[|h_{\nu,\kappa}|^2\right] = 1$. Since the channel is random for each realizations of $\mathbf{H}$, the capacity is random for every realizations and can be computed from (3.10). Thus for random MIMO channels, there is a need for an expression to quantify the capacity. The average capacity of such random channel, defined as average of capacities associated with each realization of the channel $\mathbf{H}$, is refereed to as ergodic capacity $\overline{C}$. The ergodic capacity $\overline{C}$, when CSI is unavailable at the transmitter can be formulated as

$$\overline{C} = \mathrm{E}\left[\sum_{i=1}^{r} \log_2(1 + \frac{\rho}{N_T}\lambda_i)\right] \tag{3.15}$$

3.4.3 Ergodic capacity of frequency selective MIMO channel

Frequency selectivity arises from multipath fading. When the channel is wideband, different frequencies undergo different amount of fading. This results in selective fading in different frequencies. One common technique to handle this wideband channel is to divide it into number of narrowband sub-channels, such that each sub-channel undergoes flat fading. The capacity of the wideband channel is calculated as the average of the capacities of the flat fading narrowband sub-channels.

The input-output relationship of the kth flat fading narrowband sub-channels is

$$\mathbf{y}_k = \sqrt{\frac{P_t}{N_T}}\mathbf{H}_k\mathbf{x}_k + \mathbf{n}_k \tag{3.16}$$

For the case of full rank MIMO where channel knowledge is available only at the receiver, the ergodic capacity of the random frequency selective channel $\overline{C}_{FS}$ is calculated over the average of the capacities of all individual flat fading sub-channels and can be formulated as follows [99]

$$\overline{C}_{FS} = \mathrm{E}\left[\frac{1}{N_s}\sum_{k=1}^{N_s} \log_2 \det(\mathbf{I}_{N_R} + \frac{\rho}{N_T}\mathbf{H}_k\mathbf{H}_k^H)\right] \tag{3.17}$$

3.5 Multiuser SA-based SDMA with BD adaptive beamforming

3.5.1 Overview of SA technology

Originally, SA pre-processing techniques were proposed for military communications. Due to the significant advancement in microelectronics over the past two decades, SA-based technologies become a cost-efficient solution for commercial communication systems to overcome some of the major challenges such as multipath fading, CCI, and capacity limitations especially for the cell-edge users. By exploiting the spatial diversity and the spatial processing of SA, an efficient utilization of available bandwidth and, hence, an increased system capacity is facilitated. In particular, this gain is mainly enabled by two factors:

- Spatial signal preprocessing algorithms which depend on the availability of a variety of feedback metrics and the computational power at the BS.

- Directional transmission and reception at the BS where each scheduled MS is tracked by a narrow beam for both UL and DL. The resolution of such adaptive directionality depends on the level of the centralized complexity of SA hardware technology at the BS.

It will not be possible to provide a thorough overview of SA applications to wireless systems. Therefore, this section highlights the major features of SA-based SDMA systems related to this thesis. More specifically, the provided review is aimed at the benchmark SDMA system considered in this thesis. Also, this section briefly describes the generalized BD beamforming method for multiuser SDMA system [62], where the BS directionally transmits multiple spatially multiplexed independent data streams to a group of users selected according to a scheduling criterion. Due to physical size constraints at the user side, the MSs are assumed to be equipped with limited number of multiple OAs (2 throughout this thesis). This assumption is also convenient in order to maintain affordable cost and reduced complexity at the user side. As depicted in Fig. 3.5, each SA is consisting of an array of antenna elements and is dedicated to directionally transmit/recieve a single independent spatial stream, hence, it is referred to as effective antenna according to LTE terminology.

3.5.2 Multiuser MIMO BD system model

Consider a single-cell downlink MU-MIMO system where the BS is equipped N_T transmit SAs, and communicates over multiple MIMO channels with K users. It is assumed that all
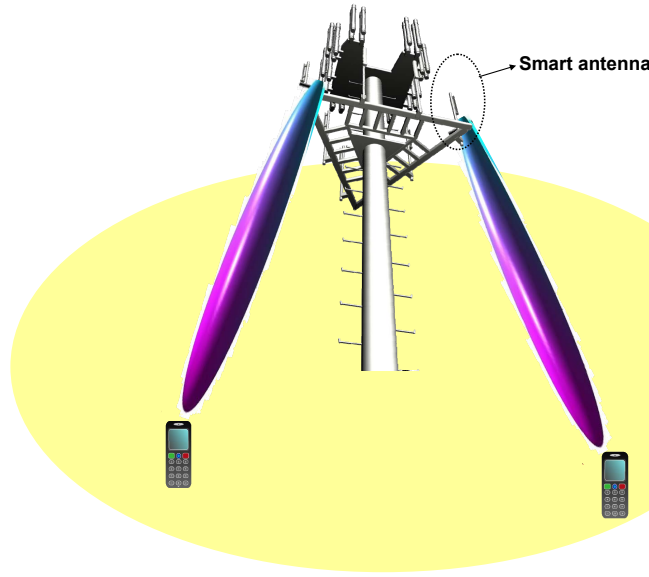
Figure 3.5: *A schematic illustration of SA-based beamforming SDMA system*

users are equipped with the same number of receiving OAs and denoted as N_R. To simplify the following analysis, it is assumed that $N_R < N_T$ and N_T is a multiplier of N_R in order to serve all users, hence, the number of served users is a natural number. Fig. 3.6 illustrates an example of the considered SDMA system where $N_R = 2$.

The flat fading MIMO channel matrix for user k is denoted as $\mathbf{H}_k$ where $h_k^{(j,i)}$ is the fading coefficient between the jth transmit antenna and the ith receive antenna of user k. For analytical simplicity, the rank r_k of $\mathbf{H}_k$ is assumed to be equal to $\min(N_R, N_T)$ for all users. Again, channel estimation errors caused by various reasons such as feedback delay, and feedback quantization error, etc. are beyond the scope of this thesis, hence, it is assumed that the BS has perfect CSI for all users. By assuming that the number of data streams s_k intended to user k is equal to N_R, the transmitted data streams to user k can be donated as a N_R-dimensional vector $\mathbf{x}_k$ where $\sum_{k=1}^{K} s_k \leq N_T$. Since CSI is available at both sides of the MIMO link, it is assumed that the MIMO transmission includes linear pre-processing and post-processing performed at both BS and MS, respectively. Prior to transmission, x_u is multiplied by a $N_T \times N_R$ precoding matrix $\mathbf{T}_k$. In this thesis, it is assumed that $\mathbf{T}_k$ is generated using the block diagonalization beamforming algorithm which is a member of the zero-forcing (ZF) type of multiuser precoding algorithms [68]. At the BS, the transmitted vectors of the K users are linearly superimposed and propagated over the channel from all N_T antennas simultaneously. It is also assumed that the elements of $\mathbf{x}_k$ are independent and identically distributed (i.i.d.) with zero
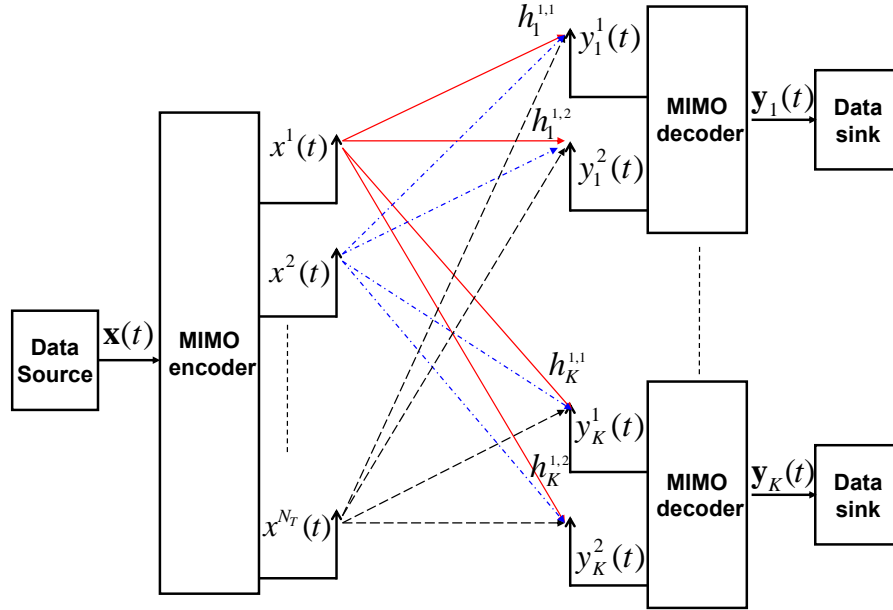
Figure 3.6: *SDMA system model with multiple MIMO users each equipped with 2 OAs*

mean and unit variance. The signal vector received at user k is

$$\mathbf{y}_k = \mathbf{H}_k \sum_{\iota=1}^{K} \mathbf{T}_\iota \mathbf{x}_\iota + \mathbf{n}_k \tag{3.18}$$

Equation (3.18) can be rewritten in the form of summation of the desired signal, the interference signal, and the noise signal as follows

$$\mathbf{y}_k = \mathbf{H}_k \mathbf{x}_k + \mathbf{H}_k \sum_{\iota=k} \mathbf{T}_\iota \mathbf{x}_\iota + \mathbf{n}_k \tag{3.19}$$

where the first term right-hand-side of (3.19) is the desired signal, the second term denotes the intracell CCI experienced by user k, and the last term $\mathbf{n}_k$ is the AWGN vector received by user k. According to the key idea of BD algorithm, $\mathbf{T}$ is designed such that $\mathbf{H}_k \mathbf{T}_\iota = 0$ for $\forall \iota \neq k$ and , hence, the intracell CCI is completely eliminated (nulled). The block matrices $\mathbf{H}_{\mathrm{S}}$ and $\mathbf{T}_{\mathrm{S}}$ can be defined as the system channel matrix and the system precoding matrix, respectively, as follows:

$$\mathbf{H}_{\mathrm{S}} = \left[\mathbf{H}_1^H \mathbf{H}_2^H \ldots \mathbf{H}_K^H \right]^H \tag{3.20}$$

$$\mathbf{T}_{\mathrm{S}} = \left[\mathbf{T}_1 \mathbf{T}_2 \ldots \mathbf{T}_K \right] \tag{3.21}$$

Under the constraint of zero intracell CCI among users within the same cell, the optimal solu-

tion can be obtained by diagonalizing the product of (3.20) and (3.21) $\tilde{\mathbf{H}}_S \mathbf{T}_S$. Now, $\tilde{\mathbf{H}}_k$ can be defined as the block matrix of the MIMO links interfering with user k as follows

$$\tilde{\mathbf{H}}_S = \left[\tilde{\mathbf{H}}_1^H \dots \tilde{\mathbf{H}}_{k-1}^H \tilde{\mathbf{H}}_{k+1}^H \dots \tilde{\mathbf{H}}_K^H \right]^H \tag{3.22}$$

In light of the above, the intracell CCI free constraint requires that $\mathbf{T}_k$ is selected to lie in the null space of $\tilde{\mathbf{H}}_k$. The details of designing the BD precoding matrices and the associated constraints can be found in [62, 68, 69].

3.6 Summary

This chapter has briefly introduced the characteristics of MIMO channel and its capacity. Also, the basic concepts of SA-based SDMA systems implementing precoding techniques were described. It was pointed out that the availability of CSI at the BS facilitates utilizing BD algorithm to eliminate intracell CCI among same-cell users. Also, it was indicated that opportunistic SA-based SDMA beamforming can be performed in cross-layer fashion. In multiuser SDMA scenario, cross-layer optimization consists of the user selection procedure and the spatial resource allocation procedure. Using UL channel sounding is of particular importance for opportunistic SA-based SDMA beamforming technologies to meet 4G requirement.

The next chapter concentrates on the cross-layer optimization problem related to SA-based SDMA system which is considered to be limited by intercell CCI. It is important to note that intercell CCI cannot be eliminated by BD algorithm because the BS in the cell of interest (CoI) has no knowledge about CSI of transmitters in adjacent cells. Therefore, Chapter 4 proposes a modified version of UL CCS, namely IWCS, to implicitly convey such knowledge of the experienced intercell CCI to the BS of CoI in order to enhance the achievable capacity associated with such optimization problem.

Chapter 4

Interference-weighted channel sounding

4.1 Introduction

This Chapter motivates the proposed modification to CCS pilots used in cellular SDMA-TDD systems. A brief overview of the signal model of CCS pilots is given and followed by a detailed mathematical model of the IWCS pilots. Moreover, the involved computational complexity with the considered MU-MIMO optimization problem is mathematically modeled and two heuristic algorithms (HAs) are proposed to reduce it. Using Monte Carlo simulations, a comparison between the performance of the different optimization metrics enabled by both CCS and IWCS is presented for both UL and DL. Finally, different forms of fairness related results are analyzed and discussed.

4.2 Problem statement

The notion of multiuser diversity opens up the following set of questions. In a spatial multiplexing opportunistic SDMA system with an excess number of SAs at the BS, how should the optimal set of spatially separable users be chosen? What is the appropriate allocation of the transmit/receive antennas (spatial beams) targeting the selected users? Since CCS pilots only provide sub-optimal metric (*i.e.* CSI), how can a better metric be provided (e.g. instantaneous SINR) for such optimization problem while maintaining the same inherent feedback bandwidth and delay efficiency? For practical reasons such as cost and physical size, the number of SAs at

the BS is greater than the number of OAs at the MS, as is the case in EUTRA. Algorithms that achieve spatial multiplexing gains such as V-BLAST receivers [126], however, require that the number of antennas at the receiver is greater than or equal to the number of transmit antennas. Consequently, the number of DL spatial beams which can be exploited is limited by the number of OAs at the MS side . Such circumstance resembles a spatial DoF for the selection of a subset of transmit SAs for DL transmission, which can be jointly optimized in a cross-layer fashion. It is worth mentioning that the time and frequency DoFs (e.g. frequency channel dependent scheduling and frequency domain link adaptation) are not considered in this thesis.

Note that according to the fourth assumption in section 1.4, it is assumed that BD algorithm can only and completely eliminate intracell CCI (interference caused by the same-cell transmitters). However, the system is still limited by intercell CCI (interference caused by the other-cell transmitters). Also, it is assumed that the intercell CCI dominates thermal noise. Therefore, throughout this chapter, wherever the term interference is mentioned, it refers to intercell CCI originated from transmitters in the adjacent cells.

4.3 Interference-aware metric for downlink optimization

In order to address the previously mentioned questions, it is suggested to exploit the channel reciprocity in TDD to jointly utilize the available DoFs for maximizing system throughput. In light of the above, the novel interference-weighted feedback concept is proposed to be applied on the UL CCS pilots. The first major contribution of this thesis is the development of the modified pilots, termed as UL IWCS pilots, which are proposed to replace the UL CCS pilots. In particular, the CCS pilots are modified to become IWCS pilots by weighting (dividing) the UL CCS pilots by the magnitude of the intercell CCI received at each MS. Afterwards, the UL IWCS pilots are utilized at the BS to extract the CSI plus the level of the intercell CCI experienced by all active MSs. Thereby, the DL SINR at each active MS is implicitly signalled to the respective BS. The key idea of applying the interference-weighting concept on the CCS pilots for a SISO case is depicted in Fig. 4.1.

Consider an UL CCS transmission of a SDMA cellular interference-limited scenario with a BS equipped with N_{BS} SAs and N_{U} active users, each equipped with N_{MS} OAs. A narrowband flat fading channel is assumed, *i.e.*, a frequency subcarrier if OFDMA or SC-SDMA is used as envisaged for in LTE-advanced. The channel transfer matrix from the uth MS is given by
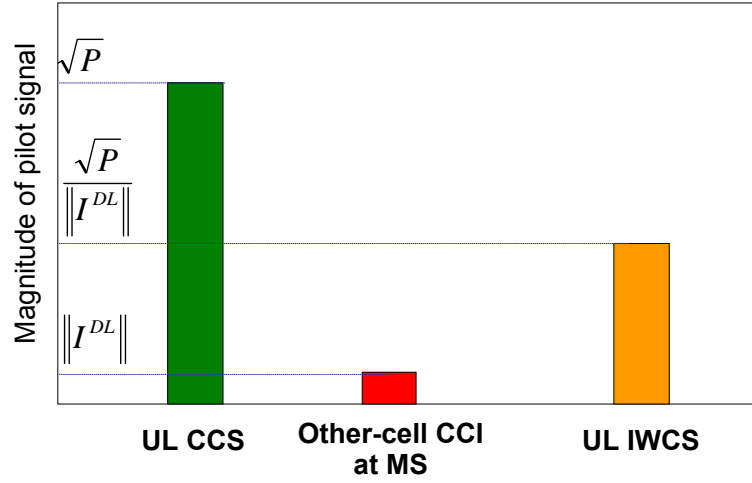
Figure 4.1: *Interference-weighting concept applied on pilot signal for a SISO case*

a complex matrix $\mathbf{H}_u \in \mathbb{C}^{N_{\mathrm{BS}} \times N_{\mathrm{MS}}}$, where $h_u^{(j,i)}$ denotes the channel fading coefficient from the ith transmit OA of the uth MS to the jth receiving SA at the BS. We assume that both the BS and MSs experience sufficient local scattering. Therefore, both real and imaginary parts of the entries of $\mathbf{H}_u$ are samples of a zero-mean Gaussian distribution. Hence, the conventional channel sounding MS-to-BS pilots transmission can be modeled as follows:

$$\mathbf{y}_u(t) = \mathbf{H}_u(t)\mathbf{x}_u(t) + \mathbf{n}(t) \tag{4.1}$$

where t is the time index. The predetermined pilot signal $\mathbf{x}_u(t)$ is N_{MS}-dimensional vector; the received signal $\mathbf{y}_u(t)$ is N_{BS}-dimensional vector; $\mathbf{n}(t)$ is the noise vector whose elements are the i.i.d. complex Gaussian noise random variables. conventional channel sounding pilots can be used to estimate two metrics: distance-dependent link gain (link budget), and the multipath fading channel coefficients (small-scale fading). By weighting (4.1) by the intercell CCI experienced by user u in the downlink, the IWCS transmission can be written as follows:

$$\mathbf{y}_u(t) = \frac{\mathbf{H}_u(t)\mathbf{x}_u(t)}{\|I_u^{\mathrm{DL}}(t-1)\|} + \mathbf{n}(t) \tag{4.2}$$

where $\|I_u^{\mathrm{DL}}(t-1)\|$ is the amplitude of the intercell CCI experienced by u^{th} MS at $(t-1)$ time interval. Consequently, the interference-weighting concept enables the sounding pilots to be used by the BS to obtain the DL interference-aware-metric $\mathbf{O}_u^{\mathrm{DL-IAM}}(t) \in \mathbb{C}^{N_{\mathrm{BS}} \times N_{\mathrm{MS}}}$ which

can be formulated as follows

$$\mathbf{O}_u^{\mathrm{DL-IAM}}(t) = \frac{\mathbf{H}_u(t)}{\|I_u^{\mathrm{DL}}(t-1)\|} \tag{4.3}$$

From information theory point of view, this metric (which can be considered as the square root of the instantaneous MIMO DL SINR) provides better feedback information compared to the CCS case. Hence, the DL joint user scheduling and transmit SA selection can be improved; as the DL interference-aware-metric can simply be used to obtain the SINR at the user side. Alternatively, quantized SINR can be fed back via the direct feedback method, but this requires transmission resources and longer time (potentially causing outdated feedback).

4.3.1 Interference estimation

From practical point of view, the CCI experienced by an entity can be estimated by allowing the entity to sense the channel when no intended transmission is taking place. For instance, the CCI sensing period can be set for an active MS to be between the end of the DL period and the beginning of the switching time (DL to UL). Then, the MS can quantize the sensed CCI during the switching time period. After that, a pilot weighted by the quantized CCI can be transmitted during the subsequent UL period. Optimizing the duration and insertion of the CCI sensing period and the quantization details of the sensed CCI are subject to future investigation.

4.3.2 Optimization methodology

The general approach used in this thesis to find the optimal solution is the brute-force search. As in the example illustrated in Fig. 4.2, each BS equipped with 4 SAs will select 2 MSs each equipped with 2 OAs to access its spatial resources. Clearly, each MS experiences independent levels of intercell CCI, and is subject to independent channel conditions on the desired link. For instance, the BS in cell 1 can schedule 2 users out of 3 possible candidates. For any active user, a BS can assign 2 out of 4 SAs to establish communication links. Using combinatorial basics, the BS has $\binom{3}{2}\binom{4}{2} = 18$ possible options to select antennas and user pairs in the given example.

The procedure followed to extract the optimization metrics provided by IWCS pilots is illustrated in the example depicted in Fig. 4.3 which is based on the example of Fig. 4.2. Basically,
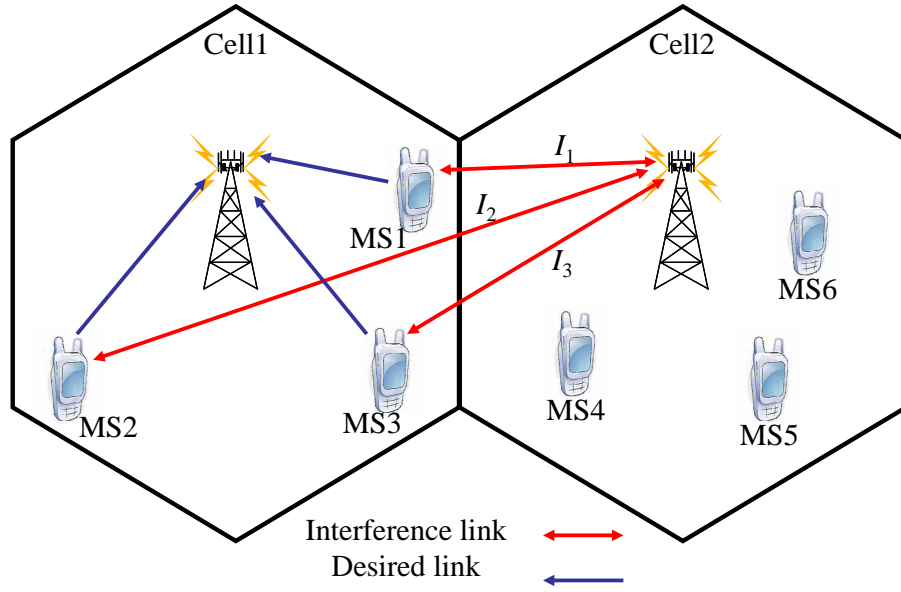
Figure 4.2: *Interference-limited multiuser MIMO system where each BS is equipped with 4 antennas, each MS is equipped with 2 antennas.*

Figure 4.3: *Interference-limited virtual MU-MIMO matrix for the example illustrated in Fig. 4.2.*

each way in which the BS can distribute the 4 SAs among 2 out of 3 users forms a possible solution. From Fig. 4.3, two arbitrary solutions are highlighted by shading them with squares of different colors and different styles for the borderline. By considering the solution shaded by blue squares of solid borderline, it can be seen that MS1 is allocated the first two SAs, while MS3 is allocated the last two antennas. Clearly, it can be seen that each SA allocation forms a (2×2) square matrix containing the coefficients of the optimization metric.

The next step is to obtain the eigenvalues of each square matrix via SVD. Afterwards, the eigenvalues of each group of selected users are summed. Finally, the summation of eigenvalues will be used to find the optimum solution among all possible solutions according to the different scheduling criteria. To examine all possible solutions, two approaches are considered: exhaustive search (ES) and HA. The details of the two searching approaches are discussed later in this chapter.

4.4 Link-protection-aware metric for uplink and downlink optimization

The main purpose of this section is to propose a method to accommodate the IWCS pilots to suit UL optimization. Since the amplitude of CCI experienced at the BS $\|I_j^{\mathrm{UL}}(t-1)\|$ (referred to as UL interference) where ($j \in 1, ..., N_{\mathrm{BS}}$) is different from the CCI experienced at the MS $\|I_u^{\mathrm{DL}}(t-1)\|$, the DL interference-aware-metric in (4.3) is not suitable for UL optimization. In order to use the IWCS pilots for UL optimization, it is proposed that the BS weights each row of the metric defined in (4.3) by the received interference at the associated SA $\|I_j^{\mathrm{UL}}(t-1)\|$ at the BS, which is assumed to be known at the BS side. Thus, the new optimization metric, referred to as link-protection-aware-metric, $\mathbf{O}_u^{\mathrm{LPAM}}(t) \in \mathbb{C}^{N_{\mathrm{BS}} \times N_{\mathrm{MS}}}$ can be formulated as follows:

$$\mathbf{O}_u^{\mathrm{LPAM}}(t) = \frac{\mathbf{H}_u^{(j)}(t)}{\|I_u^{\mathrm{DL}}(t-1)\| \|I_j^{\mathrm{UL}}(t-1)\|} \tag{4.4}$$

where $\mathbf{H}_u^{(j)}(t)$ is the jth vector in $\mathbf{H}_u(t)$.

Basically, this metric allows the BS to decide which subset of receiving antennas to use, and which users can beneficially be grouped together. In particular, the BS can use this metric to jointly select a subset of SAs experiencing favorable channel conditions and low intercell CCI to receive from a subset of users causing low intercell CCI to the neighboring cells. Since

the link-protection-aware-metric is inversely proportional to $\|I_u^{\mathrm{DL}}(t-1)\|$, a MS experiencing low interference level has higher chances to be selected. Due to channel reciprocity, a user that receives little interference from a set of users (in Tx mode) in a particular time slot only causes little interference to the same set of users (now in Rx mode) at a different time slot. Therefore, the link-protection-aware-metric decreases the probability of scheduling users that are potential strong interferers. Consequently, this forms an inherent link-protection for the already established links in the neighboring cells, which results in an enhancement in the overall system performance. Similarly, this metric can be used for DL optimization to jointly select a subset of users experiencing favorable channel conditions and low intercell CCI to receive from a subset of SAs causing low intercell CCI to the neighboring cells. Note that the link-protection-aware-metric is simultaneously used to optimize both UL and DL. Hence, the cross-layer scheduling for UL has to be the same as for DL, which reduces the scheduling time.

According to the MIMO literature [26, 27] and as discussed in the previous chapter, if the channel matrix $\mathbf{H}_u$ is known at the BS, then the instantaneous DL MIMO channel capacity of user u using fixed transmit power $\frac{P_t}{N_{\mathrm{MS}}}$ per antenna can be expressed as the sum of capacities of r SISO channels each weighted with power gain λ_{u_i} where $(i \in 1...r)$, r is the rank of the channel, and λ_{u_i} are the eigenvalues of $\mathbf{H}_u \mathbf{H}_u^H$. Assuming interference-limited system, the instantaneous MIMO capacity of user u in (3.10) can be rewritten as follows:

$$C_u = \sum_{i=1}^{r} \log_2(1 + \frac{P_t}{N_{\mathrm{MS}} \times \|I_u^{\mathrm{DL}}\|^2} \lambda_{u_i}) \tag{4.5}$$

By using the system model introduced above and (4.5), the primary objective is to find the optimum way, according to the scheduling criterion in use, in which the BS distribute N_{BS} antennas among $\frac{N_{\mathrm{BS}}}{N_{\mathrm{MS}}}$ spatially separable users out of user population of size N_{U}, where a selected user communicates with exactly N_{MS} SAs at the BS. For instance, in the case of capacity-based scheduling criterion, the optimum solution maximizes the capacity of multiuser MIMO channel at the expense of fairness.

The sample-space population (SP) (the size of the pool containing all possible solutions) of such problem is formulated later in this chapter. Thus, the resulting optimization problem can be written as follows:

$$C_{\max} = \arg\max_{v \in \mathrm{SP}} \sum_{u=1}^{\frac{N_{\mathrm{BS}}}{N_{\mathrm{MS}}}} C_u^v \tag{4.6}$$

where SP is all possible choices of allocating the beams to the members of v, while v represents a possible choice of grouping the scheduled users.

4.4.1 Summary of the optimization metrics

In DL simulations with interference awareness, three cases are compared according to the considered scheduling criteria. In the first case, the scheduler uses only perfect instantaneous measurements of the MIMO multipath fading channel coefficients (ignoring the distance-dependent link-gain). This optimization metric is fair by nature due to the uniform distribution of the users and the i.i.d. distributed fading, and it is referred to as DL blind-metric $\mathbf{O}_u^{\mathrm{DL-BM}}(t)$. In the second case, the scheduler uses instantaneous measurements of the distance-dependent link-gain. In contrast, this metric is greedy by nature because it tends, in most of the cases, to select those users which are closer to the BS, and it is referred to as DL link-gain-aware-metric $\mathbf{O}_u^{\mathrm{DL-LGAM}}(t)$. These two metrics can be obtained by the conventional channel sounding pilots and they provide the BS with no information about DL interference $\|I_u^{\mathrm{DL}}(t-1)\|$. The third case is the DL interference-aware-metric $\mathbf{O}_u^{\mathrm{DL-IAM}}(t)$ defined in (4.3). This metric can only be provided by the IWCS pilots or by explicit signalling.

In DL simulations with link-protection awareness, two cases are compared according to the considered scheduling criteria (section IV summarizes them). Particularly, the DL interference-aware-metric $\mathbf{O}_u^{\mathrm{DL-IAM}}(t)$ is compared against the link-protection-aware-metric $\mathbf{O}_u^{\mathrm{LPAM}}(t)$ defined in (4.4). These two metrics can only be provided by the IWCS pilots or via explicit signalling. Similarly, two cases are examined in UL simulations with link-protection awareness. In the first case, the scheduler uses instantaneous measurements of the CSI of each spatial stream (each row of $\mathbf{H}_u$) divided by the interference level experienced by the associated SA at the BS. This optimization metric, referred as UL interference-aware-metric, $\mathbf{O}_u^{\mathrm{UL-IAM}}(t) \in \mathbb{C}^{N_{\mathrm{BS}} \times N_{\mathrm{MS}}}$ can be written as follows:

$$\mathbf{O}_u^{\mathrm{UL-IAM}}(t) = \frac{\mathbf{H}_u^{(j)}(t)}{\|I_j^{\mathrm{UL}}(t-1)\|} \tag{4.7}$$

where j is the SA index. It is important to mention that this metric can be obtained using UL CCS pilots; since UL interference $\|I_j^{\mathrm{UL}}(t-1)\|$ is available at the BS side without feedback. The second case is the link-protection-aware-metric defined in (4.4).

4.4.2 Numerical example
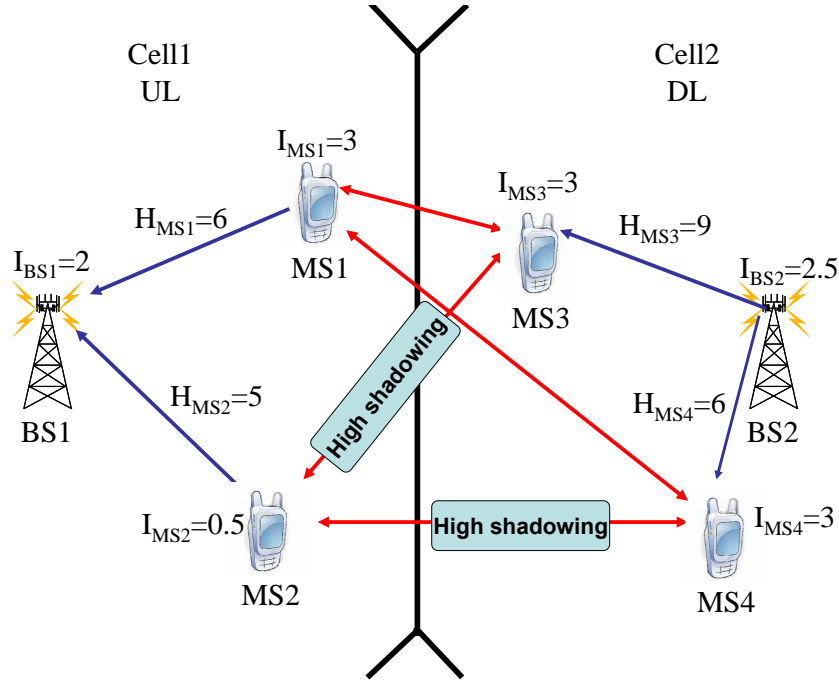
Figure 4.4: *Example of interference-limited 2-cell scenario with which the basic working principle of the link-protection-aware-metric is illustrated.*

To show the link-protection feature of the new metric defined in (4.4), a simple example is presented in Fig. 4.4. In this example, the arbitrary numbers quantifying the gain of each link and the interference experienced by each entity are used to estimate the achievable capacity using (4.5). It is assumed that cell 2 has an established DL transmission with MS3 and the argument of the current achievable DL capacity is $\frac{H_{MS3}}{I_{MS3}} = \frac{9}{3}$. Meanwhile, the BS in cell 1 attempts to select between MS1 and MS2 for UL transmission. If BS1 uses the UL interference-aware-metric, MS1 is scheduled for UL; $\frac{H_{MS1}}{I_{BS1}} = \frac{6}{2} > \frac{H_{MS2}}{I_{BS1}} = \frac{5}{2}$. Hence, the argument of the achievable UL capacity is $\frac{H_{MS1}}{I_{BS1}} = \frac{6}{2}$. As a result, it is assumed that the interference at MS3 increases to $I_{MS3} = 4.5$ due to the low shadowing conditions between MS3 and MS1. This reduces the argument of the current achievable DL capacity in cell 2 to $\frac{9}{4.5}$. Thus, the arguments of the achievable system capacity are $\frac{6}{2}$ and $\frac{9}{4.5}$.

On the other hand, if BS1 uses the link-protection-aware-metric, MS2 is scheduled for UL; $\frac{H_{MS1}}{I_{MS1} \times I_{BS1}} = \frac{6}{3 \times 2} < \frac{H_{MS2}}{I_{MS2} \times I_{BS1}} = \frac{5}{0.5 \times 2}$. Hence, the argument of the achievable UL capacity is $\frac{H_{MS1}}{I_{BS1}} = \frac{5}{2}$. Consequently, the interference at MS3 does not change (due to the high shadowing

between MS2 and MS3), and therefore, the arguments of the achievable cell capacity are $\frac{5}{2}$ and $\frac{9}{3}$ for cell 1 and cell 2, respectively. As a summary, in the first case the sum of the arguments of the cell capacity is 5 whereas in the second case the sum is 5.5. Clearly, it can be seen from this example that the link-protection-aware-metric used in the second case improves the overall spectral efficiency.

It is important to note that the usability of the optimization metrics enabled by the IWCS pilots is not limited to this numerical example. Generally, The IWCS concept is applicable for any closed-loop TDD propagation scenario where the performance is limited by the other-cell CCI.

4.5 Heuristic algorithms for computational complexity reduction

4.5.1 Introduction

In the results section, the first set of DL simulation results (Fig. 4.8 and Fig. 4.9) are obtained using the ES approach, where the scheduler broadly searches over all possible solutions, which is extremely costly from a practical standpoint. Therefore, in this section two heuristic algorithms are proposed to reduce the involved complexity in obtaining the rest of the simulation results.

4.5.2 Exhaustive search mathematical model

The complexity of exhaustive search approach for scheduling optimization of SDMA system depends on the total number of users N_{U}, the number of SAs at the BS N_{BS}, and the number of antennas at each MS N_{MS}. The search burden for the scheduler is equivalent to the SP size. Using combinatorial fundamentals, (4.8) and (4.9) can be obtained. It can be seen from (4.9) that the multiuser diversity plays significant role when $N_{\mathrm{U}} > \frac{N_{\mathrm{BS}}}{N_{\mathrm{MS}}}$; due the fact that not all users can be scheduled.

If $N_{\mathrm{U}} \leq \frac{N_{\mathrm{BS}}}{N_{\mathrm{MS}}}$

$$\mathrm{SP} = \frac{N_{\mathrm{BS}}!}{\underbrace{\left((N_{\mathrm{MS}}!)^{N_{\mathrm{U}}} \, (N_{\mathrm{BS}} - N_{\mathrm{U}} N_{\mathrm{MS}})! \right)}_{\text{SDMA DoF}}}; \tag{4.8}$$

if $N_\mathrm{U} > \frac{N_\mathrm{BS}}{N_\mathrm{MS}}$

$$\mathrm{SP} = \underbrace{\frac{N_\mathrm{U}!}{\left(\left(\frac{N_\mathrm{BS}}{N_\mathrm{MS}}\right)! \left(N_\mathrm{U} - \frac{N_\mathrm{BS}}{N_\mathrm{MS}}\right)!\right)}}_{\text{Multiuser DoF}} \underbrace{\frac{N_\mathrm{BS}!}{(N_\mathrm{MS}!)^{\left(\frac{N_\mathrm{BS}}{N_\mathrm{MS}}\right)}}}_{\text{SDMA DoF}}. \tag{4.9}$$

It is important to mention that (4.8) and (4.9) are applicable only for scenarios in which N_BS is multiple of N_MS. To gain insight into the influence of each dimension of the DoFs on the SP, Fig. 4.5, Fig. 4.6(a), and Fig. 4.6(b) are obtained while setting N_MS to 2. By comparing Fig.
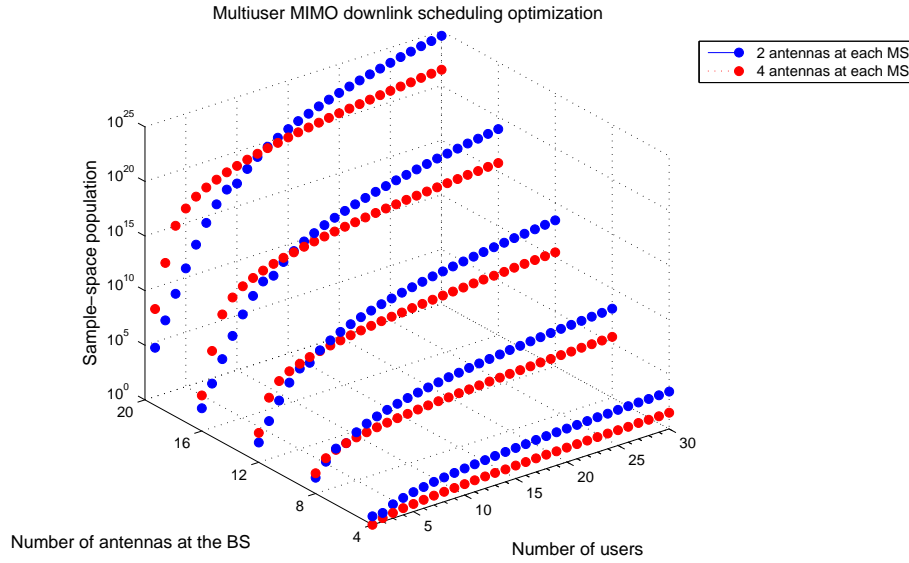
Figure 4.5: *The search complexity versus the number of SAs at the BS and the number of users, assuming 2 and 4 antennas at each MS*

4.6(a) with Fig. 4.6(b), it can be seen that SP grows polynomially with the number of users, and exponentially with the number of antennas at the BS [127]. Clearly, the ES approach is computationally expensive for large number of users and antennas, which prevents finding the optimum solution within reasonable time.

4.5.3 Proposed heuristic algorithms

In order to maintain practical optimization, two approaches are devised to significantly reduce the computational complexity of finding a solution approaching the optimum solution. The first is referred to as the interference-based user elimination approach while the second is AoA-based sectorization approach. The former aims to reduce SP by suppressing those users exposed
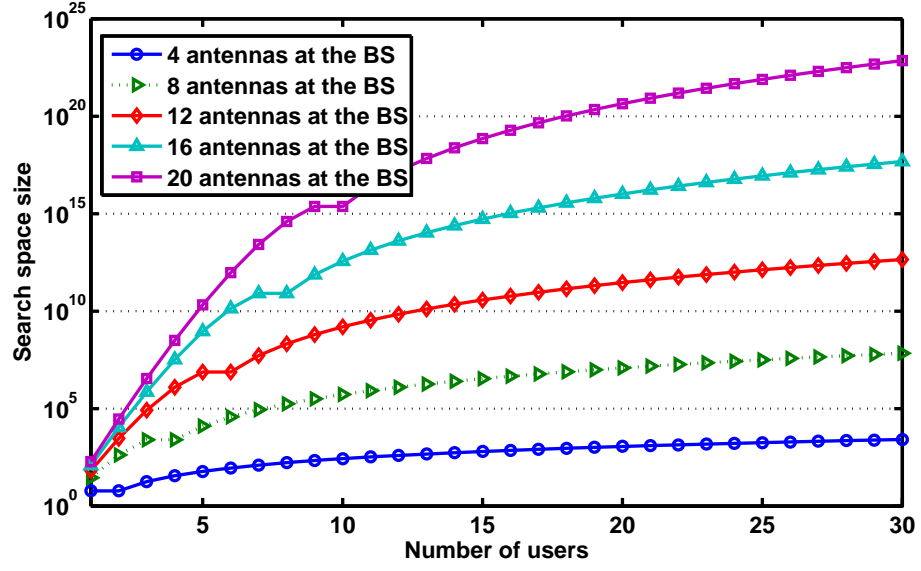
(a) The search complexity versus the number of users
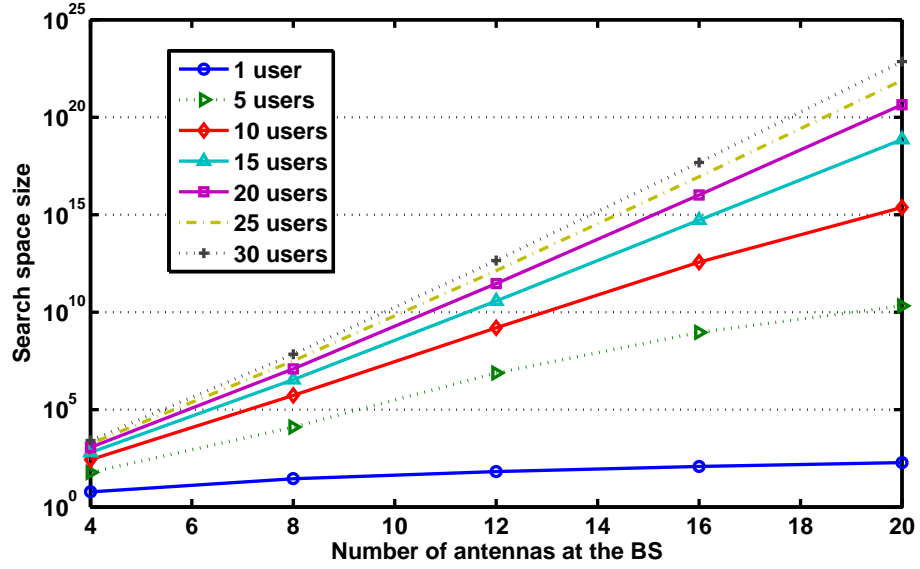
(b) The search complexity versus the number of SAs at the BS

Figure 4.6: *Cross sectional plots along each dimension of SP assuming 2 antennas at each MS*

to an interference level greater than a predetermined interference threshold. The latter converts the CoI optimization problem into smaller optimization problems, which can be optimized simultaneously. This can be done by sectorizing the cell based on the AoA of the uplink sounding channel into several sectors. Then the antennas at the BS are distributed among these sectors according to the user density of each sector. Therefore, by sectorizing the coverage space of the CoI into multiple sectors, the original SP of the CoI will be reduced significantly into smaller SPs of parallel per-sector optimization problems.

Numerical examples

To show the mechanism of the HA approach, let us consider a cell with 28 users, each equipped with 4 antennas, and the BS equipped with 16 antennas. According to (4.9), the scheduler has to broadly search through approximately 3.027×10^9 cases to find the optimum case. By applying the interference based user elimination approach, let us assume that 8 users have been found to be exposed to severe interference levels. Similarly, assume that the cell can be equally divided into four sectors with the same user density. According to the proposed HAs, the original optimization problem becomes four identical sector optimization problems. Hence, each sector has 4 associated antennas at the BS, and $\frac{28-8}{4} = 5$ admissible users, each equipped with 4 antennas. Since only one user can be supported per sector, the scheduler has to search through 5 cases per sector, which can be done in parallel for all sectors.

To show the effect of the sectorization and the number of antennas at the MS, another example is illustrated. In this example, a cell with 6 users, each equipped with 2 antennas, and the BS equipped with 12 antennas, is considered. Following the same procedure as in the previous example, assume that all users are admissible, and that the cell can be equally sectorized into only 2 sectors with the same user density. Thus, each sector has 6 associated antennas at the BS, and 3 users, each equipped with 2 antennas. According to (4.8), the original SP, that approximately equals 3.992×10^7, will be converted into 2 identical sector optimization problems, each with SP equals 120. It is worth noting in this example that the multiuser diversity has not been exploited, and a simple sectorization has been applied. However, the scheduler search burden is significantly reduced, and thus the practicability of the proposed interference-aware antenna selection and scheduling algorithm is greatly enhanced.

4.6 Scheduling criteria

Scheduling criteria can be generally classified into two groups: greedy and fair. In this thesis, the considered optimization metrics are tested using three scheduling criteria. Specifically, one greedy criterion, named maximum capacity (MC) [29, 128], and two fair criteria, named proportional-fair (PF) [50, 129] and score-based (SB) [130] approach are considered.

4.6.1 Maximum capacity scheduling criterion

MC criteria always assigns the antennas to those users with the highest eigenvalue sum, hence, it is efficient in terms of overall throughput but may look oppressive for low SINR users, typically located far from the BS (cell-edge users).

The achievable capacity according to MC scheduling criterion can be formulated as follows:

$$C^{\mathrm{MC}} = \arg\max_{v \subset \mathrm{SP}}\{C_v\} \tag{4.10}$$

Where C^{MC} is the achievable capacity using MC criterion, C_v is the instantaneous capacity of the vth option.

4.6.2 Proportional fair scheduling criterion

PF criterion seeks to assign the antennas to those users with highest eigenvalue sum relative to their current mean eigenvalue sum, which makes PF scheduler realize a reasonable trade-off between throughput efficiency and fairness.

The achievable capacity according to PF scheduling criterion can be formulated as follows:

$$C^{\mathrm{PF}} = \arg\max_{v \subset \mathrm{SP}}\left\{\frac{C_v}{\overline{C}_v}\right\} \tag{4.11}$$

Where C^{PF} is the achievable capacity using PF criterion, C_v and $\overline{C}_v$ are the instantaneous and average capacity of the vth option, respectively.

4.6.3   Score-based scheduling criterion

SB scheduler assigns the antennas to those users with the best scores. In the SB scheduling case, the score corresponds to the rank of the current eigenvalue sum among the past values observed over a window of a particular size [130].

The achievable capacity according to SB scheduling criterion can be formulated as follows:

$$C^{\text{SB}} = \underset{v \subset \text{SP}}{\arg\min} \{S_v\} \tag{4.12}$$

Where C^{SB} is the achievable capacity using SB criterion, and S_v is the rank of the instantaneous capacity of the vth option among the past values observed over a window in time of size W. The motivation behind selecting the SB scheduling criterion is because it offers a reasonable trade-off between efficiency and fairness. This feature is also customizable by changing the window size W. More specifically, setting the window size equal to 1 makes the SB criterion similar to MC criterion in terms of efficiency. Having large size for the window makes the SB criterion approaches the PF criterion in terms of fairness.

Due to the large size of the SP and the inherent integer nature of the rank in the SB criterion, several solutions can score the best rank (the first position). Therefore, out of those solutions satisfying the best rank condition, only one solution should be selected. In order to find a unique solution, MC criterion is chosen to be applied on the subset of solutions satisfying the best rank condition. More specifically, whenever the SB criterion is used in this research, the MC criterion is applied on those solutions with the first rank to select single solution. For example, consider a scenario where the SP size is 60, and assume that the current capacity values of 3 solutions are in the first position. Hence, according to the SB policy 3 solutions are qualified. Assume that the current capacity values for these solutions are 4, 7, 9 bps/HZ. By applying the MC policy on this subset of solutions, the one achieves 9 bps/Hz is selected. Throughout this thesis, wherever the SB criterion is mentioned, it means that a hybrid version of both SB and MC criteria is applied. Due to the inherent greediness of MC criterion, the hybrid version of the SB policy tends to show greedy behavior. This greedy behavior increases as the SP size is increased while keeping the window size W constant, as will be shown in the simulation results of the fairness assessment.

4.6.4   Fairness of scheduling criteria

Fairness is an important consideration in most of performance studies associated with resources sharing. In multiuser scheduling literature, typical indices of fairness such as variance, coefficient of variation (CoV), max-min ratio, and Jains fairness index [131], are used to compare the fairness of the considered scheduling criteria. According to [131], it has been shown that variance can not provide properties such as metric independence and boundedness (the index should be bounded). The max-min ratio also is unable to provide continuity, which says the index should be continuous. The difference between CoV and Jains fairness index is that the amount of CoV is between 0 and infinity while the amount of Jains fairness index is between 0 and 1. In this thesis, the CoV of the served user distance is used for a comparison. CoV is defined as the ratio of the standard deviation to a mean [132, 133], where a low CoV indicates a better fairness performance. Let d_{served} be a random variable represents the served user distance with mean value μ_{served} and standard deviation σ_{served}. Then the CoV fairness index considered in this thesis can be formulated as follows:

$$\text{CoV}(d_{\text{served}}) = \frac{\sigma_{\text{served}}}{\mu_{\text{served}}} \tag{4.13}$$

4.7 Simulation results and discussion

In this section, the performance of the different optimization metrics is assessed using the cumulative distribution function (cdf) of per-user capacity and cell capacity for both UL and DL. The per-user capacity, in the simulations of this work, is the 2×2 spatial multiplexing MIMO capacity which can be calculated using (4.5). The cell capacity is the sum capacity of the group of scheduled users. In order to shed some light on fairness of the considered optimization metrics, the cdf of the scheduled (served) user distance to the BS is obtained for all considered scheduling criteria. Finally, the relationship between the scheduling criteria and the considered optimization metrics is explored by examining the CoV of the served user distance formulated in 4.13.

A two-tier cellular platform consisting of hexagonal cells is used in the simulation. In each cell, the BS and MSs are equipped with (6 or 8) and 2 antennas, respectively. Using the parameters given in Table 4.1, the 19-cell cellular TDD system with uniform user distribution, as shown in Fig. 4.7, is simulated via Monte Carlo method. The channel matrix of uth user $\mathbf{H}_u$ is a zero-mean i.i.d. complex Gaussian random matrix. The system level performance evaluation is based on both central cell and wrap-around techniques. The DL and UL performances are
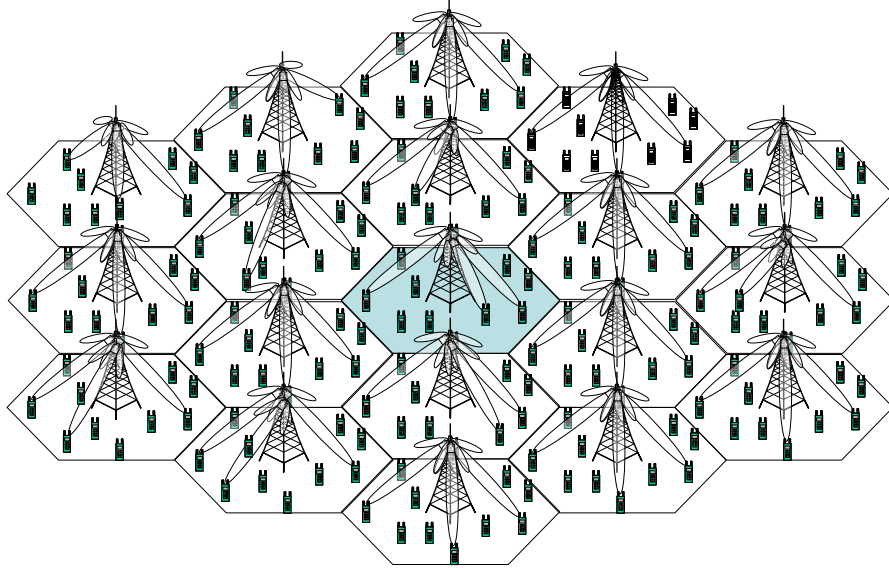
Figure 4.7: *Interference-limited multiuser MIMO system implementing orthogonal space division multiple access*

analyzed for asynchronous cells, where the two possible link-directions (UL or DL) occur with

equal probability and independently from each other. All entities (BSs and MSs) in the system use fixed transmit power of 30 dBm.

Channel propagation environment	Suburban micro cell [72]
BS-to-BS distance	300-500 m
Number of interfering tiers	2
Pilot Tx power	30 dBm
Number of users	300-1000
Carrier frequency	2 GHz
Minimum distance between MS and BS	35 m
Number of antennas at BS	6-8
Number of antennas at MS	2
log-normal shadowing variance, σ_S^2	8 dB
Correlation distance of shadowing	50 m (as in UMTS 30.03)
Path loss model (dB)	$31.5 + 35 \log 10(d)$ [72]

Table 4.1: *Simulation parameters*

In the wrap-around technique, the multicell layout is folded such that cells on the right side of the network are connected with cells on the left side and, similarly, cells in the upper part of the network get connected to cells in the lower part. The created area may be seen as borderless, but with a finite surface, and it may be visualized as a torus. The wrap-around technique is suitable for both downlink and uplink simulations. One of the main advantages of wrap-around technique is that the decision taken by a scheduler in a particular cell influences the scheduling behavior in the adjacent cells. Such an observation cannot be collected using the central cell technique. Another advantage compared to the central cell technique is that simulation data can be collected from all cells, which may reduce the required simulation time to collect sufficient statistics.

4.7.1 Downlink performance with interference awareness

The results in this subsection are only obtained for the CoI (central cell simulation technique) via ES approach. In order to avoid huge SP size, the BS is assumed to be equipped with 6 SAs, hence only 3 users are scheduled over the same time-frequency resource. The results in Fig.
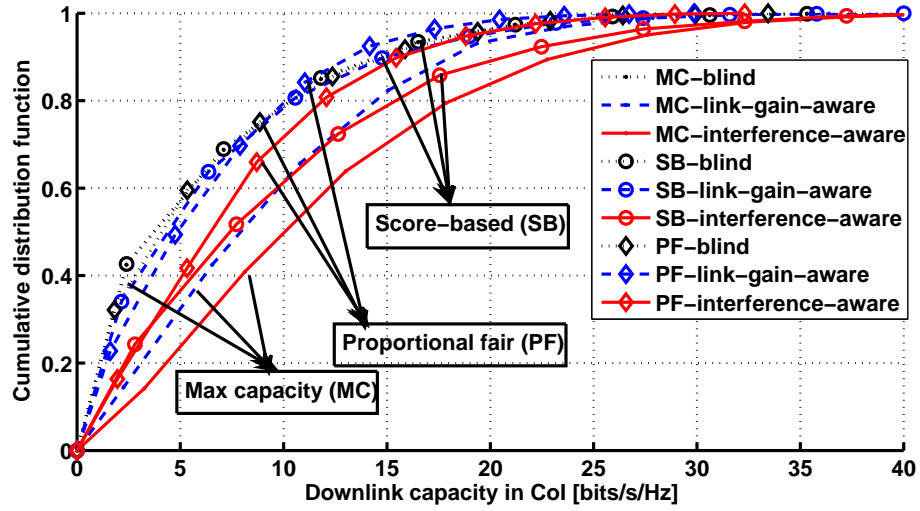
(a) Cell performance
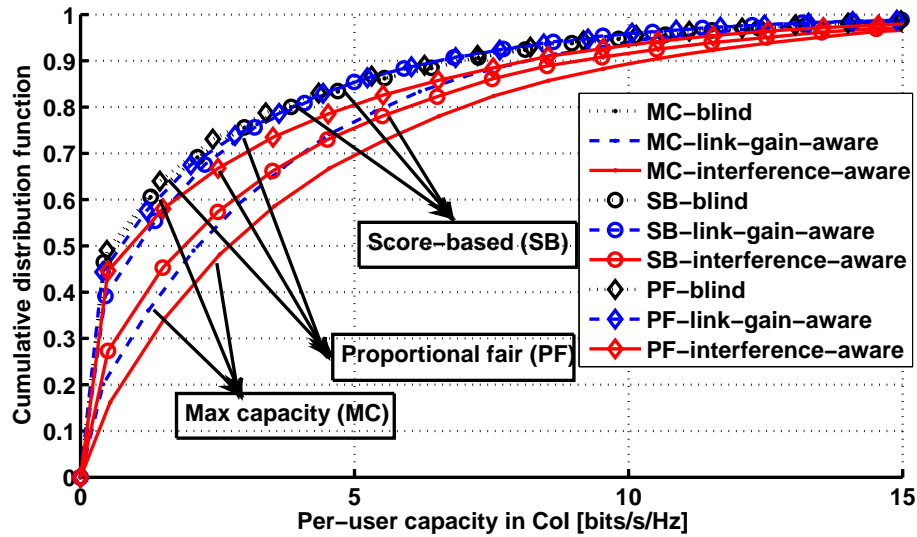
(b) User performance

Figure 4.8: *Downlink performance comparison among the DL interference-aware and both blind and link-gain-aware metrics using ES approach*

4.8(a) show that the cell throughput can be significantly enhanced if knowledge of interference is taken into account in the antenna selection and MIMO user scheduling process. For example it can be seen from Fig. 4.8(a), for the MC criterion (unmarked curves), that the median of

the DL capacity using the DL interference-aware-metric is 10 bps/Hz while it is 7.5 and 4 bps/Hz for the link-gain-aware-metric and the blind-metric, respectively. As expected from the greedy characteristics of the link-gain-aware-metric, it can be seen that it outperforms the blind-metric. The greediness of these metrics will be further discussed later when discussing fairness. Similarly, the per-user capacity in the case of the DL interference-aware-metric is substantially improved for all scheduling criteria. From Fig. 4.8(b), for the SB criterion (circle-marked curves), it can be seen that the median of the per-user capacity resulting from the DL interference-aware-metric is 2 bps/Hz while it is 1 and 0.5 bps/Hz for link-gain-aware-metric and the blind-metric, respectively. A summary of the downlink performance with interference awareness using MC, SB, and PF criteria can be found in Table 4.2, Table 4.3, and Table 4.4, respectively.

Optimization metric	Blind	Link-gain-aware	Interference-aware
Median of per-user capacity	0.7	2.5	2.8
The 10th percentile of per-user capacity	0.1	0.35	0.6
Median of cell capacity	4	7.5	10
The 10th percentile of cell capacity	0.5	1.8	2.3

Table 4.2: *Summary of the downlink performance with interference awareness using MC criterion [bps/Hz]*

Optimization metric	Blind	Link-gain-aware	Interference-aware
Median of per-user capacity	0.5	1	2
The 10th percentile of per-user capacity	0.15	0.2	0.3
Median of cell capacity	3.5	4.9	7.5
The 10th percentile of cell capacity	0.8	1	2

Table 4.3: *Summary of the downlink performance with interference awareness using SB criterion [bps/Hz]*

Optimization metric	Blind	Link-gain-aware	Interference-aware
Median of per-user capacity	0.45	0.8	1
The 10th percentile of per-user capacity	0.1	0.11	0.12
Median of cell capacity	4.2	5	6.5
The 10th percentile of cell capacity	0.85	1	1.95

Table 4.4: *Summary of the downlink performance with interference awareness using PF criterion [bps/Hz]*

The results in Fig. 4.9 are obtained for the case of cell radius of 300 m. It is shown that both

DL interference-aware-metric and link-gain-aware-metric prioritize the users closer to the BS when MC criterion is used. For instance, Fig. 4.9, for the MC criterion (unmarked curves), shows that the median of the served user distance to the BS of the DL interference-aware-metric and the link-gain-aware-metric are 160 m and 140 m, respectively, while it is 190 m for the blind-metric case. Alternatively, when the PF criterion (diamond-marked curves) is used the DL interference-aware-metric shows high level of fairness (its median is 220 m) compared to both blind-metric (its median is 175 m) and link-gain-aware-metric (its median is 210 m).
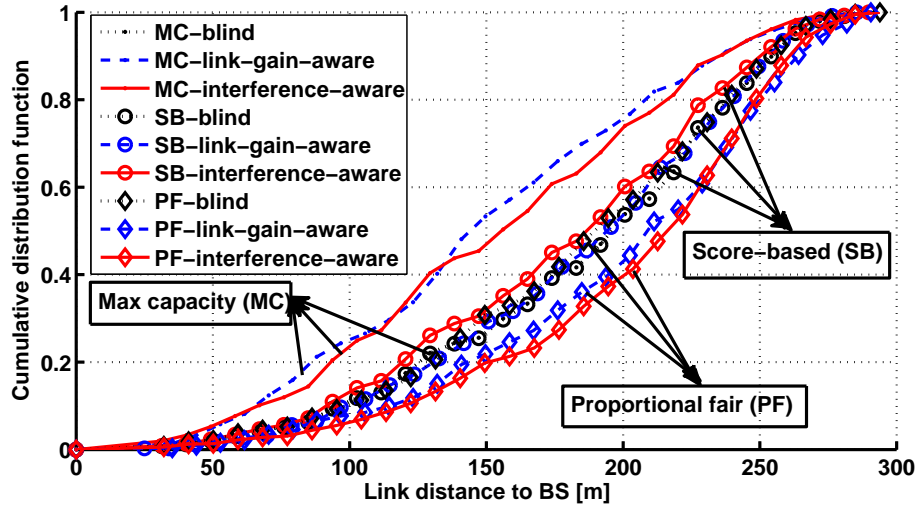
Figure 4.9: *Fairness comparison among the three considered scheduling criteria in terms of the distance between the BS and the scheduled user.*

It is worth noting that the distance associated with the blind-metric is slightly affected by using the SB and the PF criteria. This is expected due to the inherent fairness of this metric which is a consequence of the i.i.d. distributed feature of small-scale fading and the random distribution of the users.

4.7.2 Heuristic algorithms performance

In order to address the efficiency of the HAs, a DL study case has been simulated under the following assumptions: 8 SAs at the BS, 2 antennas at each MS, fixed sectorization is used to equally divide the cell into two sectors, only the best 8 users in terms of the experienced intercell CCI are considered in each cell, and MC is the scheduling criterion. It has been found using simulations that the SP has been reduced from 176400 to 80 on average (depending on the user density per sector). This is achieved at the cost that the median of the achievable capacity using DL interference-aware-metric through the HA approach converges to approximately 90% of the median of the optimum capacity under the ES approach, as seen in Fig. 4.10.
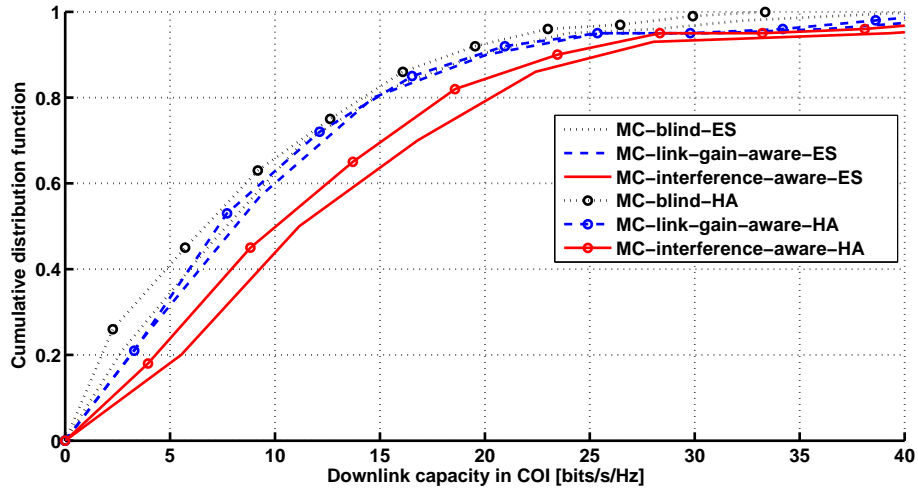
Figure 4.10: *Throughput comparison among the considered metrics in the previous section for the MC criterion via both ES and HA approaches*

Since the ES approach is computationally too expensive, simulation results for larger SP sizes cannot be obtained within reasonable time. Therefore, all the subsequent results are obtained via the HA approach due to its practicability demonstrated in Fig. 4.10. Furthermore, in order to increase the spatial SDMA DoF, the BS is assumed to be equipped with 8 SAs, hence 4 users are scheduled.

4.7.3 Uplink performance with link-protection awareness

From Fig. 4.11(a), for the MC criterion (square-marked curves), it can be seen that the UL median cell capacity using the link-protection-aware-metric is 27 bps/Hz which corresponds

to an enhancement of 12.5% of the UL median cell capacity using the UL interference-aware-metric (24 bps/Hz).
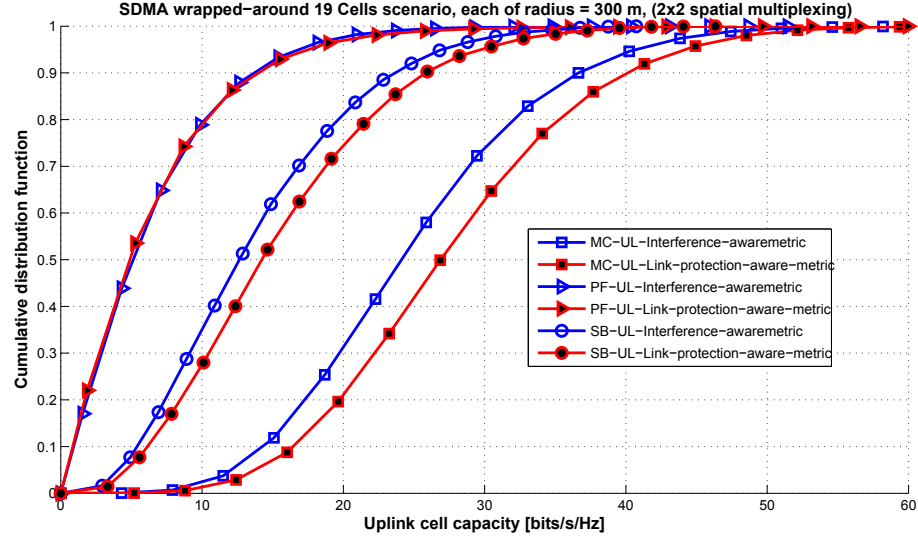
(a) Cell performance
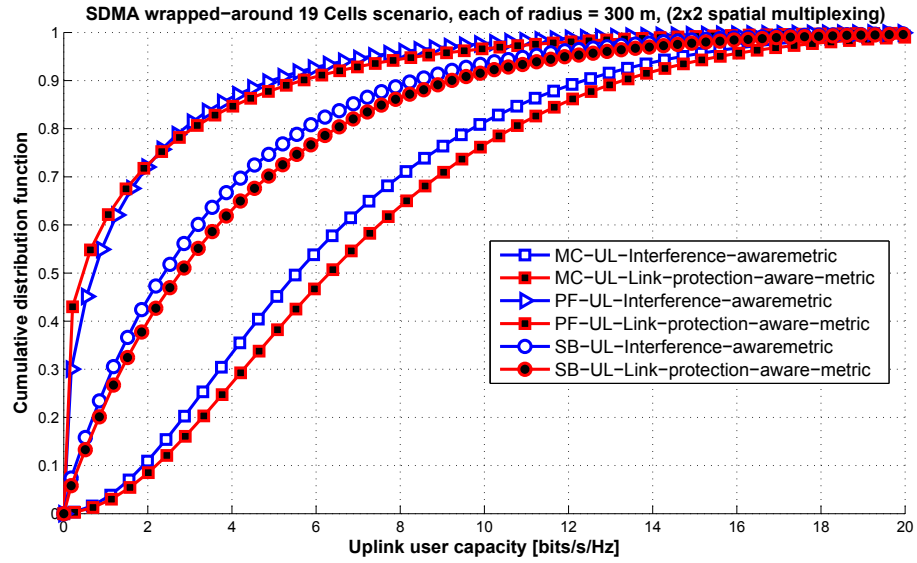
(b) User performance

Figure 4.11: *Uplink performance comparison between the UL interference-aware-metric and the link-protection-aware-metric*

This gain can be attributed to the available knowledge at the scheduler about the users potentially causing high interference to the already established links in the neighboring cells. Hence, the link-protection-aware-metric enables the scheduler to select a group of users experiencing favorable shadowing conditions on the links that contribute to interference, *i.e.*, this effec-

tively results in interference mitigation. The previous observation can be affirmed by noting that the results of the per-user capacity of the link-protection-aware-metric, which outperforms the UL interference-aware-metric for all scheduling criteria considered. For instance, from Fig. 4.11(b), for the SB criterion (circle-marked curves), it can be seen that the median of the per-user capacity resulting from the link-protection-aware-metric is 2.9 bps/Hz while it is 2.5 bps/Hz for the UL interference-aware-metric. However, the PF criterion (triangle-marked curves) does not provide a noticeable improvement due to the inherent fair nature which does not prevent strong interferers from being scheduled.

A summary of the uplink performance with link-protection awareness using MC, SB, and PF criteria can be found in Table 4.5, Table 4.6, and Table 4.7, respectively.

Optimization metric	Interference-aware	Link-protection-aware
Median of per-user capacity	5.7	6.2
The 10$^{\text{th}}$ percentile of per-user capacity	2	2.1
Median of cell capacity	24	26
The 10$^{\text{th}}$ percentile of cell capacity	14.5	16

Table 4.5: *Summary of the uplink performance with link-protection awareness using MC criterion [bps/Hz]*

Optimization metric	Interference-aware	Link-protection-aware
Median of per-user capacity	2.5	3
The 10$^{\text{th}}$ percentile of per-user capacity	0.18	0.21
Median of cell capacity	12.9	14.3
The 10$^{\text{th}}$ percentile of cell capacity	4.9	5.6

Table 4.6: *Summary of the uplink performance with link-protection awareness using SB criterion [bps/Hz]*

Optimization metric	Interference-aware	Link-protection-aware
Median of per-user capacity	0.5	0.8
The 10$^{\text{th}}$ percentile of per-user capacity	0.05	0.05
Median of cell capacity	5	5
The 10$^{\text{th}}$ percentile of cell capacity	1	1

Table 4.7: *Summary of the uplink performance with link-protection awareness using PF criterion [bps/Hz]*

4.7.4 Downlink performance with link-protection awareness

The same analysis carried out in the previous subsection discussing the UL performance is applied for the DL case. From Fig. 4.12(a), for the MC criterion (square-marked curves), it can be seen that the median of the DL capacity using the link-protection-aware-metric is 19 bps/Hz while it is 15 bps/Hz for the DL interference-aware-metric. Similarly, the per-user capacity in the case of the link-protection-aware-metric is improved for all scheduling criteria. From Fig. 4.12(b), for the SB criterion (circle-marked curves), it can be seen that the median of the per-user capacity resulting from the link-protection-aware-metric is 3.5 bps/Hz while it is 1.9 bps/Hz for the DL interference-aware-metric.

Irrespective of the nature of the employed scheduling criterion, the results show that the gain in the UL case is lower compared to the DL. This is due to the fact that the detrimental effect of line-of-sight conditions among BSs degrades the link-protection selectivity in UL. Moreover, in SDMA a user located in a cell causes interference to all beams (and groups of antennas correspondingly) other than the served one. Given that all antenna groups at the BS site are in close proximity, the large-scale fading (log-normal shadowing) on the interference links can, thus, be considered the same. Therefore, the variations among the interference links depend only on the small-scale fading.

On the other hand, the greedy nature of the hybrid SB criterion, explained in section 4.6, allows for the multiuser diversity, offered by the high user density, to be effectively exploited in DL. Furthermore, due to the relatively high variance of the statistics of DL interference, a marginal improvement is achieved using the PF criterion, as it can be seen in Fig. 4.12. However, this gain can only be seen at the high percentiles due to the fair nature of the PF criterion (triangle-marked curves).

A summary of the downlink performance with link-protection awareness using MC, SB, and PF criteria can be found in Table 4.8, Table 4.9, and Table 4.10, respectively.
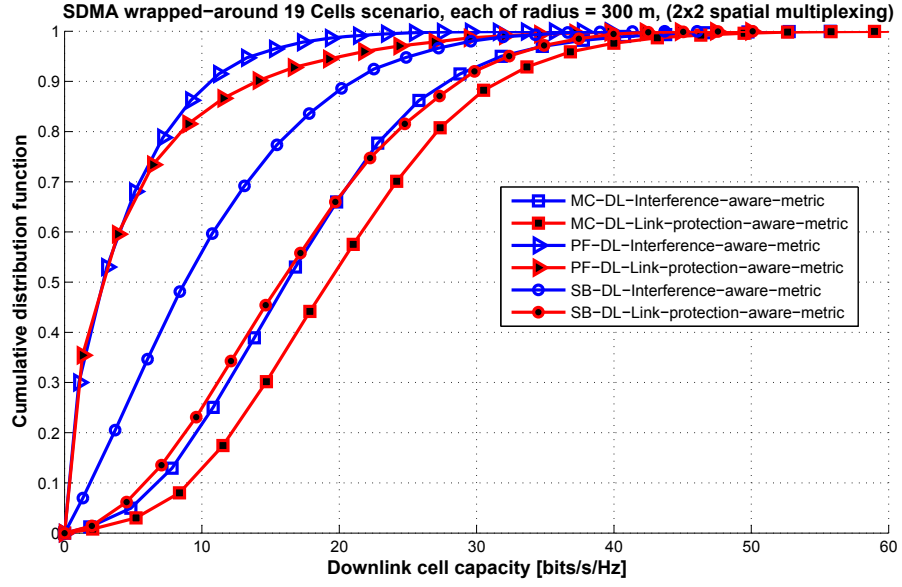
(a) Cell performance
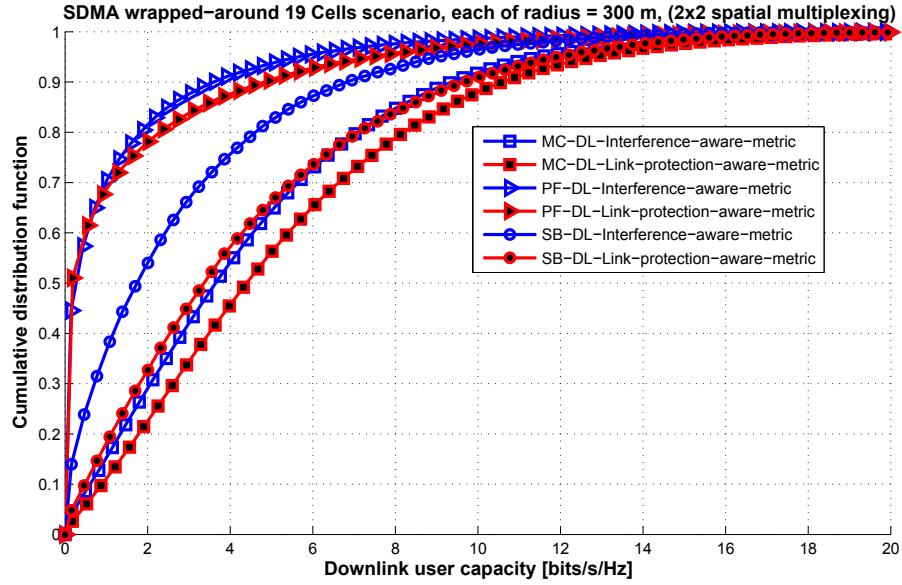
(b) User performance

Figure 4.12: *Downlink performance comparison between the DL interference-aware-metric and the link-protection-aware-metric.*

Optimization metric	Interference-aware	Link-protection-aware
Median of per-user capacity	3.6	4.5
The 10th percentile of per-user capacity	0.6	0.8
Median of cell capacity	16	19
The 10th percentile of cell capacity	7	9

Table 4.8: *Summary of the downlink performance with link-protection awareness using MC criterion [bps/Hz]*

Optimization metric	Interference-aware	Link-protection-aware
Median of per-user capacity	1.8	3.3
The 10th percentile of per-user capacity	0.1	0.5
Median of cell capacity	8	16
The 10th percentile of cell capacity	2	6

Table 4.9: *Summary of the downlink performance with link-protection awareness using SB criterion [bps/Hz]*

Optimization metric	Interference-aware	Link-protection-aware
Median of per-user capacity	0.15	0.15
The 10th percentile of per-user capacity	0.05	0.05
Median of cell capacity	3.5	3.5
The 10th percentile of cell capacity	0.5	0.5

Table 4.10: *Summary of the downlink performance with link-protection awareness using PF criterion [bps/Hz]*

4.7.5 Fairness assessment for uplink and downlink

The fairness performance of the optimization metrics for all scheduling criterion considered are evaluated by the CoV of the served user distance. Particularly, both Fig. 4.13 and Fig. 4.14 depict the CoV of the served user distance versus the user density per cell for both UL and DL, respectively. For each user density 3 groups of bars are obtained according to MC, PF, and SB scheduling criteria, respectively. Each group of bars is composed of 4 bars, which represent the CoV values of the 4 optimization metrics. Both Fig. 4.13 and Fig. 4.14 show that the blind-
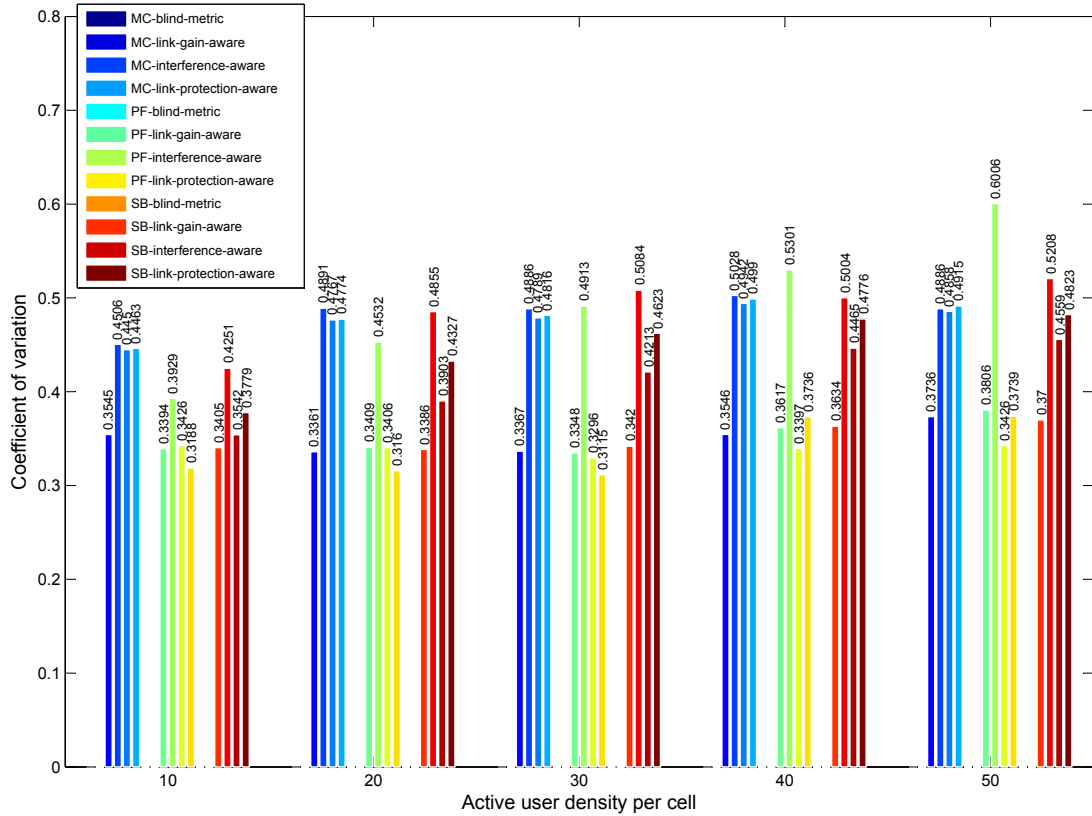
Figure 4.13: *Downlink comparison of the CoV fairness index of the served user distance among all metrics for MC, PF, and SB scheduling criteria*

metric always has low CoV values (the 1st of each group of bars), while link-gain-aware-metric always has high CoV values (the 2nd of each group of bars) regardless the scheduling criterion in use.

On the one hand, it can be seen from both Fig. 4.13 and Fig. 4.14 that using both link-gain-aware-metric and UL/DL interference-aware-metrics (the 3rd and 4th of each group of bars) results in a better fairness performance compared to link-gain-aware-metric case for all

considered scheduling criteria. On the other hand, their CoV values are higher than those associated with the blind-metric for MC and SB scheduling policies. Meanwhile, their fairness indices are lower compared to the blind-metric case when PF criterion is used. According to
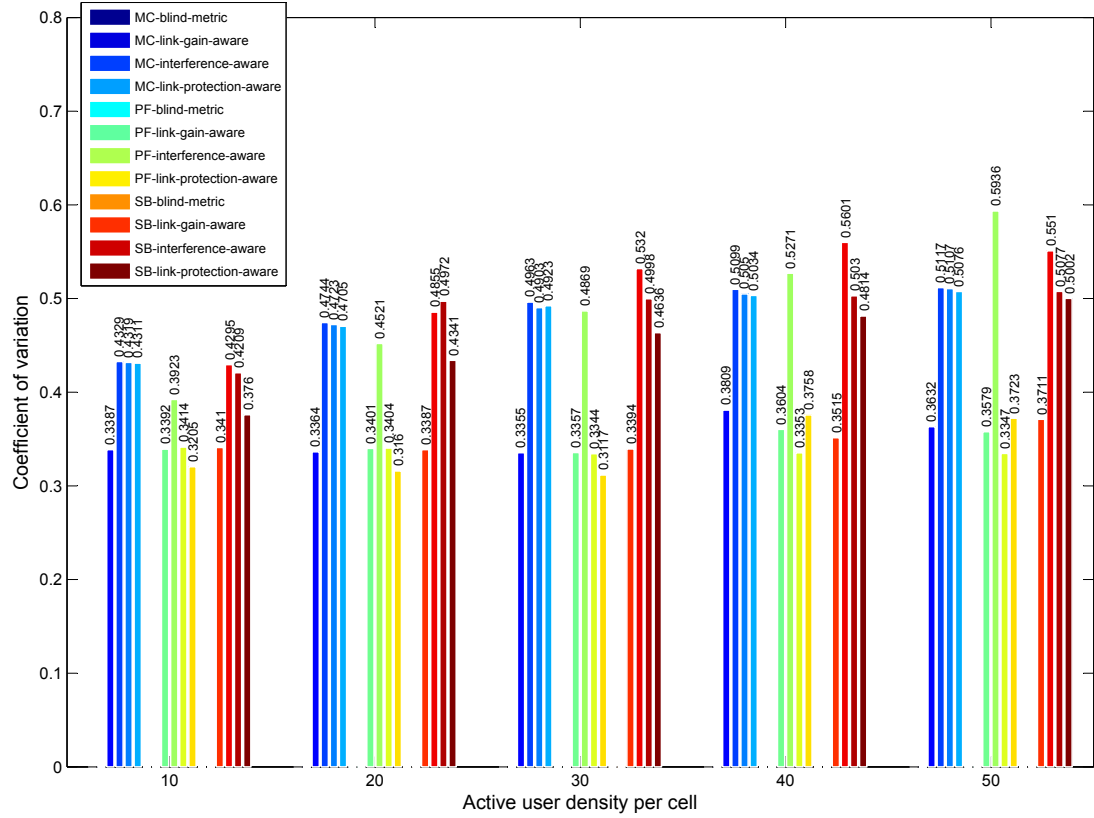
Figure 4.14: *Uplink comparison of the CoV fairness index of the served user distance among all metrics for MC, PF, and SB scheduling criteria*

[130], it was demonstrated that the PF criterion is fair and indeed opportunistic in the ideal case, however, it becomes unfair and unable to fully exploit multiuser diversity in the realistic cases with asymmetric fading statistics and data rate constraints. From the results presented in Fig. 4.13 and Fig. 4.14, such behavior can be observed. In particular, it can be noticed that by increasing the active user density, the PF criterion tends to show higher greediness compared to both MC and SB criteria when the link-gain-aware-metric is used. This behavior can be attributed to the fact that the link-gain-aware-metric accounts for the distance-dependent fading component of the channel, hence, the supported transmission rate of users far from the BS is generally less than that of close users. Therefore, it can be concluded that for high user density, the PF criterion favors close users and therefore tends to show high greediness when the optimization metric accounts for the distance-dependent fading component as in the case of

the link-gain-aware-metric.

In summary, it can be concluded from both Fig. 4.13 and Fig. 4.14 that when MC and SB criteria are used with the link-protection-aware-metric and UL/DL interference-aware-metric (the IWCS-enabled metrics), a slight degradation in the fairness performance is noted compared to the blind-metric case only. For the case of PF scheduling policy, using the IWCS-enabled metrics results in an enhanced fairness performance compared to all CCS-enabled metrics.

4.8 Summary

This chapter briefly discussed the signal model of CCS transmission. Then, the details of the new IWCS-specific modification proposed to be applied on UL CCS was presented (the first major contribution of this thesis). In particular, the novel interference-weighting method enables UL CCS pilots to convey an implicit knowledge of the experienced intercell CCI at the user side to the BS along with CSI. Afterwards, the channel diagonalization-based optimization methodology employing the interference-aware-metric provided by IWCS pilots was discussed. Also, In order to extend the usability of IWCS mechanism to UL optimization, a novel procedure was presented in which the IWCS estimated metrics are further divided by the level of the intercell CCI experienced by each SA at the BS. The resultant metric adds a link-protection awareness to the BS so the probability of selecting users causing harmful intercell CCI towards already exiting links in adjacent cells is reduced.

In order to prepare the reader to the comparative analysis results, a summary of all optimization metrics, enabled by both CCS and IWCS, was presented. Furthermore, the involved computational complexity with such optimization problem was mathematically modeled and two HAs are proposed to reduce it at the cost of negligible loss in overall performance. Additionally, the considered scheduling criteria were reviewed.

Furthermore, this chapter demonstrated that interference-limited SDMA systems with implicit signalling of intercell CCI at both transmit and receive entities, enabled by IWCS, can achieve higher throughput than SDMA systems utilizing CCS pilots. It was shown that a gain at the 10th percentile cell capacity of 150% and 35% has been achieved compared to both blind-metric and link-gain-aware-metric, respectively, for the case of DL interference-aware-metric under maximum capacity criterion. Under score-based criterion, it is shown that using the link-protection-aware-metric maintains a gain at the 10th percentile user capacity of 230% and 15%

77

compared to both downlink and uplink interference-aware-metric, respectively. Furthermore, for the case of maximum capacity, it has been found that the respective gains are 30% and 15%, respectively. However, marginal capacity gains have been obtained for the proportional fair policy which ensures fairness at the expense of throughput efficiency.

Also this chapter highlighted that utilizing the proposed HA significantly reduces the computational complexity to approximately 0.05% of the complexity of the ES approach. This reduction in complexity is achieved at the cost of 8% loss at the 10th percentile cell capacity.

Moreover, the impact of the link-protection-aware-metric and the downlink interference-aware-metric on the fairness of the scheduling criteria has been investigated. The simulation results have shown that the behavior of the scheduling criteria are not affected. On the one hand, using the IWCS enabled optimization metrics results in an enhanced system performance in terms of system throughput at the cost of a slight degradation in the fairness performance compared to the blind-metric for MC and SP criteria. On the other hand, a better fairness performance compared to all CCS enabled optimization metrics is exhibited when PF policy is used.

Finally, note that the study of this chapter is carried out using system level analysis focused on multiuser and spatial diversity techniques for closed-loop SDMA without considering the frequency domain DoF, *i.e.* the diversity offered by the orthogonality of the OFDM subcarriers. Considered as the second major contribution of this thesis, the next chapter will conduct a comparative study between conventional OFDM and a novel OFDM-based modulation technique that exploits the orthogonality of the OFDM subcarriers in a totally radical fashion. Unlike the system level analysis used in this chapter, the next chapter will use link level analysis focused on open-loop single user SISO OFDM. Integrating the analysis of both chapters has not been considered in this thesis and is subject to future work.

5 Chapter

Subcarrier-index modulation OFDM

5.1 Introduction

Generally, OFDM is a method for dividing wideband channel into independent narrowband sub-channels. Then, the sub-channels (subcarriers) are used in parallel to form what so called multicarrier communication, see Fig. 5.1. Multicarrier communication is not a new transmis-
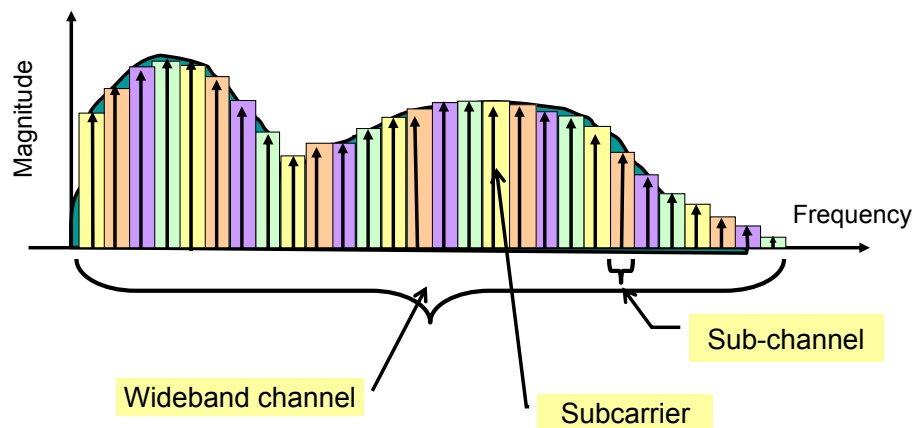
Figure 5.1: *Basic concept of OFDM*

sion method. Most of the fundamental work was done in the 1960s. OFDM is a special case of multicarrier schemes which was firstly patented at Bell Labs in 1966 [134]. Initially only analogue design was proposed, using banks of sinusoidal signal modulators and demodulators (synthesizers) to process the signal for the parallel sub-channels as depicted in Fig. 5.2.

By proposing the discrete Fourier transform (DFT) in 1971 [135] and the fast Fourier transform
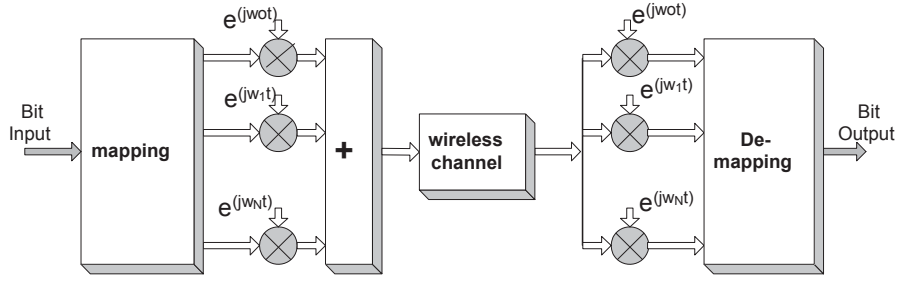
Figure 5.2: *OFDM using synthesizers*

(FFT) in 1980 [136], OFDM implementation become more cost-effective and less complex. Recent standardization bodies have rekindled interest in OFDM [80, 83, 137], especially now
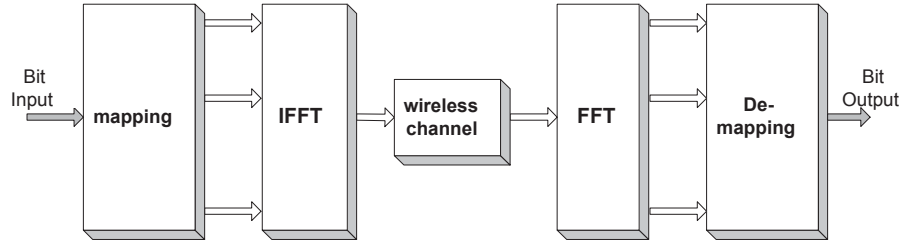
Figure 5.3: *OFDM using FFT*

that better signal processing techniques make it more practical. For example, OFDM has been adopted in several wireless standards such as WIMAX and LTE [19]. OFDM is closely related to plain FDM. It is well known that the key drawback of traditional FDM is that the guard bands waste bandwidth and thus reduce spectral efficiency. In contrast, OFDM selects channel that overlap but do not interfere with each other. Overlapping subcarriers are allowed because the subcarriers are designed so that they are easily distinguished from one another at the receiver side. The ability to separate the subcarrier hinges on a complex mathematical relationship called orthogonality.

OFDM differs from other state-of-the-art encoding techniques such as code division multiplexing (CDM) in its approach. CDM uses complex mathematical transforms to put multiple transmissions onto a single carrier; OFDM encodes a single transmission into multiple subcarriers. The mathematics underlying the code division in CDM is far more complicated than that governing OFDM [84]. When compared with the single carrier modulation techniques, OFDM is known to possess the features of high spectral efficiency and robustness against channel impairments such as impulse noise, ISI, and multipath fading [80]. In summary, OFDM is a multicarrier modulation method in which a number of orthogonal subcarriers is transmitted

simultaneously [80].

In conventional OFDM systems, modulation techniques such as BPSK and *M*-QAM map a fixed number of information bits into signal constellation symbol [87, 138]. Each signal constellation symbol represents a point in the 2-D baseband signal space [86]. The ever-increasing demand for increased data transmissions has driven several technologies that exploit new degrees of freedom such as the position of a transmit antenna in order to enhance the spectral efficiency [75, 76].

As outlined in the introduction of this thesis, the work in this chapter exploits the orthogonality of the subcarriers in a radically new way in order to add a new dimension to the complex 2-D signal plan, which is referred to as subcarrier-index dimension. The proposed SIM transmission technique employs the subcarrier-index to convey information in an OOK fashion.

5.2   Conventional OFDM signal model

This section begins with a qualitative outline to the basis of OFDM transmission. As mentioned above, OFDM system can be efficiently implemented in discrete time using inverse fast Fourier transform (IFFT) to act as a modulator and FFT to act as a demodulator [135].

Let $[B_0, B_1, ..., B_{N_{\mathrm{FFT}}-1}]$ denote data symbols corresponding to the N_{FFT} sub-channels in the OFDM system, where $B_i = s_i(t)$ for $i \in 0, ..., N_{\mathrm{FFT}}$. IFFT as a linear transformation maps complex data symbols $[B_0, B_1, ..., B_{N_{\mathrm{FFT}}-1}]$ to OFDM symbols $[b_0, b_1, ..., b_{N_{\mathrm{FFT}}-1}]$ such that

$$b_k = \sum_{n=0}^{N_{\mathrm{FFT}}-1} B_n e^{j2\pi n \frac{k}{N_{\mathrm{FFT}}}} \tag{5.1}$$

The linear mapping can be represented in a matrix form as:

$$\bar{b} = \overline{\mathbf{W}} \cdot \bar{B} \tag{5.2}$$

where

$$\overline{\mathbf{W}} = \begin{bmatrix} 1 & ... & 1 & 1 \\ 1 & W & ... & W^{N_{\text{FFT}}-1} \\ 1 & W^2 & ... & W^{2(N_{\text{FFT}}-1)} \\ . & . & . & . \\ 1 & W^{N-1} & ... & W^{N_{\text{FFT}}(N_{\text{FFT}}-1)} \end{bmatrix} \tag{5.3}$$

and

$$W = e^{j\frac{2\pi}{N_{\text{FFT}}}} \tag{5.4}$$

where $j = \sqrt{1}$ and $\overline{\mathbf{W}}$ is a symmetric and orthogonal matrix. After the IFFT, a cyclic prefix of length k_{cp} is added to each OFDM symbol block. The value of $k_{\text{cp}} \times T_s$ is assumed to be equal to or greater than the maximum delay spread of the multipath channel, where T_s is the sampling duration. The output of this block is fed into a digital-to-analogue (D/A) converter at the rate of f_s and low-pass filtered. A basic representation of the equivalent complex baseband transmitted signal is

$$x(t) = \sum_{n=0}^{N_{\text{FFT}}-1} \{B_n e^{j2\pi\frac{n}{N_{\text{FFT}}}f_s t}\} \text{ for } -\frac{k_{\text{cp}}}{f_s} < t < \frac{N_{\text{FFT}}}{f_s} \tag{5.5}$$

The transmitted OFDM signal $x(t)$ including the windowing effect is given by

$$x(t) = \sum_{l=-\infty}^{\infty} \sum_{k=-k_{\text{cp}}}^{N_{\text{FFT}}} \sum_{n=0}^{N_{\text{FFT}}-1} \{B_{n,l} e^{j2\pi\frac{n}{N_{\text{FFT}}}k}\} w(t - \frac{k}{f_s} - lT) \tag{5.6}$$

$B_{n,l}$ represents the nth data symbol transmitted during the lth OFDM symbol, $T = (N_{\text{FFT}} + k_{\text{cp}})/f_s$ is the OFDM block duration and $w(t)$ is the window or the pulse shaping function. The received signal for time-varying random channel is

$$r(t) = \int_0^{\infty} x(t - \tau)h(t, \tau)d\tau + n(t) \tag{5.7}$$

where $n(t)$ is AWGN with a diagonal covariance matrix of $E(nn^H) = \sigma^2 I$ where the noise components in the different sub-channels are uncorrelated. The received signal is sampled at $t = \frac{k}{f_S}$ for $k = -k_{\text{cp}}, ..., N_{\text{FFT}} - 1$. With no inter-symbol interference, the output of the FFT block at the receiver is

$$\tilde{B}_m = \frac{1}{N_{\text{FFT}}} \sum_{k=0}^{N_{\text{FFT}}-1} r_k e^{-j2\pi m\frac{k}{2N_{\text{FFT}}}} \tag{5.8}$$

where

$$r_k = \sum_{n=0}^{N_{\text{FFT}}-1} H_n B_n e^{j2\pi \frac{n}{2N_{\text{FFT}}}k} + n(k) \tag{5.9}$$

H_n is a complex number and is the frequency response of the time-variant channel $h(t-\tau)$ at frequency n/T. So,

$$\tilde{B}_m = \begin{cases} H_n B_n + N(n), & n = m \\ N(n), & n \neq m \end{cases} \tag{5.10}$$

Fig. 5.4 shows the typical setup of a OFDM system with digital processing techniques using FFT and IFFT transformation blocks which generates the orthogonal sub-channels.
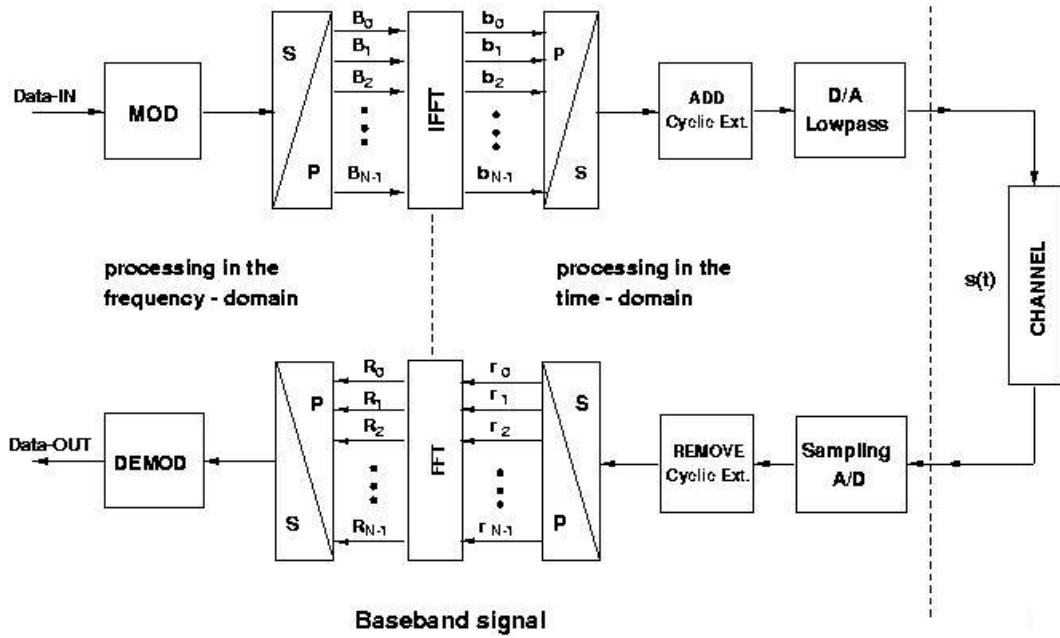
Figure 5.4: *Conventional OFDM multicarrier transmission system*

83

5.3 Subcarrier-index modulation OFDM

The main concept of SIM OFDM is explained using the system depicted in Fig. 5.5. According to the basic OFDM system illustrated in Fig. 5.5(a), an arbitrary binary bit-stream B of length $(N_{\mathrm{FFT}} \times \log_2(M))$ bits is transmitted using all N_{FFT} subcarriers, where N_{FFT} and M represent the FFT size and the signal constellation size, respectively. In the example, a square 4-QAM technique is used, $N_{\mathrm{FFT}} = 16$, and the block size is 32. Please note that all the available subcarriers are active and the indices of the modulated subcarriers are labeled using italic numbers in Fig. 5.5(a).

Unlike traditional OFDM depicted in Fig. 5.5(a), the SIM OFDM technique splits the serial bit-stream B into two bit-substreams of the same length as in this example. As depicted in Fig. 5.5(b), the first bit-substream B_{OOK} is on the right side of the splitting point while the second bit-substream B_{QAM} is on the left side. In general, the number of bits in the first bit-substream B_{OOK} is equal to the FFT size. Also, it is assumed that all subcarriers are dedicated for data transmission. Compared to the conventional OFDM system in Fig. 5.5(a), SIM OFDM has an additional module named subcarrier-index modulator.

The functionality of this module can be summarized in two main functions. Firstly, based on the bit-value of each bit in , the subcarrier-index modulator forms two subsets from B_{OOK} (ones and zeroes). By comparing the cardinality of these subsets, the type of the majority bit-value can be determined. For instance, consider the case in Fig. 5.5(b) where B_{OOK} is in the following form (1111010101101001). In this example, the subcarrier-index modulator logically forms two subsets namely B_{OOK}^0 and B_{OOK}^1. The subset of the zero bit-values B_{OOK}^0 will be in the form (000000) and according to the location of each zero within B_{OOK}, the associated set of indices will be {5,7,9,12,14,15}. Similarly, the subset B_{OOK}^1 will be in the form (1111111111), while the associated set of indices will be {1,2,3,4,6,8,10,11,13,16}. Since the the size of B_{OOK}^1 is greater than the size of B_{OOK}^0, the majority bit value is 1 for this example.

Secondly, the location of each bit in B_{OOK} is associated with the index of each subcarrier. Then, the group of subcarriers associated with the subset of the majority bit-value (ones in this example) are selected to be modulated by the second bit-substream B_{QAM} while the remaining subcarriers are turned-off (suppressed before the signal modulation). In other words, the bit-substream B_{OOK} is used in an OOK fashion to activate those subcarriers whose indices correspond to the majority bit-value. The type of the majority bit-value (one or zero) can be

(a) Conventional OFDM

(b) SIM OFDM

Figure 5.5: *OFDM sytem with the following parameters: FFT size: 16 subcarriers, modulation type: 4QAM (each subcarrier is loaded by 2 bits), and symbol transmit power: 1 W*

85

estimated using the Hamming weight of B_{OOK} (the Hamming weight of a binary bit stream is the number of ones). The number of bits of the majority bit-value N_{maj} can be formulated as follows:

$$N_{\text{maj}} = \max\{N_{\text{ones}}^{B_{\text{OOK}}}, (N_{\text{FFT}} - N_{\text{ones}}^{B_{\text{OOK}}})\} \tag{5.11}$$

where $N_{\text{ones}}^{B_{\text{OOK}}}$ is Hamming weight of B_{OOK}. Clearly, if $N_{\text{ones}}^{B_{\text{OOK}}} \geq N_{\text{FFT}}/2$ then ones are majority, otherwise zeroes are majority. In the serial-to-parallel (S/P) module, the bit-substream B_{QAM} is multiplexed to modulate the activate subcarriers whose indices are labeled using italic magnified-numbers in Fig. 5.5(b).

5.3.1 Majority bit-value signalling

As in the example illustrated in Fig. 5.5, the size of B_{QAM} is equal to $N_{\text{FFT}}/2 < N_{\text{maj}}$, hence, the number of excess subcarriers can be formulated as follows:

$$N_{\text{ex}} = N_{\text{maj}} - \frac{N_{\text{FFT}}}{2} \tag{5.12}$$

In this example, $N_{\text{ex}} = 2$ subcarriers are used as control subcarriers to explicitly signal the type of the majority bit-value to the receiver, see Fig. 5.5(b). This approach is followed throughout this work to signal the type of the majority bit-value in order to de-map B_{OOK} at the receiver side. A flowchart illustration of this algorithm is depicted in Fig. 5.6. According to Fig. 5.6, the bit-value of the majority bit-value is equal to one when $N_{\text{ex}} = 0$. Therefore, no signalling is needed since this case is assumed to be predefined in the system. Alternatively, signalling the type of the majority bit-value can be avoided, and all excess subcarriers can be used for data transmission which results in better spectral efficiency. In order to estimate the status of each received subcarrier, a coherent OOK detector is used at the receiver side [86]. However, the receiver can only detect the combination of N_{maj} active subcarriers and $N_{\text{FFT}} - N_{\text{maj}}$ inactive subcarriers. Afterwards, the receiver uses the two possibilities of the majority bit-value (1 or 0) to construct two possible hypotheses of B_{OOK}. Then, each of the two hypotheses is attached to the estimated B_{QAM} to form two different versions of the original bit-stream B. Finally, the version with less errors is selected.
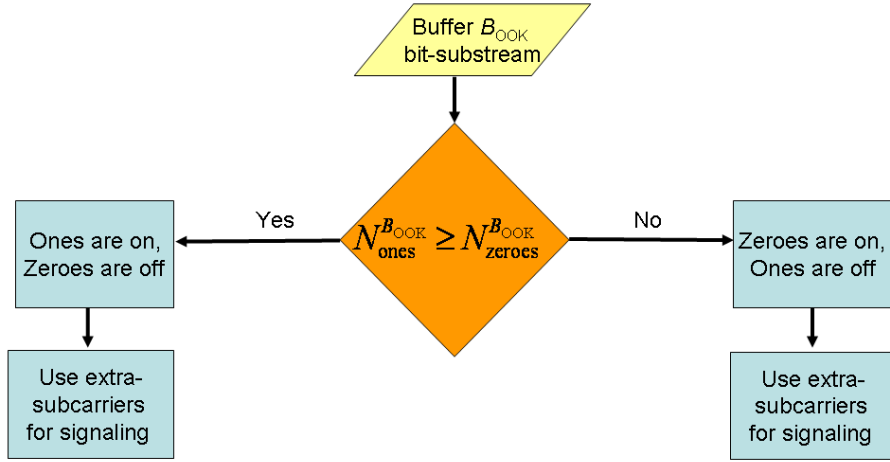
Figure 5.6: *Exemplary algorithm for the majority bit-value signalling*

5.3.2   Power allocation policies

There are two possible policies to deal with the power originally allocated to the inactive subcarriers, namely the power reallocation policy (PRP) and the power saving policy (PSP). In PRP, the power originally allocated to the inactive subcarriers is equally redistributed among the active ones. Thus, the power allocated to each active subcarrier is increased compared to conventional OFDM. This results in a better BER performance as will be shown later in the results section.

On the one hand, the average SNR of an active subcarrier, assuming unity channel gain, under PRP $\overline{\gamma}_{\text{sc}}^{\text{PRP}}$ can be written as follows:

$$\overline{\gamma}_{\text{sc}}^{\text{PRP}} = 10 \log_{10} \left(\frac{P_{\text{Tx}}}{E[N_{\text{maj}}]} \right) - 10 \log_{10}(n_{\text{sc}}), \quad \text{dB} \tag{5.13}$$

where P_{Tx} is the total transmit power allocated to the OFDM symbol, $E[N_{\text{maj}}]$ is the average number of majority bit-value, and n_{sc} is the per-subcarrier average AWGN. It is important to note that for an uncoded bits-stream, *i.e.* a sequence of independent bits, the number of the majority bits is binomially distributed random variable, and $E[N_{\text{maj}}] \approx \frac{N_{\text{FFT}}}{2}$ for the case of
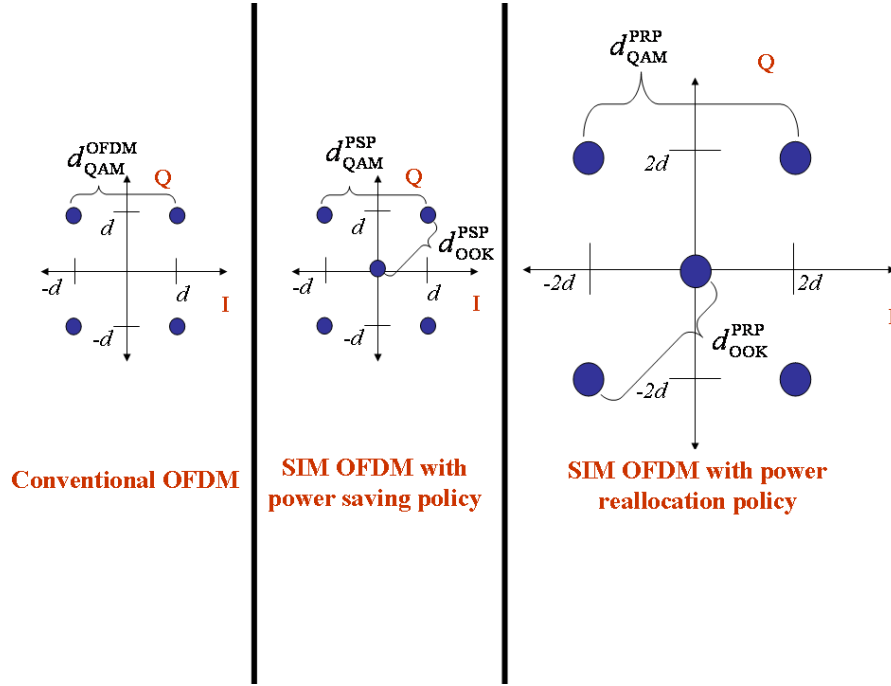
Figure 5.7: *Comparison of the Euclidean distance of conventional OFDM against SIM OFDM for different power allocation policies*

equiprobable bits. As it can be seen from the example in Fig. 5.5, the power of each active subcarrier is increased by $\frac{1}{10} - \frac{1}{16} = \frac{3}{80}$ W. Moreover, a gain of 4 bits per OFDM symbols ($N_{\text{ex}} = 2$ multiplied by $\log_2(M = 4) = 2$) can be achieved according to the example. This gain in the symbol throughput is further discussed in section 5.3.3. It is important to remember that, in this work, the excess subcarriers are used to explicitly signal the bit-value of the majority bits to the receiver.

On the other hand, PSP completely suppresses the power originally allocated to the inactive subcarriers, which results in a better power efficiency. Hence, the average SNR of an active subcarrier under PSP $\overline{\gamma}_{\text{sc}}^{\text{PSP}}$ can be written as follows:

$$\overline{\gamma}_{\text{sc}}^{\text{PSP}} = 10 \log_{10} \left(\frac{P_{\text{Tx}}}{N_{\text{FFT}}} \right) - 10 \log_{10}(n_{\text{sc}}), \quad \text{dB} \tag{5.14}$$

Assuming that $N_{\text{ex}} = 0$, Fig. 5.7 shows the influence of both PRP and PSP on the Euclidian distance compared to the case when conventional OFDM is used.

In Fig. 5.7 $d_{\text{QAM}}^{\text{PSP}}, d_{\text{OOK}}^{\text{PSP}}, d_{\text{QAM}}^{\text{PRP}}, d_{\text{OOK}}^{\text{PRP}}$ and $d_{\text{QAM}}^{\text{OFDM}}$ denote the Euclidean distance between two adjacent symbols of the following: SIM OFDM QAM with PSP, SIM OFDM OOK with PSP,

SIM OFDM QAM with PRP, SIM OFDM OOK with PRP, and conventional OFDM QAM, respectively.

5.3.3 Spectral efficiency

Assuming all active subcarriers are used for data transmission, the error-free spectral efficiency of SIM OFDM and conventional OFDM can be formulated as follows, respectively:

$$T^{\text{SIM OFDM}} = 1 + \frac{\text{E}[N_{\text{maj}}]}{N_{\text{FFT}}} \log_2(M) \quad [\text{bps/Hz}] \tag{5.15}$$

$$T^{\text{OFDM}} = \log_2(M) \quad [\text{bps/Hz}] \tag{5.16}$$

As for the case of uncoded data with 4-QAM, $\text{E}[N_{\text{maj}}]$ is approximately equal to $\frac{N_{\text{FFT}}}{2}$ for equiprobable bits (as highlighted in section 5.3.2). Consequently, $T^{\text{SIM OFDM}} \approx T^{\text{OFDM}}$ since $1 + \frac{\text{E}[N_{\text{maj}}]}{N_{\text{FFT}}} \log_2(M) \approx \log_2(M)$ when $M = 4$. Therefore, a marginal improvement in the spectral efficiency over 4-QAM conventional OFDM is anticipated. However, the average N_{maj} can be increased by manipulating the bit probabilities, which is subject to future investigation. Fig.
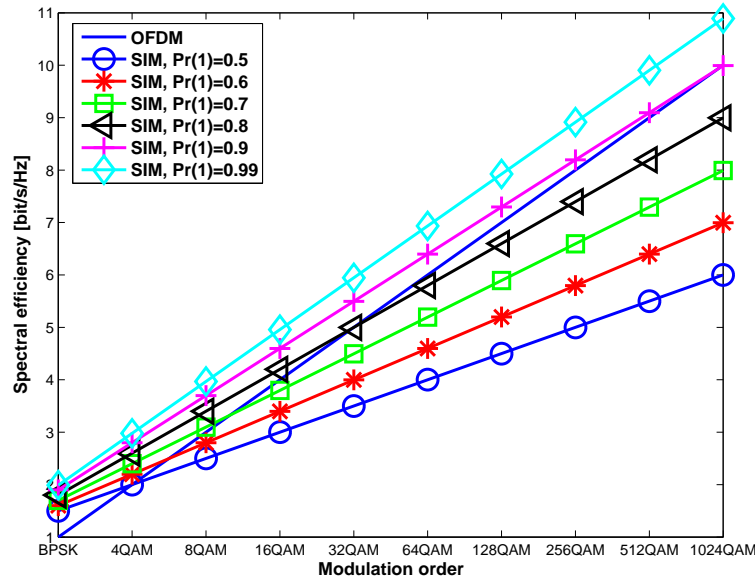
Figure 5.8: *Average spectral efficiency of both SIM OFDM and OFDM for different constellation size, and different bit probability within a finite codeword.* Pr(1): probability of the logical bit-value one within a finite codeword.

5.8 has been obtained using (5.15) to provide insight about the influence of the bit probability on the average spectral efficiency using SIM OFDM technique for higher modulation orders.

This motivates the importance of studying the effect of adding an interleaver and/or channel coder before the subcarrier-index modulator which has not been considered in this thesis.

5.4 Generalization of SIM

From a generalization point of view, using OOK to map the first bit-substream [139] can be considered as a spacial case of using two different constellation sizes (*i.e.* high-order QAM and low-order QAM) for modulation. In this generic case, the original bit-stream is divided into three portions: a first bit-substream, a second bit-substream, and a third bit-substream as in Fig. 5.9. Then, the subcarrier-index modulator encodes the first bit-substream by associating each
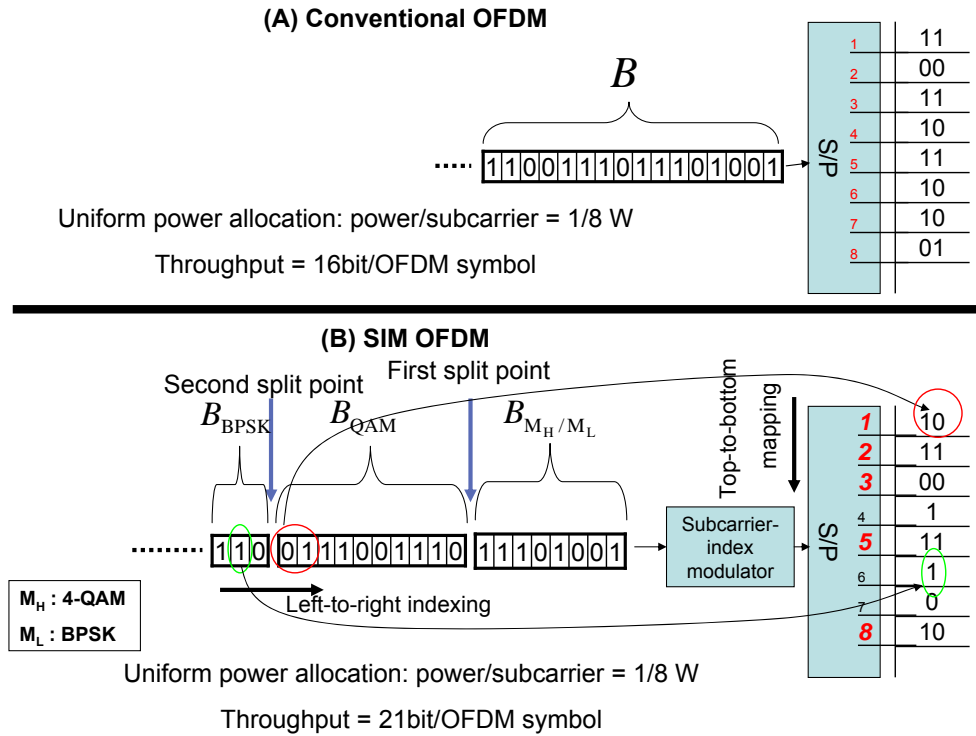
Figure 5.9: *Generic implementation of SIM OFDM where two different modulation types are used instead of OOK modulation.*

indexed subcarrier with the index of each bit in the first bit-substream. Afterwards, two subsets of bit-values (ones and zeros) are identified within the first bit-substream. The next step is to select two different modulation alphabets M_H and M_L (*i.e.* 4-QAM and BPSK) to be assigned to the first and the second subsets of the first bit-substream. For spectrally-efficient implementation, the majority subset of the first bit-substream is allocated the high-order modulation (e.g.

4-QAM), while the minority subset is allocated the low-order modulation (e.g. BPSK). Finally, the second bit-substream is mapped by modulating the subcarriers belonging to the majority subset according to the constellation size of M_{H}, and the third bit-substream is mapped by modulating the subcarriers belonging to the minority subset according to the constellation size of M_{L}. Fig. 5.9 illustrates an example on SIM using two different modulation instead of OOK modulation.

While the above implementation of the subcarrier-index have been carried out for the frequency domain, the underlaying concept can easily be generalized towards other dimensions such as time, space, or even combination of them. Accordingly, the generic version of the subcarrier-index modulation can be referred to as the domain-specific resource-index modulation. For instance, the index-modulation concept can be referred to as time-slot-index modulation (TSIM) in the time domain. Similarly, for the spatial domain case, it can be referred to as antenna-index modulation (AIM). Therefore, different domain resources may be used in addition to or as an alternative to the frequency domain resource. The next subsections provide examples about extending the generalized concept of SIM into different domains.

5.4.1 Time domain scenario: TSIM scheme

In the time domain, a transmission frame is subdivided into smaller time units of equivalent (however, not necessarily) length (time-slots). The time-slot can be indexed to be associated with the first portion of the bit-stream. Then, the time-slots are assigned different modulation types to encode the second and the third portions. Fig. 5.10 illustrates a simple example where the first portion, consisting of the information bits (110110), is only associated with the indices of the time-slots. Not that in this example the index-modulation concept is not utilized in the frequency domain, hence, at any time-slot all subcarriers use the same constellation size, *i.e.* M_H is used for all subcarriers at the second time-slot.
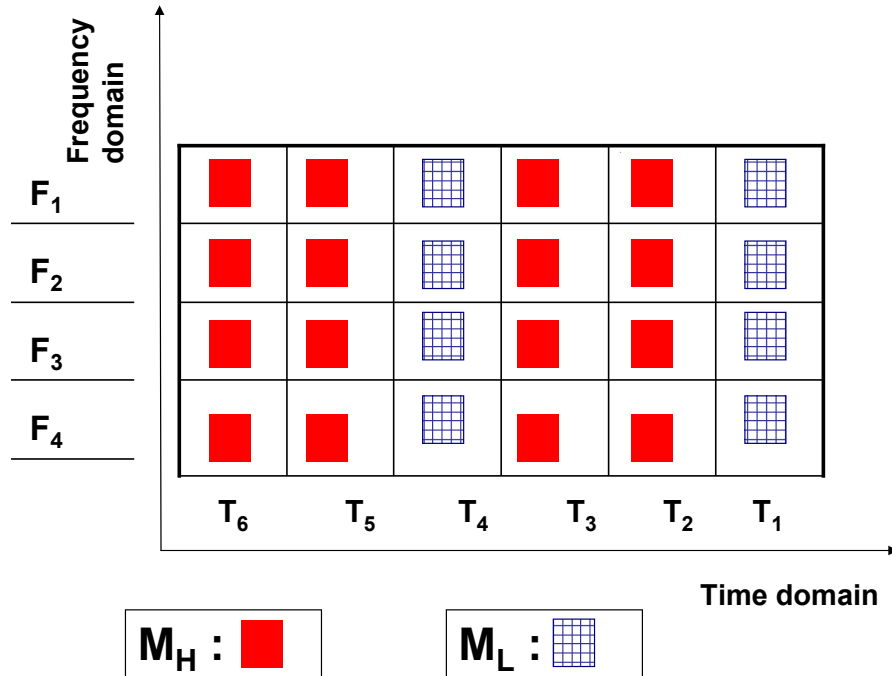
Figure 5.10: *An example on TSIM scheme where the first bit-substream (110110) is only mapped into the time domain*

5.4.2 Spatial domain scenario: AIM scheme

In the spatial domain, in spatial multiplexing MIMO systems with independent spatial streams, multiple antenna locations can be indexed to be associated with the information bits of the first bit-substream. Alternatively, in smart antenna based MIMO systems such as grid-of-beams (GoB), multiple beams can be indexed and used to convey information as depicted in Fig. 5.11. According to the example in Fig. 5.11, the first portion, consisting of the information bits (0011), is associated with the indices of four beams. The first two beams transmit the second bit-substream using M_L, while the M_H is used by the last two beams to transmit the third bit-substream.
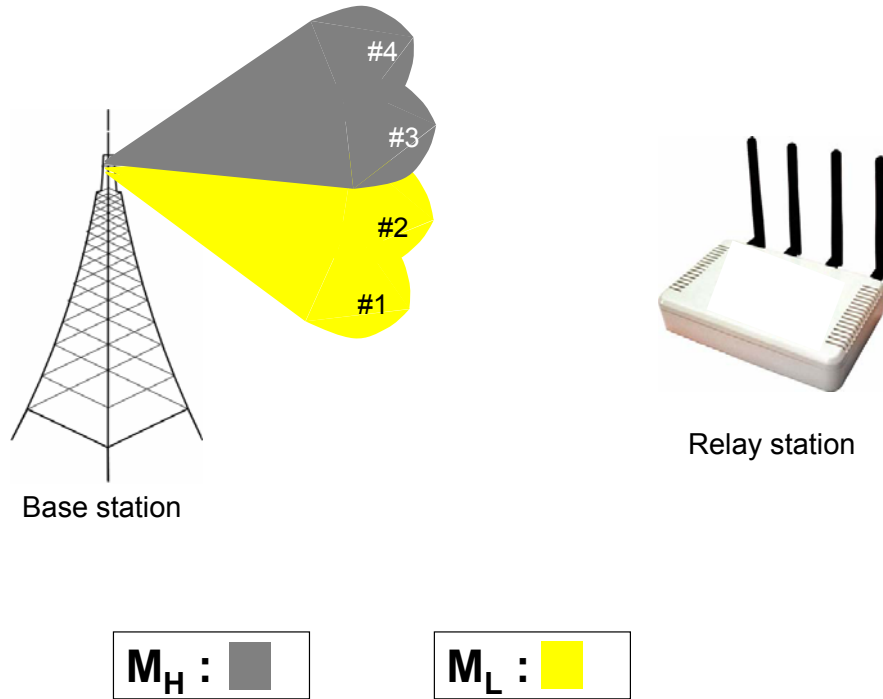
Figure 5.11: *An example on AIM scheme where the first bit-substream (1100) is mapped into the spatial domain (grid-of-beams).*

5.4.3 Combined domains scenario: SIM/TSIM schemes

Finally, it is possible to simultaneously apply the index-modulation concept to two or more domains. For example, consider a scenario of 4 subcarriers associated with the binary word (1110) and 4 time-slots associated with the binary word (0110). For the frequency domain two groups of modulation levels, each of size 2, are formed G_L, and G_H. In the example illustrated

in Fig. 5.12, the members of each modulation group are defined as follows: G_L : {$M_L \equiv$ off, $M_H \equiv$ 8-QAM}, and G_H : {$M_L \equiv$ BPSK, $M_H \equiv$ 4-QAM}. Now, the binary word 1110 can be mapped to the frequency domain as follows: (G_H G_H G_H G_L). Similarly, the binary

0 F_1	off	8-QAM	8-QAM	off
1 F_2	BPSK	4-QAM	4-QAM	BPSK
1 F_3	BPSK	4-QAM	4-QAM	BPSK
1 F_4	BPSK	4-QAM	4-QAM	BPSK
	T_1	T_2	T_3	T_4
	0	1	1	0

Mapping key : in frequency domain: 1 : G_H , 0 : G_L , in time domain: 1 : M_H , 0 : M_L

Figure 5.12: *An example on a combination of SIM and TSIM schemes where the index-modulation concept is applied to both frequency and time domains.*

word 0110 can be mapped to the time domain as follows: (M_L M_H M_H M_L). The resultant mapping of the time-frequency block (chunk) can be found in the Fig. 5.12.

5.5 Analytical BER calculation for SIM OFDM

The computation of the analytical bit error performance of SIM OFDM involves analyzing two consecutive estimation processes. The first process is to estimate the status of all N_{FFT} subcarriers (active or inactive) in order to estimate the first bit-substream B_{OOK} using coherent OOK detector. The second estimation process is related to the conventional OFDM-based system, which transmits the second bit-substream B_{QAM} using *M*-ary amplitude/phase modulation (*M*-APM) symbols only using the active subcarriers. As explained in 5.3.2, the power allocation policy has an impact on the average SNR of each active subcarrier. In what follows, B_{OOK} and B_{QAM} are assumed to be of equal lengths, and the excess subcarriers (if any) are used to signal the bit-value of the majority bit-value as highlighted earlier. In this work, the excess subcarriers are not used for data transmission in order to maintain the same OFDM symbol throughput

compared to conventional OFDM which makes the BER comparison fair.

Throughout the computations, the two estimation processes are assumed to be independent to simplify the calculations. The considered APM for the second process is a square 4-QAM. The bit-stream B is correctly estimated if and only if both estimation processes are correct. Let A_1 and A_2 represent the first and the second estimation processes, respectively. Since B_{OOK} and B_{QAM} are of equal length, the respective probabilities are $P(A_1) = P(A_2) = \frac{1}{2}$. Now, let $P_{\text{sc}}(E)$ be the error probability for A_1 (the subcarrier activity) and $P_{\text{q}}(E)$ be the error probability for A_2 (the 4-QAM symbol recovery) at the receiver side. The overall probability $P_{\text{e}}(E)$ can be formulated using the law of total probability as follows:

$$
\begin{aligned}
P_{\text{e}}(E) &= P_{\text{e}}(E \mid A_1)P(A_1) + P_{\text{e}}(E \mid A_2)P(A_2) \\
&= \frac{1}{2}P_{\text{sc}}(E) + \frac{1}{2}P_{\text{q}}(E)
\end{aligned}
\tag{5.17}
$$

In what follows, the error probability of each estimation process is considered separately using both PRP and PSP.

5.5.1 Analytical BER of estimating B_{OOK} (P_{sc})

The estimation process of the subcarrier activity using coherent OOK detector (A_1) is similar to M-ary ASK (M-ASK) detection [86]. For the binary case (on or off) the symbol error ratio (SER) expression over a Rayleigh fading channel can be written as follows [140]:

$$
P_{\text{s}} = \frac{1}{2}\left(1 - \sqrt{\frac{\overline{\gamma}_s}{1 + \overline{\gamma}_s}}\right)
\tag{5.18}
$$

where $\overline{\gamma}_s \triangleq \overline{\alpha^2}\frac{\overline{E}_s}{N_o^{\text{sc}}}$ denotes the average SNR per symbol, and α, $\overline{E}_s$, and N_o^{sc} are the amplitude of fading coefficient, the average symbol energy, and the average symbol noise power, respectively. $\overline{E}_s$ can be calculated by dividing the total transmit power allocated to the OFDM symbol P_{Tx} by the number of the subcarriers associated with the OOK estimation process. The power reallocation policy results in having $\overline{E}_s$ unchanged. Particularly, this is because all the subcarriers are associated with the OOK estimation process, and P_{Tx} is still the same compared to the case where all subcarriers are active. In other words, the effective average SNR during the OOK detection using PRP $\overline{\gamma}_s^{\text{OOK}-\text{PRP}}$ is equal to $\overline{\gamma}_s$. Meanwhile, the power saving policy suppresses the power originally allocated to the $(N_{\text{FFT}} - N_{\text{maj}})$ inactive subcarriers. By defining ϵ as the

ratio of the active subcarriers $\frac{N_{\text{maj}}}{N_{\text{FFT}}}$, the used OFDM symbol power is $\epsilon \times P_{\text{Tx}}$. Also, note that the OOK estimation process considers both active and inactive subcarriers. Therefore, the average symbol energy is $\epsilon \times \overline{E}_s$. Hence, the effective average SNR during the OOK detection using PSP $\overline{\gamma}_s^{\text{OOK}-\text{PSP}}$ is equal to $\epsilon \times \overline{\gamma}_s$. Note that for binary ASK, the BER P_{b} and SER P_{s} are equal [86], hence, two versions of P_{sc} can be formulated for both PRP and PSP, respectively.

$$P_{\text{sc}}^{\text{PRP}} = \frac{1}{2}\left(1 - \sqrt{\frac{\overline{\gamma}_s}{1+\overline{\gamma}_s}}\right) \tag{5.19}$$

$$P_{\text{sc}}^{\text{PSP}} = \frac{1}{2}\left(1 - \sqrt{\frac{\epsilon \times \overline{\gamma}_s}{1+\epsilon \times \overline{\gamma}_s}}\right) \tag{5.20}$$

By letting $\phi_s^{\text{PRP}} = \sqrt{\frac{\overline{\gamma}_s}{1+\overline{\gamma}_s}}$ and $\phi_s^{\text{PSP}} = \sqrt{\frac{\epsilon\times\overline{\gamma}_s}{1+\epsilon\times\overline{\gamma}_s}}$ (5.19) and (5.20) can be simplified to (5.21) and (5.22), respectively, as follows:

$$P_{\text{sc}}^{\text{PRP}} = \frac{1 - \phi_s^{\text{PRP}}}{2} \tag{5.21}$$

$$P_{\text{sc}}^{\text{PSP}} = \frac{1 - \phi_s^{\text{PSP}}}{2} \tag{5.22}$$

5.5.2 Analytical BER of estimating B_{QAM} (P_{q})

According to [140], SER expression for *M*-ary QAM over a Rayleigh fading channel is:

$$\begin{aligned} P_{\text{s}} &= 2\left(\frac{\sqrt{M}-1}{\sqrt{M}}\right)\left(1 - \sqrt{\frac{1.5\overline{\gamma}_s}{M-1+1.5\overline{\gamma}_s}}\right) - \left(\frac{\sqrt{M}-1}{\sqrt{M}}\right)^2 \\ &\quad \times \left[1 - \sqrt{\frac{1.5\overline{\gamma}_s}{M-1+1.5\overline{\gamma}_s}}\left(\frac{4}{\pi}\tan^{-1}\sqrt{\frac{M-1+1.5\overline{\gamma}_s}{1.5\overline{\gamma}_s}}\right)\right] \end{aligned} \tag{5.23}$$

Note that $\overline{\gamma}_s \triangleq \overline{\gamma}\log_2(M)$, where $\overline{\gamma}$ denotes the average SNR per bit. Also, note that for uncoded data the average BER can be approximated as $P_{\text{b}} = \frac{P_{\text{s}}}{\log_2 M}$ [140], which becomes $P_{\text{b}} = \frac{P_{\text{s}}}{2}$ for $M = 4$. Hence, P_q for square 4-QAM can be written as follows:

$$P_{\text{q}} = -\frac{1}{8} - \frac{1}{2}\sqrt{\frac{\overline{\gamma}_s}{2+\overline{\gamma}_s}} + \frac{1}{2\pi}\sqrt{\frac{\overline{\gamma}_s}{2+\overline{\gamma}_s}}\tan^{-1}\sqrt{\frac{2+\overline{\gamma}_s}{\overline{\gamma}_s}} \tag{5.24}$$

which can be simplified to

$$P_{\mathrm{q}} = -\frac{1}{8} - \frac{\theta_s}{2} + \frac{\theta_s}{2\pi} \tan^{-1}\left(\frac{1}{\theta_s}\right) \tag{5.25}$$

where $\theta_s = \sqrt{\frac{\overline{\gamma}_s}{2+\overline{\gamma}_s}}$. The impact of both PRP and PSP on $\overline{E_s}$ can be analyzed in the same way as in 5.5.1. Since $0.5 \leq \epsilon \leq 1$, using PSP enhances the average symbol energy which is equal to $\frac{\overline{E_s}}{\epsilon}$. This is due to the fact that the 4-QAM estimator considers only the active subcarrier, where $\mathrm{P_{Tx}}$ is equally redistributed among them at the transmitter. Therefore, the effective average SNR during the 4-QAM detection using PRP $\overline{\gamma}_s^{\mathrm{QAM-PRP}}$ is equal to $\frac{\overline{\gamma}_s}{\epsilon}$.

For the power saving policy, $\epsilon \times \mathrm{P_{Tx}}$ is redistributed among the active subcarriers, which leaves $\overline{E_s}$ unchanged compared to the case when all the subcarriers are active. Hence, the effective average SNR during the 4-QAM detection using PSP $\overline{\gamma}_s^{\mathrm{QAM-PSP}}$ is equal to $\overline{\gamma}_s$. The influence of both PRP and PSP on $\overline{E_s}$ can be inferred from the variation in the Euclidean distance as depicted in Fig. 5.7. The two versions of P_{q} associated with PRP and PSP can be written as follows, respectively:

$$P_{\mathrm{q}}^{\mathrm{PRP}} = -\frac{1}{8} - \frac{1}{2}\sqrt{\frac{\overline{\gamma}_s}{2\epsilon + \overline{\gamma}_s}} + \frac{1}{2\pi}\sqrt{\frac{\overline{\gamma}_s}{2\epsilon + \overline{\gamma}_s}} \tan^{-1}\sqrt{\frac{2\epsilon + \overline{\gamma}_s}{\overline{\gamma}_s}} \tag{5.26}$$

$$P_{\mathrm{q}}^{\mathrm{PSP}} = -\frac{1}{8} - \frac{1}{2}\sqrt{\frac{\overline{\gamma}_s}{2 + \overline{\gamma}_s}} + \frac{1}{2\pi}\sqrt{\frac{\overline{\gamma}_s}{2 + \overline{\gamma}_s}} \tan^{-1}\sqrt{\frac{2 + \overline{\gamma}_s}{\overline{\gamma}_s}} \tag{5.27}$$

By letting $\theta_s^{\mathrm{PRP}} = \sqrt{\frac{\overline{\gamma}_s}{2\epsilon + \overline{\gamma}_s}}$ and $\theta_s^{\mathrm{PSP}} = \sqrt{\frac{\overline{\gamma}_s}{2 + \overline{\gamma}_s}}$, (5.26) and (5.27) can be simplified to (5.28) and (5.29), respectively, as follows:

$$P_{\mathrm{q}}^{\mathrm{PRP}} = -\frac{1}{8} - \frac{\theta_s^{\mathrm{PRP}}}{2} + \frac{\theta_s^{\mathrm{PRP}}}{2\pi} \tan^{-1}\left(\frac{1}{\theta_s^{\mathrm{PRP}}}\right) \tag{5.28}$$

$$P_{\mathrm{q}}^{\mathrm{PSP}} = -\frac{1}{8} - \frac{\theta_s^{\mathrm{PSP}}}{2} + \frac{\theta_s^{\mathrm{PSP}}}{2\pi} \tan^{-1}\left(\frac{1}{\theta_s^{\mathrm{PSP}}}\right) \tag{5.29}$$

5.5.3 Analytical BER of estimating B (P_{e})

By substituting (5.21), (5.22), (5.28), and (5.29) into (5.17), the overall bit error probability using both PRP and PSP can be formulated as in (5.30) and (5.31), respectively.

$$P_{\mathrm{e}}^{\mathrm{PRP}} = \frac{1}{2}\left[\frac{1-\phi_s^{\mathrm{PRP}}}{2}\right] + \frac{1}{2}\left[-\frac{1}{8} - \frac{\theta_s^{\mathrm{PRP}}}{2} + \frac{\theta_s^{\mathrm{PRP}}}{2\pi}\tan^{-1}\left(\frac{1}{\theta_s^{\mathrm{PRP}}}\right)\right] \tag{5.30}$$

$$P_{\mathrm{e}}^{\mathrm{PSP}} = \frac{1}{2}\left[\frac{1-\phi_s^{\mathrm{PSP}}}{2}\right] + \frac{1}{2}\left[-\frac{1}{8} - \frac{\theta_s^{\mathrm{PSP}}}{2} + \frac{\theta_s^{\mathrm{PSP}}}{2\pi}\tan^{-1}\left(\frac{1}{\theta_s^{\mathrm{PSP}}}\right)\right] \tag{5.31}$$

5.6 Simulation results and discussion

In the simulation, a single cell scenario with 500 m radius is assumed and the users are uniformly distributed in the cell. Table 5.1. shows the system parameters considered for the simulation.

Parameters	Values
Carrier frequency	5 GHz
System Bandwidth	100 MHz
Sampling Interval	10 ns
FFT length	1024
Constellation size	4
Speed	60 km/h

Table 5.1: *Simulation parameters*

5.6.1 Link level simulation model

The distance dependent path loss model is described in (5.32)

$$g = A + 10\mu\log_{10}(d/d_0) + \xi, \tag{5.32}$$

where $A = 20\log_{10}(4\pi d_0/\lambda)$ with d_0=100 m, and λ is the wavelength. The quantity μ is the pathloss exponent. The log-normally distributed random variable ξ models shadowing effects and with a standard deviation of 8 dB.

The multipath frequency-selective time-varying channel is modeled using the deterministic

channel model or Monte Carlo model approach described in [96, 97]. According to [96], the scattering components are assumed to be laying in confocal elliptical scattering zones where the transmitter and receiver at the common focal points. Each elliptical zone represents the set of paths for which distance between the transmitter and receiver remains same i.e., all the waves have the same propagation delay time. Every elliptical scattering zone undergoes a propagation delay $\tau_\varrho = \tau_0 + \varrho\Delta\tau$, $\varrho = 0, 1, ..., L-1$, where τ_0 is the propagation delay of the LOS component, $\Delta\tau$ defines the difference in path delays between adjacent elliptical zones and L defines the number of multipath components.

The multipath channel at time t is modelled as a finite impulse response (FIR) filter with tap delay equal to $\Delta\tau$ and the tap coefficients given by $\mathbf{h}(t, \tau) = [h(t, \tau_0) \ h(t, \tau_1) \ ... \ h(t, \tau_{L-1})]$. The received signal $y(t)$ is the convolution of transmitted time-domain OFDM signal $x(t)$ and the time-variant multipath channel $h(t, \tau)$ and is given as

$$y(t) = \mathbf{x}(t) * \mathbf{h}(t, \tau) = \sum_{\varrho=0}^{L-1} x(t - \tau_\varrho) \times h(t, \tau_\varrho) \tag{5.33}$$

where $y(t)$ is the received signal at time t, $x(t - \tau_\varrho)$ is the OFDM signal transmitted at $t - \tau_\varrho$ and $h(t, \tau_\varrho)$ is the channel coefficient corresponding to the ϱth path at time t.

The frequency-selective time-variant multipath channel $h(t, \tau)$ with a discrete multipath channel power delay profile (PDP) $\rho[\varrho]$ given in Table 5.2 is simulated.

Path index ϱ	Propagation delay τ_ϱ (ns)	Path power $\rho[\varrho]$
1	0	1.0
2	50	0.6095
3	100	0.4945
4	150	0.3940
5	200	0.2371
6	250	0.1900
7	300	0.1159
8	350	0.0699
9	400	0.0462

Table 5.2: *Multipath channel power delay profile*

The simulated channel can be mathematically modeled as follows [97].

$$h(t,\tau) = \frac{1}{\sqrt{N_\mathrm{h}}} \sum_{\varrho=1}^{L} \underbrace{\rho[\varrho]}_{\text{PDP}} \sum_{m=1}^{N_\mathrm{h}} \underbrace{\left[\cos(2\pi f_{\varrho,m}t + \theta_{\varrho,m}) + j\sin(2\pi f_{\varrho,m}t + \theta_{\varrho,m}) \right]}_{\text{Doppler weighted signal}} \times \underbrace{\delta(\tau - \tau_\varrho)}_{\text{path delay}}$$

(5.34)

where $f_\mathrm{d,max}$ is the maximum Doppler frequency, $f_{\varrho,m} = f_\mathrm{d,max}sin(2\pi u_{\varrho,m})$ is the discrete Doppler frequency, $\theta = 2\pi u_{\varrho,m}$ is the discrete Doppler phase, $u_{\varrho,m}$ is an independent and uniform distributed random variable in the range [0,1] for all ϱ and m, N_h is the number of harmonic functions, and L is the number of the multipath channel taps.

A sample realization of the simulated channel is presented in Fig. 5.13. The channel is assumed to be slow time-varying such that it is assumed to be constant for one OFDM symbol duration.
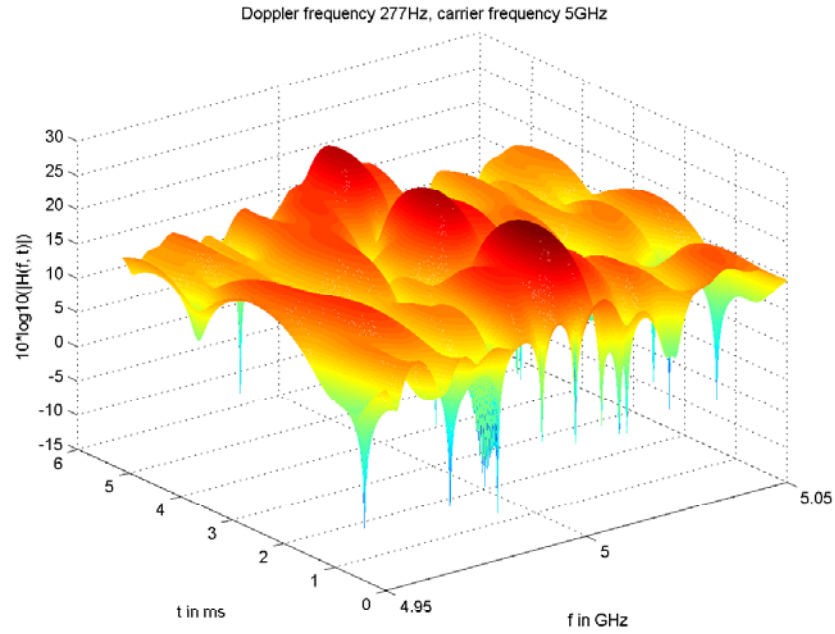
Figure 5.13: *Sample of channel realization for 500 OFDM symbols.*

5.6.2 Uncoded data with power reallocation policy

Compared to conventional OFDM, Fig. 5.14 shows that using SIM OFDM approximately results in a SNR gain of 26-22=4 dB for a BER of 10^{-3}. Also, it can be noticed that this gain is almost the same with increasing SNR. The reasons are twofold: First, the increment in the activated subcarrier power, quantified in (5.13), improves the detection quality of the signal constellation symbols. Second, the inherent high error rate performance of the coherent OOK detector, used to estimate the subcarrier activity, enhances the overall BER performance.
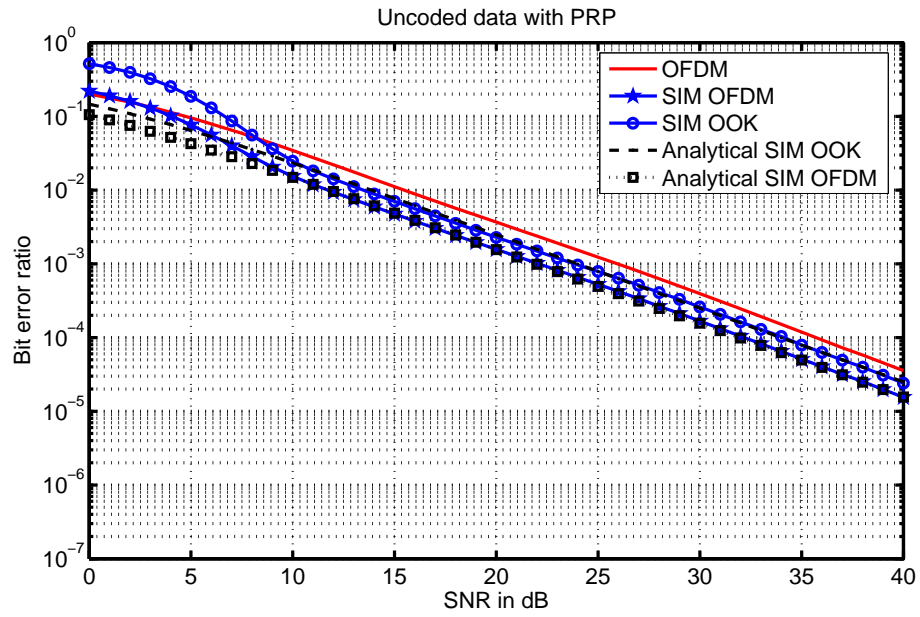
Figure 5.14: *Comparison of bit error ratio between SIM OFDM and OFDM for uncoded data under power reallocation policy*

5.6.3 Uncoded data with power saving policy

In contrast to conventional OFDM, a SNR gain of approximately 26-25=1 dB is achieved using SIM OFDM for a BER of 10^{-3}, see Fig. 5.15. Since the power originally allocated to the inactive subcarriers is totally suppressed, there is no increment in the activated subcarrier SNR as illustrated in (5.14). Hence, this marginal gain can be attributed to the inherent good BER performance of the coherent OOK detector used to estimate the first bit-substream. Most importantly, however, there is a 3-dB enhancement in the power efficiency compared to conventional OFDM since only half transmit power is used.
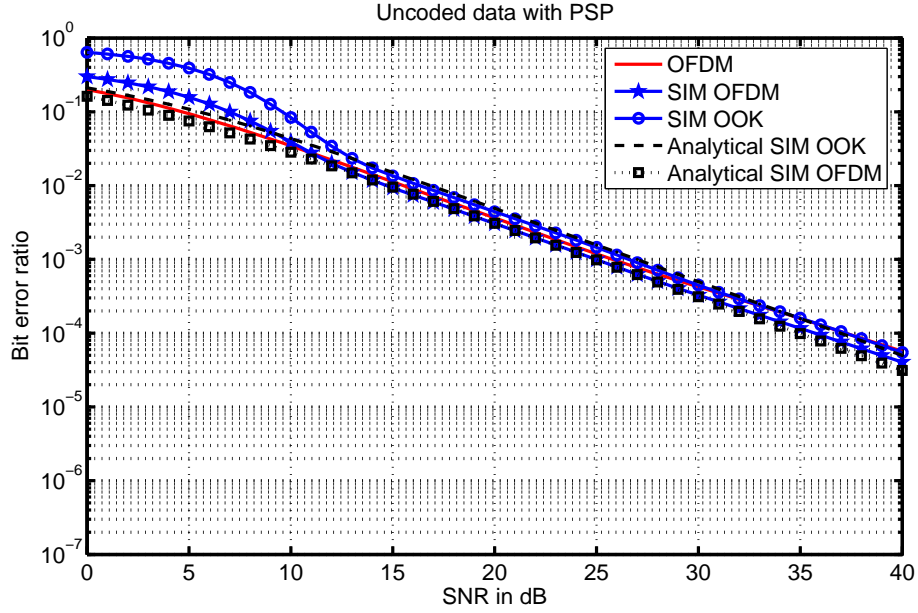
Figure 5.15: *Comparison of bit error ratio between SIM OFDM and OFDM for uncoded data under power saving policy*

5.6.4 Coded data with power reallocation policy

Fig. 5.16 shows the results for coded data using a convolutional encoder with $\frac{3}{4}$ coding rate where the constraint length vector is $[1\,2\,3]$ and the code-generator matrix is $[1\,1\,1\,1;\,0\,3\,1\,2;\,0\,2\,5\,5]$. Channel coding and interleaving are applied to each OFDM symbol. Channel coding is applied to the bits before splitting the incoming bit-stream into two bit-substreams. The bits received after OFDM demodulation and detection are block de-interleaved and then decoded using hard Viterbi decoder. For sake of brevity, the details of channel coding and decoding techniques are not considered in this thesis. The interested reader can refer to [93, 141] for detailed description.

By comparing the BER of SIM OFDM against conventional OFDM, it can be seen that the SNR gain is about 36-32=4 dB for a BER of 10^{-6} and it slightly decreases with increasing SNR. Note that this gain is similar to the gain achieved in the uncoded case. This observation affirms the results obtained in Fig. 5.14, while the significant enhancement in the BER curves compared to the uncoded data case is solely due to the channel coding gain.
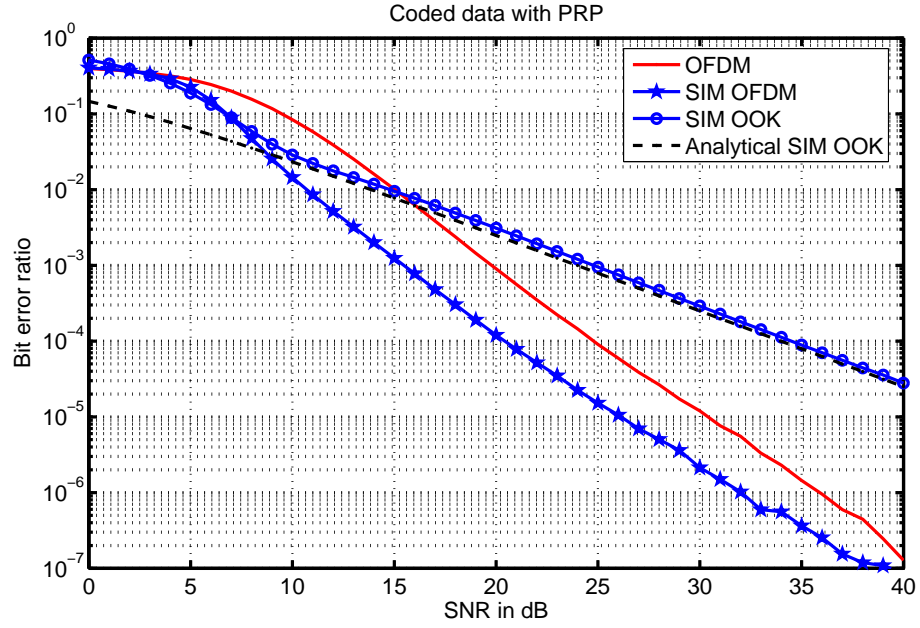
Figure 5.16: *Comparison of bit error ratio between SIM OFDM and OFDM for coded data*

5.7 Summary

In this chapter the key advantages of SIM OFDM were presented and can be summarized as follows:

- Exploit a new dimension for information transmission.

- Per subcarrier allocated transmit power increases when PRP is used, which results in improved error rate performance compared to conventional OFDM.

- PSP makes SIM OFDM a potential candidate for power efficient systems and green radio applications.

- Reduction in the inter-subcarrier-interference and more robustness in frequency selective fading channels Note that this feature is subject to future assessment since ideal synchronization is assumed throughout this work.

- Extra-subcarriers provide potential gain in the spectral efficiency.

- Simple subcarrier status detection using existing technology (coherent OOK detection).

- According to the second algorithm for detecting the type of the majority bit-value,which subject to further study in the future, additional overhead can be completely avoided.

Furthermore, an analytical model of BER of SIM OFDM was derived in this chapter. Also, a generalization of the SIM concept was presented with aid of examples which demonstrated the simplicity of extending the SIM concept to other dimensions such as time, and space. Finally, this chapter demonstrated via simulations that SIM OFDM always increases system reliability and/or spectral efficiency. However, power efficiency can be traded of against BER performance compared to conventional OFDM. In all the results presented in this chapter, it was clearly shown that both analytical and simulation results match closely. However, since the current analytical BER assumes that the two consecutive estimation process of SIM OFDM are independent and does not consider the error probability of estimating the type of the majority bit-value, a mismatch in the results can be noticed at the low SNR regime.

Chapter 6

Conclusions and future developments

6.1 Conclusions

In chapter 4, it has been shown that interference-limited systems with implicit signalling of the interference at both transmit and receive entities, enabled by the interference-weighted channel sounding, can achieve higher throughput than systems which utilize the conventional channel sounding pilots.

Compared to both blind-metric and link-gain-aware-metric, simulations results show that a gain at the 10th percentile cell capacity of 150% and 35%, respectively, has been achieved when downlink interference-aware-metric is used with maximum capacity criterion. By considering the score-based policy, simulations show that using the link-protection-aware-metric results in a gain at the 10th percentile user capacity of 230% and 15% compared to both downlink and uplink interference-aware-metric, respectively. Moreover, for the case of maximum capacity, it has been found that the respective gains are 30% and 15%, respectively. However, marginal capacity gains have been obtained for the proportional fair policy which ensures fairness at the expense of throughput efficiency.

Utilizing the proposed heuristic algorithm significantly reduces the computational complexity to approximately 0.05% of the complexity of the exhaustive search approach. This reduction in complexity is achieved at the cost of 8% loss at the 10th percentile cell capacity.

Furthermore, the impact of the link-protection-aware-metric and the downlink interference-

aware-metric on the fairness of the scheduling criteria has been investigated. The simulation results have shown that the behavior of the scheduling criteria are not affected. On the one hand, using the IWCS enabled optimization metrics results in an enhanced system performance in terms of system throughput at the cost of a slight degradation in the fairness performance compared to the blind-metric for MC and SP criteria. On the other hand, a better fairness performance compared to all CCS enabled optimization metrics is exhibited when PF policy is used.

In the context of research aimed at finding new degrees of freedom for better spectral efficiency such as spatial modulation (SM), and space shift keying (SSK) [75, 78], and in order to meet the continuous demand for increased data rates, an efficient OFDM-based modulation technique is developed in this thesis, specifically in chapter 5, and can be considered as the second major contribution of this thesis.

The underlying idea of SM was a main source of inspiration for the thesis to exploit the subcarrier orthogonality of SU-SISO OFDM wireless systems in an innovative fashion to add a new dimension to the complex 2-D signal plan. The resultant new dimension devised in this thesis is referred to as subcarrier-index dimension.

A novel spectral efficient multi-carrier modulation scheme has been developed to utilize the subcarrier-index dimension. The new SIM scheme maps a stream of bits into the indices of the available subcarriers in an on-off keying fashion. In this context, the subcarrier-index modulator activates a subset of subcarriers whose indices are associated with those bits of the majority bit-value to guarantee no degradation in the throughput compared to 4-QAM OFDM. Moreover, the subcarrier-index detection involves negligible complexity at the receiver.

In order to support the simulation results, a closed form expression of the error probability of SIM OFDM using different power allocation policies is derived. The analytical and simulation results of the error probability match closely for different power allocation policies. Furthermore, simulation results show error probability performance gain of 4 dB over 4-QAM OFDM systems for both coded and uncoded data without power saving policy. Alternatively, power saving policy maintains an average gain of 1 dB while only using half OFDM symbol transmit power.

Two algorithms are proposed to detect the type of the majority bit-value at the receiver. The first detection algorithm relies on explicit signalling where the excess-subcarriers are used to

convey this control information. The second detection algorithm can be classified as a non-coherent detection approach since signalling is no longer required. The details of the second algorithm are subject to further study. SIM OFDM always increases system reliability and/or spectral efficiency, but power efficiency can be traded of against BER performance compared to pure OFDM.

One of the powerful features of the SIM concept is its extendability to other dimensions such as time and space. This feature makes the generalized version of SIM, referred to as domain-specific resource-index modulation, a promising technique to enhance throughput and/or power efficiency.

6.2 Limitations and future work

Throughout this thesis a perfect channel estimation is assumed. Therefore, investigating the effect of realistic channel estimation on the system performance merits more work to be conducted in the future.

Also, A full buffer scenario has been used by the system level simulator. However, In real MU-MIMO scenarios, different Internet-based services are expected in future wireless communication applications. Hence, a realistic traffic model has to be integrated with the simulator. Consequently, different traffic models have to be investigated in order to assess their compatibility with the considered optimization problem.

Furthermore, after implementing an appropriate traffic model, the fairness measurements can be extended to use different fairness analysis approaches such as the Jain's fairness index [131, 142].

Moreover, since a hybridization of OFDMA/SDMA is envisaged for LTE-advanced systems, involving the frequency domain diversity techniques will be a very relevant topic to study in such optimization problem. However, the involved computational complicity will increase rapidly. Therefore, further complexity reduction algorithms could be investigated.

The analytical model derived in Chapter 5 assumed that SIM OFDM detection consist of two independent estimation processes. However, this is not generally correct. For instance, erroneous detection of the subcarrier activity results in estimation errors in the second estimation process (e.g. 4-QAM detection). Therefore, by considering that the two estimation processes are de-

pendent, the derivation of the analytical BER performance will be more correct. Consequently, the gap between the analytical and simulation results in the low SNR regime is expected to be diminished significantly.

In the future, one of the main goals is to study the influence of different interleaving and/or channel coding methods on the distribution of the excess-subcarriers, and to investigate the involved trade-off between spectral efficiency and BER performance. Also, since only hard decoding is considered in this work, the performance of the proposed SIM OFDM technique with soft decoder is subject to future investigation.

In an attempt to further exploit the gain in the subcarrier SNR, future research directions will involve adaptive power/modulation techniques as potential candidates to be integrated with the SIM concept.

Note that the study associated with IWCS concept was carried out using system level analysis and focused on multiuser and spatial diversity techniques for closed-loop SDMA without considering the frequency domain DoF. In contrast, the comparative study between conventional OFDM and SIM OFDM used link level analysis and focused on open-loop single user SISO OFDM without considering the DoFs of the study associated with the IWCS concept. Hence, both of the studies were conducted separately from each other. Therefore, an interesting future direction of this work could be the integration of both concepts within the framework of cross-layer optimization in wireless networks.

A possible framework that combines both concepts can be a smart antenna-aided multicarrier transmission system where the available DoFs (space, frequency, and multiuser) can be jointly optimized. In such system, the generalized form of the SIM concept can be implemented on a per-link basis.

Channel estimation example: MIMO-OFDM scenario

The channel frequency response (CFR) at the receiver can be estimated by training sequence based method, also known as pilot aided channel estimation (PACE). Training based methods use pilot signals in specific sub-channels to estimate the channel and interpolate the values to the remaining sub-channels. The disadvantage of this method is that it consumes fixed amount of bandwidth for channel estimation. But offers the advantage of decoupling data detection and channel estimation, thereby reducing the receiver complexity [88]. A simple extension of channel estimation techniques used in SISO OFDM system to MIMO OFDM system is not favorable, since the received signal is a sum of signals from multiple transmit antennas and the pilot signals from the transmit antennas need to be perfectly de-correlated to estimate the multiple channels between transmit and receive arrays. In order to achieve this, one pilot-subcarrier is allocated to only one antenna at a time. This approach has certain drawbacks such as high PAPR and reduced pilot sub-channels for each antenna. Fig. A.1 and Fig. A.2 show the MIMO OFDM setup with pilot based channel estimation at both transmitter and receiver. The system has N_{FFT} sub-channels, N_T transmit and N_R receive antennas. The total number of pilot and data sub-channels are N_P and $N_{\mathrm{FFT}} - N_P$ respectively. In the simple least squares channel estimation, the pilot sub-channels are uniformly distributed among the N_T transmit antennas allowing N_P/N_T pilot sub-channels per transmit antenna. Let us assume that there are N_P pilot sub-channels and N_T transmit antennas. In this method, the total number of the pilot sub-channels should be a multiple of N_T; to allow a uniform distribution among the N_T
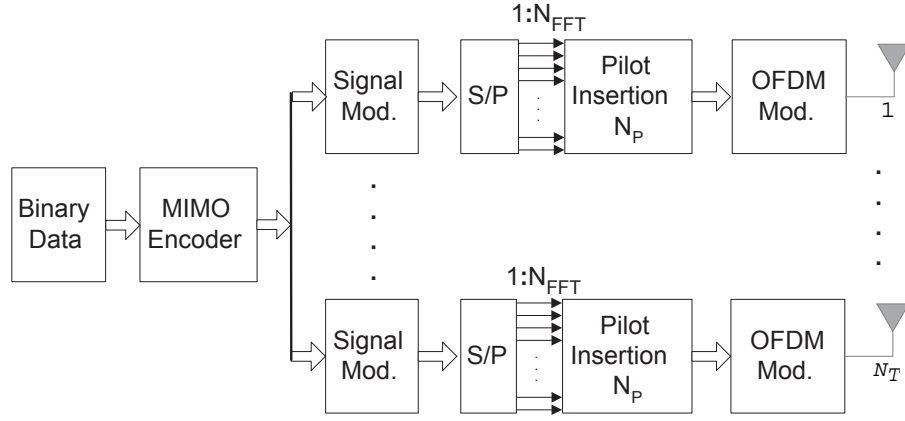
Figure A.1: *Example on MIMO-OFDM transmitter using PACE for channel estimation*
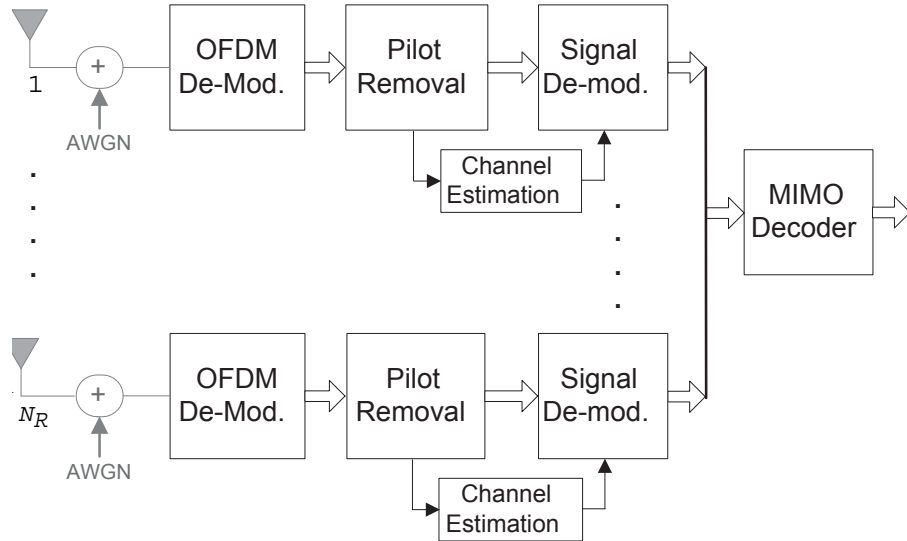
Figure A.2: *Example on MIMO-OFDM receiver using PACE for channel estimation*

transmit antennas. Hence, the pilot sub-channels are divided into N_T groups. The pilot sub-channel arrangement is such that only one transmit antenna uses that sub-channel and no pilot signal is transmitted in the same sub-channel by other antennas. Let K_κ where $\kappa = 1, 2, \ldots N_T$ be the set of pilot sub-channels used by κ^{th} transmit antenna to transmit pilot tones.

$$
\begin{aligned}
K_\kappa &= \frac{N_{FFT}}{N_P}(mN_T + 0.5) + \kappa - 2 \\
m &= 0, 1, \ldots N_P/N_T - 1; \quad \kappa = 1, 2, \ldots N_T
\end{aligned}
\tag{A.1}
$$

In frequency-selective channels, the pilot tones are equi-spaced on the FFT grid as in (A.1). In the sub-channels $k_\kappa \in K_\kappa$ each receive antenna receives pilot signal only from the κth transmit antenna and no signal from the other transmit antennas. For example, let $N_{FFT} = 64, N_P = 16$, and, $N_T = 4$, which means each antenna has 4 pilot sub-channels. Using (A.1), the first antenna will transmit its pilots on those subcarriers with indices 1, 21, 33, and 49, while the second antenna transmits on 2, 22, 34, and 50. Accordingly, the same goes for the rest of antennas.

The receive antenna ν estimates the channel transfer function in the pilot sub-channels corresponding to each transmit antenna.

$$
\hat{H}_{\nu,\kappa} = \frac{Y_\nu(k_\kappa)}{X(k_\kappa)} = H_{\nu,\kappa}(k_\kappa) + \frac{I_\nu(k_\kappa) + n_\nu(k_\kappa)}{X(k_\kappa)}
\tag{A.2}
$$

$$
k_\kappa \in K_\kappa; \quad \kappa = 1, 2, \ldots N_T; \quad \nu = 1, 2, \ldots N_R
\tag{A.3}
$$

where $Y_\nu(k_\kappa)$ is the received signal at the νth receive antenna in the pilot sub-channel k_κ, $X(k_\kappa)$ is the known transmit pilot signal at the sub-channel k_κ from the κth transmit antenna, $H_{\nu,\kappa}(k_\kappa)$ is the channel transfer function (CTF) between κ^{th} transmit and ν^{th} receive antenna at the k_κ^{th} sub-channel, $I_\nu(k_\kappa)$ and $n_\nu(k_\kappa)$ are the interference and noise component at the νth receive antenna in the k_κ^{th} sub-channel.

Appendix B

Publications

B.1 Published

- R. Abu-alhiga, H. Haas. *Implicit Pilot-Borne Interference Feedback for Multiuser MIMO TDD Systems*, the 10th International Symposium on Spread Spectrum Techniques and Applications (ISSSTA) 2008, August 25th - 28th, Bologna, Italy.

- R. Abu-alhiga, H. Haas. *Interference-Weighted Channel Sounding for Cellular SDMA-TDD Systems*. 69th IEEE Vehicular Technology Conference (VTC) 2009, April 26th - 29th, Barcelona, Spain.

- R. Abu-alhiga, H. Haas. *Subcarrier Index Modulation OFDM*. the 20th International Symposium on Personal, Indoor and Mobile Radio Communications (PIMRC) 2009, September 13th - 16th, Tokyo, Japan.

B.2 Pending

- R. Abu-alhiga, H. Haas. *Implicit Co-Channel Interference Signalling and Optimum Cross-Layer Scheduling in Cellular SDMA-TDD*. Submitted to IEEE Transaction on Wireless communications.

Implicit Pilot-Borne Interference Feedback for Multiuser MIMO TDD Systems

Rami Abu-alhiga and Harald Haas

Institute for Digital Communications, School of Engineering and Electronics, University of Edinburgh

EH9 3JL Edinburgh, UK. {r.abu-alhiga, h.haas}@ed.ac.uk

Abstract—In closed-loop future time division duplex (TDD) wireless systems, where channel reciprocity is maintained, uplink (UL) channel sounding method is considered as one of the most promising feedback methods due to its bandwidth and delay efficiency. However, in TDD interference-limited systems, conventional channel sounding pilots only provide instantaneous channel state information at the transmitter (CSIT), but knowledge about the level of the interference at the receiver cannot be obtained. Therefore, a scheduler cannot optimally exploit the available degree of freedom (DoF) in order to maximize the system capacity (e.g. the downlink (DL) sum capacity). In this paper, a novel interference feedback scheme is proposed to provide the base station (BS) with implicit knowledge about the interference level received by each mobile station (MS). It is proposed to weight the uplink channel sounding pilots by the level of the received interference at each MS. The weighted uplink channel sounding pilots act as a bandwidth-efficient and delay-efficient means for providing the BS with both, CSIT and the level of interference received by each active user. The performance of a system using weighted sounding pilots is compared against a system using non-weighted sounding pilots for both greedy (maximum capacity) as well as fair scheduling criteria such as proportional fair and score based scheduling policies. It is shown that the throughput is increased while fairness is not compromised.

I. Introduction

Multiple input multiple output (MIMO) communication is widely acknowledged as the key technology for achieving high data rates in future wireless systems (e.g. the evolved universal terrestrial radio access (EUTRA) study item launched in the 3rd generation partnership project (3GPP) long term evolution (LTE) concept [1], [2]). The availability of CSIT by the BS is a key enabler in multiuser communications to optimally incorporate elements from various spatial technologies such as adaptive beamforming, antenna selection, spatial multiplexing, and spatial division multiple access (SDMA) in order to increase the overall system capacity. For instance, in 3GPP LTE framework, link performance can be improved by adapting the characteristics of the transmitted MIMO signal to the current channel conditions [3]–[5]. Such techniques are sometimes referred to as closed-loop transmission methods.

According to the 3GPP Release 8 specification documents [1], the BS is equipped with a number of smart antennas (effective antennas) which is greater than the number of the antennas at the MS. If this is combined with the adaptive directionality feature of the antennas at the BS adopted in the 3GPP LTE framework, a group of users can be dynamically scheduled to receive simultaneously on a particular time-frequency resource over different spatial channels (in SDMA fashion) [6], [7]. In other words, a directional antenna assignment based on the channel quality of the different spatial channels can be performed leading to MIMO channel-dependent scheduling. While initial interest was focused on single-user links, more recently there have been a number of investigations in multiuser MIMO communication [7], [8].

In general, there are two methods for providing a BS with instantaneous knowledge of the fading channel conditions between the BS and MS [4], [9]. The first method is called direct feedback and involves the MS measuring the DL channel and transmitting a feedback message to the BS over the uplink, e.g. short-term signal-to-interference-plus-noise-ratio (SINR) reports. In addition, this feedback message must contain enough information to enable the BS to perform the closed-loop transmission on the DL (e.g., a quantized channel response). In systems where the BSs are equipped with large number of transmit antennas, the amount of feedback information needed to accurately specify the DL channel response of all possible spatial channels can be significant. The second method is called channel sounding and involves the BS estimating the DL channel based on channel response estimates obtained from reference signals (pilots) received from the MS during UL transmission. The key assumption behind channel sounding is that the UL and DL channels are reciprocal, which is reasonable to assume in TDD systems.

In a cellular environment, especially with frequency reuse of one, there will often be co-channel interference (CCI) from other cells, which becomes the dominating channel impairment. Hence, knowledge of the CSIT at the BS is only incomplete information in such interference-limited environments. Therefore, considering only the uplink CSIT at the BS as the selection metric of the antenna subsets for multiuser scenarios will be sub-optimal due to the fact that each user is exposed to different interference levels. Thus, by providing an implicit knowledge of the interference level for each user at the BS, the antenna selection process can be made more efficient. Therefore, the envisaged scheduler jointly assigns the optimum subset of antennas dependant on channel fading conditions and schedules the optimum group of users dependant on the received interference level.

In a TDD system, there are several convincing reasons for applying channel sounding rather than direct feedback. Firstly, in direct feedback, the air interface must enable the MS to estimate the channel between its antennas and, for instance, eight transmit antennas at the BS. Such estimation imposes a heavy processing load on a MS in a direct feedback scheme, while in a channel sounding scheme it takes place at the BS side [10]. Secondly, direct feedback schemes tend to have much higher latency between the time of the channel estimation and the time of the subsequent DL transmission. This difference in latency can have serious consequences on the performance of closed-loop transmission schemes in mobile channels. But, the direct feedback channel can also be

used to send a low rate quantized information about the SINR at the MS to the BS. Such feature is generally not available in channel sounding. Due to the superiority of channel sounding in terms of overhead, complexity, estimation reliability, and delay, it is considered here, and with the proposed modification outlined in the next section, the level of interference at the MS can be signalled to the BS.

The rest of the paper is organized as follows. Section II presents the interference sounding technique. The scheduling criteria used for assessment are summarized in Section III. Section IV proposes two complexity reduction approaches. System model and simulation results are presented in Sections V and VI, respectively. Finally, conclusions are given in Section VII.

II. INTERFERENCE FEEDBACK SIGNALING USING CHANNEL SOUNDING PILOTS

This section motivates the proposed modification to the conventional sounding pilots (the main contribution of this paper). A brief overview of the conventional sounding pilots is giving and followed by a detailed mathematical model of the modified sounding pilots.

The notion of multiuser diversity opens up the following set of questions. In a spatial multiplexing system with an excess of directional antennas at the BS, how should the optimal set of spatially separable users be chosen? What is the appropriate allocation of the transmit antennas (spatial resources) targeting the selected users? Since conventional soundings pilots only provide sub-optimal metric, how can a better metric be provided, e.g. instantaneous SINR, for such optimization problem while maintaining the same inherent feedback bandwidth and delay efficiency?

In this paper, it is assumed that the number of directional antennas at the BS is greater than the number of antennas at the MS, as is the case in EUTRA. Algorithms that achieve spatial multiplexing gains such as vertical Bell labs layered space-time (V-BLAST) algorithm [11], however, require that the number of antennas at the receiver is greater than or equal to the number of transmit antennas. Such circumstance resembles a spatial DoF for the selection of a subset of transmit antennas for DL transmission. In addition, the multiuser Dof is another dimension of diversity as shown later. It is worth mentioning that the frequency domain DoF (e.g. frequency channel dependent scheduling and frequency domain link adaptation) is not considered in this paper.

Furthermore, in EUTRA uplink sounding, the MS transmits a sounding waveform on the uplink and the BS estimates the uplink channel to the MS from the received sounding waveform. The sounding pilot sequences are chosen to be orthogonal among all of the users' antennas and also are designed to have a low peak to average power ratio (PAPR) in the time domain. In 3GPP technical documents the details of uplink sounding are given [9], [12].

In order to answer the previously mentioned questions, it is suggested here to exploit the channel reciprocity in TDD to jointly utilize these degrees of freedom for maximizing total throughput. In order to enable the BS to extract the CSI plus the level of interference at all active MSs, it is proposed to weight the uplink channel sounding pilots by the magnitude of the interference received at each MS (resembling implicit signalling of the instantaneous DL SINR).

Consider an EUTRA-like cellular interference-limited scenario with a BS equipped with N_{BS} antennas and N_U active users, each equipped with N_{MS} antennas. The conventional MS-to-BS sounding pilots transmission can be modeled as follows:

$$y_u(i) = H_u(i)x_u(i) + n(i) \qquad (1)$$

where u is the user index, and i is the time index. The predetermined pilot signal $x_k(i)$ is N_{MS}-dimensional vector; the received signal $y_u(i)$ is N_{BS}-dimensional vector; $n(i)$ is the independent, identically distributed (i.i.d.) complex Gaussian noise. The channel of user u at time instant i is represented by $H_u(i)$, which is an $N_{MS} \times N_{BS}$ matrix with complex entries. Fundamentally, conventional sounding pilots can be used to estimate two metrics: distance-dependent link gain, and the multipath fading channel matrix $H_u(i)$. By weighting (1) by the interference experienced by user u, the interference-weighted channel sounding transmission can be written as follows:

$$y_u(i) = \frac{H_u(i)x_u(i)}{\|I_u^{DL}(i)\|} + n(i) \qquad (2)$$

where $\|I_u^{DL}\|$ is the amplitude of the interference experienced by user u at the end of the previous DL. Consequently, the interference-weighting concept enables the sounding pilots to be used to obtain $\frac{\|H_u(i)\|^2 \|x_u(i)\|^2}{\|I_u^{DL}(i)\|^2}$ (instantaneous SINR), which is the optimal metric for DL joint scheduling and transmit antenna selection.
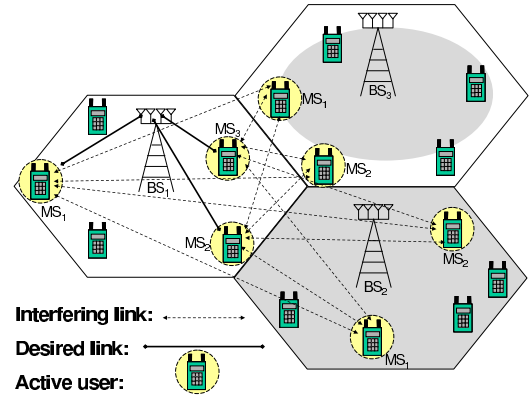
Fig. 1. Interference-limited multiuser MIMO system where each BS is equipped with 4 antennas, each MS is equipped with 2 antennas, and the active users are highlighted using dashed line circles.

In the example illustrated in Fig. 1, each BS equipped with 4 directional antennas will select 2 MSs each equipped with 2 antennas to access its spatial resource. Clearly, each MS is vulnerable to independent level of interference over the interfering links, and sees independent channel conditions over the desired link. For instance, the BS in the white cell can schedule 2 users out of 3 active users requesting access to the spatial resources. For any active user, 2 antennas out of 4 can be selected as transmit antennas. Using combinatorial basics, the BS has 18 possible selections. In general the problem statement can be formulated as follows: in how many ways

can a BS distribute N_{BS} antennas among $\frac{N_{\text{BS}}}{N_{\text{MS}}}$ users out of user population of size N_{U}, where a selected user will be receiving exactly from N_{MS} antennas? Then, which is the one that maximizes the DL multiuser capacity?

In the simulations, three cases are examined in which 3 different channel metrics will be used by the BS scheduler to exhaustively search over all possible solutions for the optimal solution according to 3 different scheduling criteria. In the first case, the scheduler uses only perfect instantaneous measurements of the MIMO multipath fading channel coefficients (ignoring the link gain). This scheduler is fair by nature due to the uniform distribution of the users and the i.i.d. distributed fading, and it will be referred to as blind scheduler. In the second case, the scheduler uses instantaneous measurements of the distance-dependent link gain. In contrast, this scheduler is greedy by nature because it tends, in most of the cases, to select those users which are closer to the BS, and it will be referred to as link-gain-aware scheduler. In the third case, the scheduler uses instantaneous measurements of the CSI divided by the interference level at the MS; this scheduler will be referred as interference-aware scheduler.

According to MIMO literature (e.g. [5]), the capacity of MIMO channel can be expressed as the sum of capacities of r single input single output (SISO) channels each weighted with power gain λ_{u_i} where ($i \in 1...r$), r is the rank of the channel, and λ_{u_i} are the eigenvalues of $H_u H_u^H$. Thus, the MIMO capacity can be written as follows:

$$C_u = \sum_{i=1}^{r} \log_2(1 + \frac{x_u^2}{N_{\text{MS}} \times \|I_u^{DL}\|^2} \lambda_{u_i}) \qquad (3)$$

To extract the channel metrics needed for each of the blind and the link-gain-aware schedulers, the channel of each possible spatial $N_{\text{MS}} \times N_{\text{MS}}$ MIMO channel must be diagonalized via the singular value decomposition (SVD) for each user. Then, the BS assembles multiple sets of orthogonal assignments of the directional antennas (antennas cannot be shared by different users due to the SDMA orthogonality constraints). Then, the BS associates each set of antenna assignment with all possible selections of the scheduled users. After that, the BS sums the eigenvalues of each possible assignment of the directional antennas for each possible selection of the scheduled subset of users. The sum of the eigenvalues will be used differently by each scheduler according to the scheduling criterion in order to find the optimum solution through exhaustive search (ES) over all possible solutions.

In the proposed method, modified eigenvalues (weighted by the interference level) are obtained at the BS by applying channel decomposition on the UL channel estimated from the weighted sounding pilots. Analogously, the sum of the modified channel eigenvalues of each possible spatial channel forms the basis for the optimization. A key advantage of this idea is that a significant amount of signal processing needed for conveying the interference received at all MSs is moved from the MS to the BS, which generally can tolerate higher processing power since there are no power limitations. Another key advantage of the proposed method is that no extra overhead is needed to convey such knowledge of interference to the BS. It is important to notice that in EUTRA-like systems, the channel sounding pilots are different from the demodulation pilots and are not used for any data

detection processes. Hence, the coherent UL data detection will not be affected by the interference weighting method because the channel sounding pilots are not involved in the data demodulation process.

As an outlook, this paper also proposes a method to accommodate the interference-weighted uplink sounding pilots to support UL scheduling. Since the interference experienced at the BS $\|I_j^{UL}\|$ where ($j \in 1...N_{\text{BS}}$) is different from the one experienced at the MS $\|I_u^{DL}\|$, it is proposed that the BS weights the metric estimated using the interference-weighted UL sounding pilots $\frac{\|H_u\|^2 \|x_u(i)\|^2}{\|I_u^{DL}\|^2}$ by the power of the received interference at each directional antenna $\|I_j^{UL}\|^2$, which is assumed to be known at the BS side. Thus, the new uplink scheduling metric $\frac{\|H_u\|^2 \|x_u(i)\|^2}{\|I_u^{DL}\|^2 \|I_j^{UL}\|^2}$ allows the BS to decide which subset of receiving antennas to use, and which users can be beneficially grouped together. In particular, a BS can use this metric to jointly select a subset of antennas experiencing healthy channel conditions and low interference to receive from a subset of users causing low interference to the neighboring cells, which forms a link-protection for the active MSs in the neighboring cells (shaded and semi-shaded cells in Fig. 1). The key assumption is that the intercell CCI experienced by a MS during DL and the interference caused by the same MS towards the MSs in the neighboring cells during UL are reciprocal, this is indicated using double-arrows for the interfering links in Fig. 1. This holds as long as fixed transmit power is used by all entities, and the same set of entities from the neighboring cells are to be scheduled for the subsequent scheduling period.

III. SCHEDULING CRITERIA

In this paper, each one of the considered antenna selection metrics is examined for three scheduling criteria. Specifically, one greedy criterion, named maximum capacity (MC), and two fair criteria, named proportional-fair (PF) [13], [14] and score-based (SB) [15] are considered. MC criteria always select the antenna's assignment of the users with the highest eigenvalue sum, hence, it is efficient in terms of overall throughput but may look oppressive for low SINR users, typically located far from the BS. PF criterion seeks to select the antenna's assignment of the users with highest eigenvalue sum relative to their current mean eigenvalue sum, which makes PF scheduler realize a reasonable trade-off between throughput efficiency and fairness. SB scheduler selects the antenna's assignment of the users with the best scores. In SB criterion, the score corresponds to the rank of the current eigenvalue sum among the past values observed over a window of a particular size. The achievable capacity according to each scheduling criterion can be formulated as follows:

$$C^{\text{MC}} = \underset{u \in 1...N_{\text{U}}}{\arg\max}\{C_u\} \qquad (4)$$

$$C^{\text{PF}} = \underset{u \in 1...N_{\text{U}}}{\arg\max}\{\frac{C_u}{T_u}\} \qquad (5)$$

$$C^{\text{SB}} = \underset{u \in 1...N_{\text{U}}}{\arg\min}\{S_u\} \qquad (6)$$

Where C^{MC}, C^{MC}, and C^{MC} are the achievable capacity using MC, PF, and SB criteria, respectively, C_u is the instantaneous capacity of user u, T_u is the current average capacity,

and S_u is the rank of the current capacity among the past values observed over of certain window in time.

IV. Heuristic Algorithms For Computational Complexity Reduction

In this paper, the simulation results are obtained using ES approach, where the scheduler broadly searches over all possible solutions. However, in this section we propose two heuristic algorithms (HA) to reduce the involved complexity. The exhaustive optimization complexity of scheduling for multiuser MIMO downlink system depends on the total number of users N_U, the number of directional transmit antennas at the BS N_{BS}, and the number of receive antennas at each MS N_{MS}. The search burden for the optimal scheduler is proportional to the sample-space population (SP) (the size of the pool containing all valid combinations of the spatial resources assignments). Using combinatorial fundamentals, (7) and (8) can be obtained. (7) and (8) are general formulation of the SP as a function of N_U, N_{BS}, and N_{MS}.

It can be seen from (8) that the multiuser diversity is exploited if and only if $N_U > \frac{N_{BS}}{N_{MS}}$.

If $N_U \leq \frac{N_{BS}}{N_{MS}}$

$$\text{SP} = \underbrace{\frac{N_{BS}!}{\left((N_{MS}!)^{N_U} \times (N_{BS} - N_U N_{MS})!\right)}}_{\text{MIMO DoF}}; \qquad (7)$$

if $N_U \geq \frac{N_{BS}}{N_{MS}}$

$$\text{SP} = \underbrace{\frac{N_U!}{\left(\left(\frac{N_{BS}}{N_{MS}}\right)! \times \left(N_U - \frac{N_{BS}}{N_{MS}}\right)!\right)}}_{\text{Multiuser DoF}} \times \underbrace{\frac{N_{BS}!}{(N_{MS}!)^{\left(\frac{N_{BS}}{N_{MS}}\right)}}}_{\text{MIMO DoF}}. \qquad (8)$$

It is important to mention that (7) and (8) are applicable only for scenarios in which N_{BS} is multiple of N_{MS}. To practically tackle this optimization problem, SP must be reduced. Two approaches are proposed in this paper to reduce SP. Namely, the interference-based user elimination approach, and the angle of arrival (AoA) based sectorization approach. The former aims to reduce SP by suppressing those users exposed to interference level greater than a predetermined interference threshold. The latter converts the cell of interest (CoI) optimization problem into smaller optimization problems, which can be optimized simultaneously. This can be done by sectorizing the cell based on the AoA of the uplink sounding channel into many sectors. Then the antennas at the BS are distributed among these sectors according to the user density of each sector. Therefore, by sectorizing the coverage space of the CoI into multiple sectors, the original SP of the CoI will be reduced significantly into smaller SPs of parallel per-sector optimization problems.

V. Simulation Platform

The simulation is carried out under the assumption of hexagonal multicell layout with frequency reuse of one. The 3GPP spatial channel model has been used to model the propagation channel [1], [16]. Using the parameters given in Table I, a 19-cell cellular TDD system with uniform user distribution is simulated via Monte Carlo method. The DL performance in the CoI is analyzed for a asynchronous CCI scenario, where the two possible link-directions (UL or DL) are equally likely to occur for each interfering cell independently from each other.

TABLE I
SIMULATION PARAMETERS

BS-to-BS distance	300 m
Number of interfering tiers	2
Transmitting power	30 dBm
Number of users	200
Number of antennas at BS	6
Number of antennas at MS	2
shadowing standard deviation	8 dB
Path loss model (dB)	$31.5 + 35 \log 10(d)$

VI. Simulation Results

The main assessment metrics are the per-user DL MIMO capacity in the CoI which can be calculated using (3), and the CoI DL cell capacity which is defined as the sum capacity of the three scheduled users. In order to shed some light on fairness of the considered feedback methods, the cumulative distribution function (cdf) of the served user distance to the BS is obtained for all considered scheduling criteria. The results in Fig. 2 show that the cell throughput can be significantly enhanced if knowledge of interference is taken into account in the antenna selection and MIMO user scheduling process. For example from Fig. 2, for the MC criterion, it can be seen that the median of the DL capacity of the interference-aware scheduler is 10 bits/s/Hz while it is 7.5 and 4 bits/s/Hz for the link-gain-aware and the blind schedulers, respectively. Analogously, the per-user capacity in the case of the interference-aware scheduler is substantially improved for all scheduling criteria. From Fig. 3, for the SB criterion, it can be seen that the 90th percentile of the per-user capacity resulting from the interference-aware scheduler is 9.5 bits/s/Hz while it is 7 and 7.5 bits/s/Hz for link-gain-aware and the blind schedulers, respectively. Fig. 4 shows that both the interference-aware and the link-gain-aware schedulers prioritize the users closer to the BS when MC criterion is used. For instance, Fig. 4, for the MC criterion, shows that the median of the served user's distance to the BS of the interference-aware and the link-gain-aware schedulers are 160 m and 140 m, respectively, while it is 190 m for the blind scheduler. Alternatively, when the PF criterion is used the interference-aware scheduler shows high level of fairness (its median is 220 m) compared to both of the blind (its median is 175 m) and the link-gain-aware (its median is 210 m) schedulers. It is worth noting that the blind scheduler fairness is slightly affected by using the SB and the PF criteria. This is expected due to the inherent fairness of this scheduler which is a consequence of ignoring the link gain, the random distribution of the users, and the i.i.d. distributed fading.

In order to address the efficiency of the HA, a study case has been simulated under the following assumptions: 8 directional antennas at the BS, 2 antennas at each MS, fixed sectorization is used to equally divide the cell into two sectors, only the best 8 users in terms of the experienced interference are considered in each cell, and MC is the scheduling criterion. It has been found using simulations that the SP has been reduced from
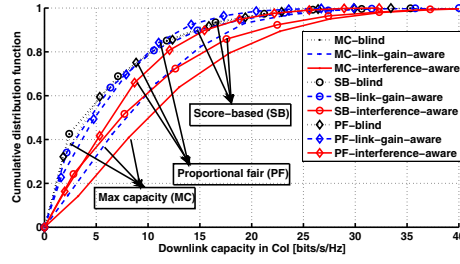
Fig. 2. Throughput comparison among the three considered schedulers using three different scheduling criteria.
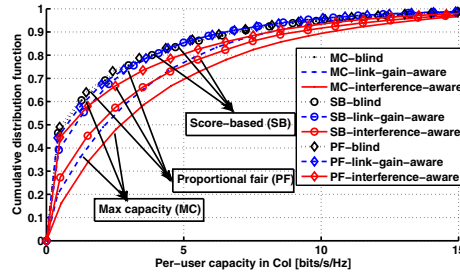

Fig. 3. User capacity comparison among the three considered schedulers using three different scheduling criteria.
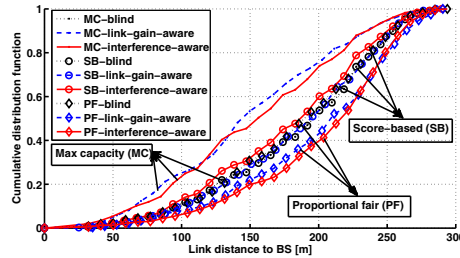

Fig. 4. Fairness comparison among the three considered schedulers using three different scheduling criteria.

176400 to 80 on average, at the cost that the median of the achievable capacity under the HA converges to approximately 90% of the median of the achievable capacity under the ES, as seen in Fig. 5.

VII. Conclusions

It has been shown that interference-limited systems with instantaneous interference knowledge, enabled by the interference-weighted sounding pilots, can achieve higher throughput than systems which utilize the classical non-weighted sounding pilots. Furthermore, the interference-aware scheduler outperforms both blind and link-gain-aware schedulers even when fair scheduling criteria are used. Using the proposed heuristic algorithms significantly reduces the com-
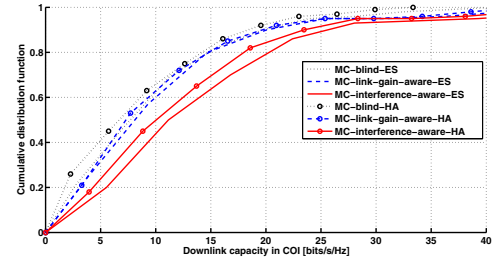

Fig. 5. Throughput comparison among the three considered schedulers using MC scheduling criterion via both ES and HA approaches.

putational complexity to approximately 0.05% of the involved complexity of the exhaustive search approach.

References

[1] 3rd Generation Partnership Project (3GPP), Technical Specification Group Radio Access Network, *Physical Channels and Modulation (Release 8)*, 3GPP Std. TS 36.211, Rev. 1.2.0.
[2] ——, *Summary of MIMO Schemes for EUTRA*, 3GPP Std. R1-051 238.
[3] A. Maaref and S. Aissa, "A Cross-Layer Design for MIMO Rayleigh Fading Channels," in *Canadian Conference on Electrical and Computer Engineering*, vol. 4, May 2–5 2004, pp. 2247–2250.
[4] D. J. Love, R. W. Heath Jr., W. Santipach, M. L. Honig, "What is the Value of Limited Feedback for MIMO Channels," *IEEE Communications Magazine*, Oct. 2004.
[5] E. Telatar, "Capacity of Multi-Antenna Gaussian Channels," *European Transaction on Telecommunications*, vol. 10, no. 6, pp. 585–595, Nov. 1996.
[6] J. K. Cavers, "Single-User and Multiuser Adaptive Maximal Ratio Transmission for Rayleigh Channels," *IEEE Transactions on Vehicular Technology*, vol. 49, no. 6, Nov. 2000.
[7] W. Choi, A. Forenza, J. G. Andrews, and R. W. Heath Jr., "Capacity of Opportunistic Space Division Multiple Access with Beam Selection," in *IEEE Global Telecommunications Conference (GLOBECOM)*, Nov. 2006, pp. 1–5.
[8] Z. Shen, R. Chen, J. Andrews, R. Heath, and B. Evans, "Low Complexity User Selection Algorithms for Multiuser MIMO Systems with Block Diagonalization," in *39th Asilomar Conference on Signals, Systems and Computers.*, Oct. 2005, pp. 628–632.
[9] 3rd Generation Partnership Project (3GPP), Technical Specification Group Radio Access Network, *Uplink Sounding for Obtaining MIMO Channel Information at NodeB in EUTRA*, 3GPP Std. R1-060 668, 2006.
[10] B. Hassibi and B. M. Hochwald, "How Much Training is Needed in Multiple-Antenna Wireless Links?" *IEEE Transactions on Information Theory*, vol. 49, pp. 951–963, 2003.
[11] G. J. Foschini, "Layered Space-Ttime Architecture for Wireless Communication in a Fading Environment when Using Multi-Element Antennas," *Bell Labs Technical Journal*, vol. 1, no. 2, pp. 41–59, Sep. 1996.
[12] 3rd Generation Partnership Project (3GPP), Technical Specification Group Radio Access Network, *EUTRA Downlink Pilot Requirements and Design*, 3GPP Std. R1-050 714, 2005.
[13] E.F. Chaponniere, P.J. Black, J.M. Holtzman, D.N.C. Tse, "Transmitter Directed Code Division Multiple Access System Using Path Diversity to Equitably Maximize Throughput," *US Patent 6449490*, 2002.
[14] P. Viswanath, D. Tse, and R. Laroia, "Opportunistic Beamforming Using Dumb Antennas," in *IEEE International Symposium on Information Theory*, 2002, p. 449.
[15] T. Bonald, "A Score-Based Opportunistic Scheduler for Fading Radio Channels," in *Proceedings of the 5th European Wireless Conference (EWC)*, Barcelona, Spain, Feb. 24–27, 2004.
[16] 3rd Generation Partnership Project (3GPP), Technical Specification Group Radio Access Network, *Spatial Channel Model for Multiple Input Multiple Output (MIMO)*, 3GPP Std. TR 25.996, Rev. 6.0.0, Jun. 2006.

Interference-Weighted Channel Sounding for Cellular SDMA-TDD Systems

Rami Abu-alhiga and Harald Haas

Institute for Digital Communications, School of Engineering and Electronics, The University of Edinburgh
EH9 3JL Edinburgh, UK. {r.abu-alhiga, h.haas}@ed.ac.uk

Abstract—In future time division duplex (TDD) wireless systems, where channel reciprocity is maintained, uplink (UL) channel sounding method is considered as one of the most promising feedback methods due to its bandwidth and delay efficiency. Conventional channel sounding only conveys the channel state information (CSI) of each active user to the base station (BS). Due to the limitation in system performance because of co-channel interference (CCI) from adjacent cells in interference-limited scenarios, CSI is only a suboptimal metric for multiuser spatial multiplexing optimization. Interference-weighted channel sounding (IWCS) is a spectrally efficient feedback technique that provides the base station (BS) with implicit knowledge about the interference experienced by each active user. The main contribution of this paper is to propose a novel way to make the IWCS pilots usable for improved UL performance. In this context, it is proposed to weight the metric obtained from the IWCS pilots by the interference experienced at the BS. The resultant new metric, which is implicitly dependent on downlink (DL) and UL interference, provides link-protection awareness and is used to jointly improve spectral efficiency in UL as well in DL. Using maximum capacity scheduling criterion, the link-protection aware metric results in a gain in the median system sum capacity of 26.7% and 12.5% in DL and UL respectively compared to the case when conventional channel sounding techniques are used.

I. Introduction

Multiple-input multiple-output (MIMO) communication is widely recognized as the key technology for achieving high data rates and for providing significant capacity improvements [1]. In a multiuser MIMO context, opportunistic approaches have recently attracted considerable attention [2, 3]. Opportunistic resource allocation in a multiuser MIMO scenario is still an open issue. Wong *et al.* [4] consider a multiuser MIMO system and focused on multiuser precoding. In DL multiuser MIMO channels, dirty-paper coding (DPC) [5], which uses successive interference precancelation by employing complex encoding and decoding, can achieve the maximum throughput [6]. This technique is computationally expensive and complex and its contribution primarily is to present bounds on the achievable sum capacity under a per-cell equal power constraint. Therefore, many alternative practical precoding approaches are proposed to offer a trade-off between complexity and performance [7–9]. One of the most attractive approaches is block diagonalization (BD), which supports orthogonal multiple stream transmission and the precoding matrix of each user is designed to lie in the null space of all remaining channels of other users, and hence the intra-cell multiuser interference is avoided [9].

In a multiuser MIMO context, SDMA multiplexes users in the same radio frequency spectrum (i.e. without separation in time, frequency or code) by granting the channel to spatially separable users. This multiple access technique can be achieved through exploitation of the spatial degree of freedom (DoF) represented by the excess number of directional (smart) antennas at the BS. Particularly, the BS steers orthogonal beams (spatial streams) to spatially dispersed MSs (mobile stations) [3]. The joint beam selection and user scheduling for orthogonal SDMA-TDD system is a key problem addressed in this paper. It is well known that the availability of CSI for all users at the BS is a key enabler in multiuser communications to optimally incorporate different precoding techniques such as BD, adaptive beamforming, or antenna selection, in order to increase the overall system spectral efficiency. Basically, there are two methods for providing a BS with CSI for all MSs. The first method is called direct feedback and involves the MS to measure the DL channel and to transmit a feedback message to the BS via the UL. The second method is called channel sounding and involves the BS to estimate the DL channel based on channel response estimates obtained from reference signals (pilots) received from the MS during UL transmission. Channel sounding offers advantages in terms of overhead, complexity, estimation reliability, and delay. Clearly, TDD systems offer a straightforward way for the BS to acquire the CSI enabled through channel reciprocity [10, 11]. The details of UL channel sounding can be found, for instance, in the technical documents of the evolved universal terrestrial radio access (EUTRA) study item launched in the 3rd generation partnership project (3GPP) long term evolution (LTE) concept, and particularly in [11, 12].

In a cellular environment, especially when full frequency reuse is considered, CCI becomes a key challenge as it can significantly degrade the performance of multiuser MIMO systems [13]. In other words, if the BS schedules a group of users only based on the available CSI, the scheduling decision might be *optimum* for a noise limited system, but high CCI at the respective MSs might render the scheduling decision greatly suboptimum. The signal-to-interference-plus-noise ratio (SINR) would be a more appropriate metric in interference limited scenarios, but this metric cannot directly be obtained from channel sounding. Thus, the challenge is to implicitly provide knowledge of interference observed by each user to the BS in addition to CSI. If, furthermore, interference observed at the BS itself is taken into account, the substream selection and user scheduling process can be jointly improved [14]. Using the concept of interference-weighted channel sounding pilots proposed in [14], the level of interference at each MS can implicitly be signalled to the BS.

In this paper, a further enhancement is proposed to integrate the usability of the IWCS enabled metrics for UL cross-layer optimization of directional antenna selection and user scheduling. The optimization metric enabled by this enhancement provides the scheduler with knowledge of the potential interference caused by the candidate users to already established links in the neighboring cells. The rest of the paper

is organized as follows. Section II gives a brief background about the interference-weighted channel sounding technique proposed in [14] and presents the new link-protection-aware metric. Scheduling criteria and system model are summarized in section III. Simulation results are discussed in section IV. Finally, conclusions are given in section V.

II. Interference-Weighted Channel Sounding

In multiuser spatial multiplexing systems, it is assumed that the number of directional antennas at the BS is greater than the number of antennas at the MS, as is the case in EUTRA. In addition to the multiuser DoF, this constitutes a spatial DoF for the selection of a subset of antennas for DL or UL transmission. In this context, an interesting question arises, namely which subset of antennas jointly optimizes UL and DL. It is worth mentioning that the time and frequency domain DoFs are not considered in this study.

In order to enable the BS to extract the CSI plus the level of interference experienced at all active MSs, it is proposed in [14] to weight the UL channel sounding pilots by the magnitude of the interference received at each MS. Thereby, the SINR at MS is implicitly signalled to the respective BS.

A. Interference-Aware Metric for Downlink Optimization

Consider the uplink channel sounding transmission of a SDMA cellular interference-limited scenario with a BS equipped with N_{BS} antennas and N_{U} active users, each equipped with N_{MS} antennas. A narrow-band flat-fading channel is assumed, which is satisfied if single carrier frequency division multiple access (also known as DFT-spread orthogonal frequency division multiplexing) is used, as envisaged for in EUTRA systems. The channel transfer matrix from the uth MS is given by a complex matrix $\mathbf{H}_u \in \mathbb{C}^{N_{\mathrm{BS}} \times N_{\mathrm{MS}}}$, where $H_u^{(j,i)}$ denotes the channel fading coefficient from the ith transmit antenna of the uth MS to the jth directional receive antenna at the BS. We assume that both the BS and MSs experience sufficient local scattering. Therefore, the entries of $\mathbf{H}_u$ are samples of a zero-mean Rayleigh distribution. Hence, the conventional channel sounding MS-to-BS pilots transmission can be modeled as follows:

$$\mathbf{y}_u(q) = \mathbf{H}_u(q)\mathbf{x}_u(q) + \mathbf{n}(q) \qquad (1)$$

where q is the time index. The predetermined pilot signal $\mathbf{x}_u(q)$ is N_{MS}-dimensional vector; the received signal $\mathbf{y}_u(q)$ is N_{BS}-dimensional vector; $\mathbf{n}(q)$ is the noise vector whose elements are the independently, identically distributed (i.i.d.) complex Gaussian noise random variables. conventional channel sounding pilots can be used to estimate two metrics: distance-dependent link gain, and the multipath fading channel coefficients. By weighting (1) by the interference experienced by user u in the downlink, the interference-weighted channel sounding transmission can be written as follows:

$$\mathbf{y}_u(q) = \frac{\mathbf{H}_u(q)\mathbf{x}_u(q)}{\|I_u^{\mathrm{DL}}(q-1)\|} + \mathbf{n}(q) \qquad (2)$$

where $\|I_u^{\mathrm{DL}}(q-1)\|$ is the amplitude of the CCI experienced by u^{th} MS at the $(q-1)$ time interval. Consequently, the interference-weighting concept enables the sounding pilots to be used by the BS to obtain DL interference-aware-metric $\mathbf{O}_u^{\mathrm{DL-IAM}}(q)$ which can be formulated as follows

$$\mathbf{O}_u^{\mathrm{DL-IAM}}(q) = \frac{\mathbf{H}_u(q)}{\|I_u^{\mathrm{DL}}(q-1)\|} \qquad (3)$$

From information theory point of view, this metric (the square root of instantaneous MIMO DL SINR) is optimal for DL joint user scheduling and transmit directional antenna selection; as it can simply be used to obtain the SINR at the user side. Alternatively, quantized SINR can be fed back via dedicated feedback channel, but this requires transmission resources and time (potentially causing outdated feedback).

B. Optimization Methodology

In the example illustrated in Fig. 1, each BS equipped with 4 directional antennas will select 2 MSs each equipped with 2 antennas to access its spatial resources. Clearly, each MS experiences independent levels of interference, and is subject to independent channel conditions on the desired link. For instance, the BS in cell 1 can schedule 2 users out of 3 possible candidates. For any active user, a BS can assign 2 out of 4 directional antennas to establish communication links. Using combinatorial basics, the BS has $\binom{3}{2}\binom{4}{2} = 18$ possible options to select antennas and user pairs in the given example.
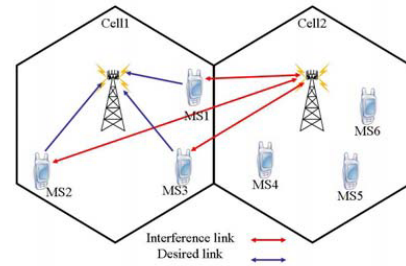
Fig. 1. Interference-limited multiuser MIMO system where each BS is equipped with 4 antennas, each MS is equipped with 2 antennas.

The procedure followed to extract the optimization metrics provided by IWCS pilots is illustrated in the example depicted in Fig. 2. Basically, each way in which the BS can distribute the 4 directional antennas among 2 out of 3 users forms a possible solution. From Fig. 2, two arbitrary solutions are highlighted by shading them with squares of different colors and different styles for the borderline. By considering the solution shaded by blue squares of solid borderline, it can be seen that MS1 is allocated the first two directional antennas, while MS3 is allocated the last two antennas. Clearly, it can be seen that each antenna allocation forms a square matrix containing the coefficients of the optimization metric. The next step is to obtain the eigenvalues of each square matrix via singular value decomposition (SVD). Afterwards, the eigenvalues of each group of selected users are summed. Finally, the summation of eigenvalues will be used differently according to the scheduling criterion in order to find the optimum solution among all possible solutions. To examine all possible solutions, a heuristic algorithm approach, also proposed in [14], is used for complexity reduction purposes.

C. Link-Protection-Aware Metric for Uplink and Downlink Optimization

The main purpose of this paper is to propose a method to accommodate the IWCS pilots to suit UL optimization. Since the amplitude of CCI experienced at the BS $\|I_j^{\mathrm{UL}}(q-1)\|$
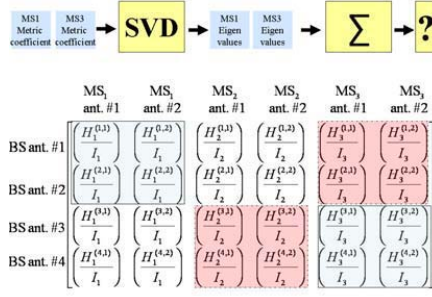
Fig. 2.   Interference-limited virtual multiuser MIMO matrix for the example illustrated in Fig. 1.

(referred to as UL interference) where $(j \in 1, \ldots, N_{\mathrm{BS}})$ is different from the CCI experienced at the MS $\|I_u^{\mathrm{DL}}(q-1)\|$, the DL interference-aware-metric in (3) is not suitable for UL optimization. In order to use the IWCS pilots for UL optimization, it is proposed that the BS weights each row of the metric defined in (3) by the received interference at the associated directional antenna $\|I_j^{\mathrm{UL}}(q-1)\|$ at the BS, which is assumed to be known at the BS side. Thus, the new optimization metric, referred to as link-protection-aware-metric, $\mathbf{O}_u^{\mathrm{LPAM}}(q)$ can be formulated as follows:

$$\mathbf{O}_u^{\mathrm{LPAM}}(q) = \frac{\mathbf{H}_u(q)}{\|I_u^{\mathrm{DL}}(q-1)\|\|I_j^{\mathrm{UL}}(q-1)\|} \qquad (4)$$

Basically, this metric allows the BS to decide which subset of receiving antennas to use, and which users can beneficially be grouped together. In particular, the BS can use this metric to jointly select a subset of directional antennas experiencing preferable channel conditions and low CCI. Since the link-protection-aware-metric is inversely proportional to $\|I_u^{\mathrm{DL}}(q-1)\|$, a MS experiencing low interference level has higher chances to be selected. Due to channel reciprocity, a user that receives little interference from a set of users (in Tx mode) in a particular time slot only causes little interference to the same set of users (now in Rx mode) at a different time slot. Therefore, the link-protection-aware-metric decreases the probability of scheduling users that are potential strong interferers. Consequently, this forms an inherent link-protection for the already established links in the neighboring cells, which results in an enhancement in the overall system performance. Similarly, this metric can be used for DL optimization to jointly select a subset of users experiencing preferable channel conditions and low CCI to receive from a subset of directional antennas causing low CCI to the neighboring cells. Note that the link-protection-aware-metric is simultaneously used to optimize both UL and DL. Hence, the cross-layer scheduling for UL has to be the same as for DL, which reduces the scheduling time.

According to MIMO literature [1], if the channel matrix $\mathbf{H}_u$ is known at the BS, then the DL capacity of single user MIMO channel can be expressed as the sum of capacities of r single-input single-output (SISO) channels each weighted with power gain λ_{u_i} where $(i \in 1, \ldots, r)$, r is the rank of the channel, and λ_{u_i} are the eigenvalues of $\mathbf{H}_u\mathbf{H}_u^H$. Assuming interference-

limited system, the MIMO capacity can be written as follows:

$$C_u = \sum_{i=1}^{r} \log_2(1 + \frac{x_u^2}{N_{\mathrm{MS}} \times \|I_u^{\mathrm{DL}}\|^2} \lambda_{u_i}) \qquad (5)$$

Using the system model previously introduced and (5), the optimization problem can be written as follows: According to an optimization utility function, the objective is to find the optimum way in which the BS distribute N_{BS} antennas among $\frac{N_{\mathrm{BS}}}{N_{\mathrm{MS}}}$ spatially separable users out of user population of size N_{U}, where a selected user communicates with exactly N_{MS} directional antennas at the BS. For instance, in the case of capacity-based optimization utility function, the optimum solution maximizes the capacity of multiuser MIMO channel at the expense of fairness. The sample-space population (SP) (the size of the pool containing all possible solutions) of such problem is formulated in [14]. The resulting optimization problem can be written as follows:

$$\arg\max_{v \subset \mathrm{SP}} \sum_{u=1}^{\frac{N_{\mathrm{BS}}}{N_{\mathrm{MS}}}} C_u^v \qquad (6)$$

D. Summary of the Optimization Metrics

In DL simulations, two cases are compared according to the considered scheduling criteria (section III summarizes them). Particularly, the DL interference-aware-metric $\mathbf{O}_u^{\mathrm{DL-IAM}}(q)$ is compared against the link-protection-aware-metric $\mathbf{O}_u^{\mathrm{LPAM}}(q)$ defined in (4). These two metrics can only be provided by the IWCS pilots or via explicit signalling. Similarly, two cases are examined in UL simulations. In the first case, the scheduler uses instantaneous measurements of the CSI divided by the interference level at the BS. This optimization metric, referred to as UL interference-aware-metric, $\mathbf{O}_u^{\mathrm{UL-IAM}}(q)$ can be written as follows:

$$\mathbf{O}_u^{\mathrm{UL-IAM}}(q) = \frac{\mathbf{H}_u(q)}{\|I_j^{\mathrm{UL}}(q-1)\|} \qquad (7)$$

where j is the directional antenna index. It is important to mention that this metric can be obtained using conventional channel sounding pilots since UL interference $\|I_j^{\mathrm{UL}}(q-1)\|$ is available at the BS without feedback. The second case is the link-protection-aware-metric defined in (4).

E. Numerical Example

To show the link-protection feature of the new metric defined in (4), a simple example is presented in Fig. 3. In this example, the arbitrary numbers quantifying the gain of each link and the interference experienced by each entity are used to estimate the achievable capacity using (5). It is assumed that cell 2 has an established DL transmission with MS3 and the argument of the current achievable DL capacity is $\frac{\mathrm{H_{MS3}}}{\mathrm{I_{MS3}}} = \frac{9}{3}$. Meanwhile, the BS in cell 1 attempts to select between MS1 and MS2 for UL transmission. If BS1 uses the UL interference-aware-metric, MS1 is scheduled for UL; $\frac{\mathrm{H_{MS1}}}{\mathrm{I_{BS1}}} = \frac{6}{2} > \frac{\mathrm{H_{MS2}}}{\mathrm{I_{BS1}}} = \frac{5}{2}$. Hence, the argument of the achievable UL capacity is $\frac{\mathrm{H_{MS1}}}{\mathrm{I_{BS1}}} = \frac{6}{2}$. As a result, it is assumed that the interference at MS3 increases to $\mathrm{I_{MS3}} = 4.5$ due to the low shadowing conditions between MS3 and MS1. This reduces the argument of the current achievable DL capacity in cell 2 to $\frac{9}{4.5}$. Thus, the arguments of the achievable system capacity are $\frac{6}{2}$ and $\frac{9}{4.5}$. On the other hand, if
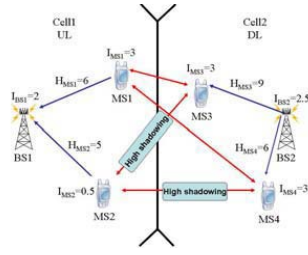
Fig. 3. Example of interference-limited 2-cell scenario with which the basic working principle of the link-protection-aware-metric is illustrated.

BS1 uses the link-protection-aware-metric, MS2 is scheduled for UL; $\frac{H_{MS1}}{I_{MS1} \times I_{BS1}} = \frac{6}{3 \times 2} < \frac{H_{MS2}}{I_{MS2} \times I_{BS1}} = \frac{5}{0.5 \times 2}$. Hence, the argument of the achievable UL capacity is $\frac{H_{MS1}}{I_{BS1}} = \frac{5}{2}$. Consequently, the interference at MS3 does not change (due to the high shadowing between MS2 and MS3), and therefore, the arguments of the achievable cell capacity are $\frac{5}{2}$ and $\frac{9}{3}$ for cell 1 and cell 2, respectively. As a summary, in the first case the sum of the arguments of the cell capacity is 5 whereas in the second case the sum is 5.5. Clearly, it can be seen from this example that the link-protection-aware-metric used in the second improves the overall spectral efficiency.

III. SCHEDULING CRITERIA AND SIMULATION PLATFORM

In this paper, the considered optimization metrics are tested using three scheduling criteria. Specifically, one greedy criterion, named maximum capacity (MC), and two fair criteria, named proportional-fair (PF) and score-based (SB), are considered. The details of the considered scheduling criteria and their achievable capacity can be found in [14] and the references within. It is important to mention that due to the large size of the SP, and the inherent integer nature of the rank in the SB criterion, several solutions can score the best rank (the first position). Therefore, out of those solutions satisfying the best rank condition, only one solution should be selected. In order to come out with a unique solution, MC criterion is chosen, in this work, to be applied on the subset of solutions satisfying the best rank condition. Throughout this paper, wherever the SB criterion is mentioned, it means that a hybrid version of both SB and MC criteria is applied. Due to the inherent greediness of MC criterion, the hybrid version of the SB policy tends to show greedy behavior. This greedy behavior increases as the SP size is increased.

TABLE I
SIMULATION PARAMETERS

Channel propagation environment	Suburban micro cell [12]
Number of users	1000
Lognormal shadowing standard deviation, σ_S	8 dB
Path loss model (dB)	$31.5 + 35 \log 10(d)$

A wrapped-around two-tier cellular platform consisting of hexagonal cells with a BS-to-BS distance of 300 m is used in the simulation. In each cell, BS and MSs are equipped with 8 and 2 antennas, respectively. Using the parameters given in Table I, the 19-cell cellular TDD system with uniform

user distribution is simulated via Monte Carlo method. The channel matrix of uth user $\mathbf{H}_u$ is a zero-mean i.i.d. complex Gaussian random matrix for the uncorrelated MIMO Rayleigh fading channel. The DL and UL performances are analyzed for asynchronous cells, where the two possible link-directions (UL or DL) occur equally likely and are cell independent. All entities (BSs and MSs) in the system use fixed transmit power of 30 dBm.

IV. SIMULATION RESULTS AND DISCUSSION

The performance of the different optimization metrics are assessed using the cumulative distribution function (cdf) of per-user capacity and cell capacity for both UL and DL. The per-user capacity is the 2×2 spatial multiplexing MIMO capacity which can be calculated using (5). The cell capacity is the sum capacity of the group of scheduled users.

A. The Uplink Performance

From Fig. 4(a), for the MC criterion, it can be seen that the UL median cell capacity using the link-protection-aware-metric is 27 bits/s/Hz which corresponds to an enhancement of 12.5% of the UL median cell capacity using the UL interference-aware-metric (24 bits/s/Hz). This gain can be attributed to the available knowledge at the scheduler about the users potentially causing high interference to the already established links in the neighboring cells. Hence, the link-protection-aware-metric enables the scheduler to select a group of users experiencing preferable shadowing conditions on the links that contribute to interference, i.e., this effectively results in interference mitigation. The previous observation can be affirmed by looking at the results of the per-user capacity of the link-protection-aware-metric, which outperforms the UL interference-aware-metric for all scheduling criteria considered. For instance, from Fig. 4(b), for the SB criterion, it can be seen that the median of the per-user capacity resulting from the link-protection-aware-metric is 2.9 bits/s/Hz while it is 2.5 bits/s/Hz for the UL interference-aware-metric. However, the PF criterion does not provide a noticeable improvement due to the inherent fair nature which hardly prevents strong interferers from being scheduled.

B. The Downlink Performance

The same analysis carried out in the previous subsection discussing the UL performance is applied for the DL case. From Fig. 5(a), for the MC criterion, it can be seen that the median of the DL capacity using the link-protection-aware-metric is 19 bits/s/Hz while it is 15 bits/s/Hz for the DL interference-aware-metric. Similarly, the per-user capacity in the case of the link-protection-aware-metric is improved for all scheduling criteria. From Fig. 5(b), for the SB criterion, it can be seen that the median of the per-user capacity resulting from the link-protection-aware-metric is 3.5 bits/s/Hz while it is 1.9 bits/s/Hz for the DL interference-aware-metric.

Irrespective of the nature of the employed scheduling criterion, the results show that the gain in the UL case is lower compared to DL. This is due to the fact that the detrimental effect of line-of-sight conditions among BSs degrades the link-protection selectivity in UL. Moreover, in SDMA a user located in a cell causes interference to all beams (and groups of antennas correspondingly) other than the served one. Given that all antenna groups at the BS site are in close proximity, the large-scale fading (log-normal shadowing) on the interference links can, thus, be considered the same. Therefore, the
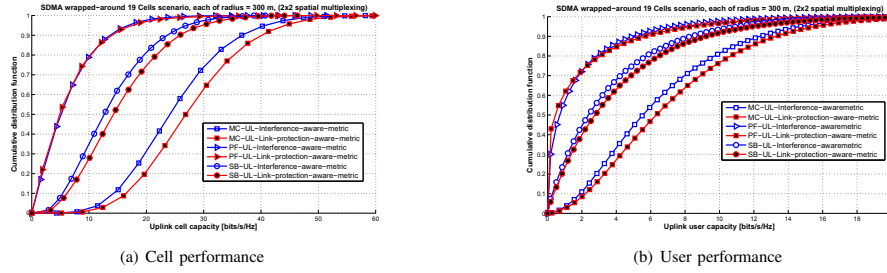
(a) Cell performance   (b) User performance

Fig. 4. Uplink performance comparison between the UL interference-aware-metric and the link-protection-aware-metric.

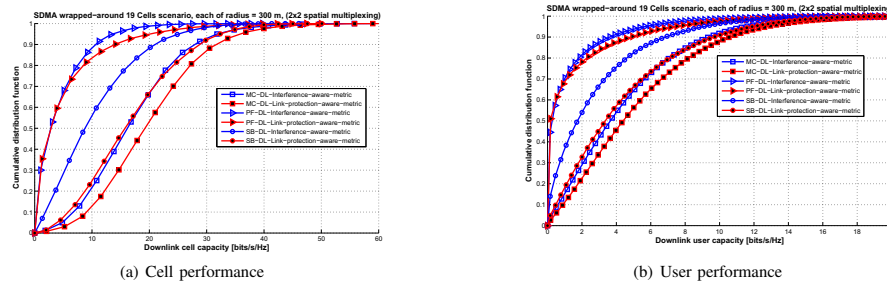
(a) Cell performance   (b) User performance

Fig. 5. Downlink performance comparison between the DL interference-aware-metric and the link-protection-aware-metric.

variations among the interference links depend only on the small-scale fading. On the other hand, the greedy nature of the hybrid SB criterion, explained in section III, allows for the multiuser diversity, offered by the high user density, to be effectively exploited in DL. Furthermore, due to the relatively high variance of the statistics of DL interference, a marginal improvement is achieved using the PF criterion, as it can be seen in Fig. 5. However, this gain can only be seen at the high percentiles due to the fair nature of the PF criterion.

V. CONCLUSIONS

It has been shown that interference-limited systems with implicit signalling of the interference experienced by the users, enabled by the interference-weighted channel sounding, can achieve higher throughput than systems which utilize the conventional channel sounding pilots. By considering the score-based policy, simulations show that using the link-protection-aware-metric results in a gain in the median user capacity of 78% and 13% compared to both DL and UL interference-aware-metric, respectively. For the case of maximum capacity, it has been found that the respective gains are 19% and 18%, respectively. However, marginal capacity gains have been obtained for the proportional fair policy which ensures fairness at the expense of throughput efficiency.

REFERENCES

[1] E. Telatar, "Capacity of Multi-Antenna Gaussian Channels," *European Transaction on Telecommunications*, vol. 10, no. 6, pp. 585–595, Nov. 1996.

[2] P. Viswanath, D. Tse, and R. Laroia, "Opportunistic Beamforming Using Dumb Antennas," in *Proc. of the International Symposium on Information Theory*. Lausanne , Switzerland: IEEE, 30 Jun.–5 Jul. 2002, p. 449.

[3] W. Choi, A. Forenza, J. G. Andrews, and R. W. Heath Jr., "Capacity of Opportunistic Space Division Multiple Access with Beam Selection," in *Proc. of the Global Telecommunications Conference (GLOBECOM 06)*. San Francisco, USA: IEEE, 27 Nov.–1 Dec. 2006, pp. 1–5.

[4] K.-K. Wong, R. Murch, and K. Letaief, "A Joint-Channel Diagonalization for Multiuser MIMO Antenna Systems," *IEEE Transactions on Wireless Communications*, vol. 2, no. 4, pp. 773–786, July 2003.

[5] M. Costa, "Writing on Dirty Paper," *IEEE Transactions on Information Theory*, vol. 29, no. 3, pp. 439–441, May 1983.

[6] H. Weingarten, Y. Steinberg, and S. Shamai, "The Capacity Region of the Gaussian MIMO Broadcast Channel," in *Proc. of the International Symposium on Information Theory (ISIT 04)*, Chicago, USA, 27 Jun.–2 Jul. 2004, pp. 174–182.

[7] C. Wang and R. Murch, "Adaptive Cross-Layer Resource Allocation for Downlink Multi-User MIMO Wireless System," in *Proc. of the 61st Vehicular Technology Conference (VTC 05)*, vol. 3, Stockholm, Sweden, 30 May–1 Jun. 2005, pp. 1628–1632.

[8] C.-B. Chae, D. Mazzarese, and R. W. Heath, "Coordinated Beamforming for Multiuser MIMO Systems with Limited Feedforward," *Fortieth Asilomar Conference on Signals, Systems and Computers (ACSSC)*, pp. 1511–1515, Oct.-Nov. 2006.

[9] R. Chen, R. W. Heath, and J. G. Andrews, "Transmit Selection Diversity for Unitary Precoded Multiuser Spatial Multiplexing Systems With Linear Receivers," *IEEE Transactions on Signal Processing*, vol. 55, no. 3, pp. 1159–1171, March 2007.

[10] D. J. Love, R. W. Heath Jr., W. Santipach, M. L. Honig, "What is the Value of Limited Feedback for MIMO Channels," *IEEE Communications Magazine*, Oct. 2004.

[11] 3rd Generation Partnership Project (3GPP), Technical Specification Group Radio Access Network, *Uplink Sounding for Obtaining MIMO Channel Information at NodeB in EUTRA*, 3GPP Std. R1-060 668, 2006.

[12] ——, *Physical Channels and Modulation (Release 8)*, 3GPP Std. TS 36.211, Rev. 1.2.0.

[13] R. Blum, "MIMO Capacity with Interference," *IEEE Journal on Selected Areas in Communications*, vol. 21, no. 5, pp. 793–801, Jun. 2003.

[14] R. Abualhiga and H. Haas, "Implicit Pilot-Borne Interference Feedback for Multiuser MIMO TDD Systems," in *Proc. of the International Symposium on Spread Spectrum Techniques and Applications (ISSSTA)*. Bologna, Italy: IEEE, Aug. 25–28, 2008, pp. 334–338.

Subcarrier-Index Modulation OFDM

Rami Abu-alhiga and Harald Haas

Institute for Digital Communications, Joint Research Institute for Signal and Image Processing, School of Engineering
The University of Edinburgh, EH9 3JL Edinburgh, UK. {r.abu-alhiga, h.haas}@ed.ac.uk

Abstract—A new transmission approach, referred to as subcarrier-index modulation (SIM) is proposed to be integrated with the orthogonal frequency division multiplexing (OFDM) systems. More specifically, it relates to adding an additional dimension to the conventional two-dimensional (2-D) amplitude/phase modulation (APM) techniques, i.e. amplitude shift keying (ASK) and quadrature amplitude modulation (QAM). The key idea of SIM is to employ the subcarrier-index to convey information to the receiver. Furthermore, a closed-form analytical bit error ratio (BER) of SIM OFDM in Rayleigh channel is derived. Analytical and simulation results show error probability performance gain of 4 dB over 4-QAM OFDM systems for both coded and uncoded data without power saving policy. Alternatively, power saving policy retains an average gain of 1 dB while using 3 dB less transmit power per OFDM symbol.

I. INTRODUCTION

In conventional OFDM systems, modulation techniques such as BPSK (binary phase shift keying), and multilevel quadrature amplitude modulation (M-QAM) map a fixed number of information bits into signal constellation symbol. Each signal constellation symbol represents a point in the 2-D baseband signal space [1]. The continuous demand for increased data transmission rates has driven numerous technologies that exploit new degrees of freedom for better spectral efficiency [2, 3]. In [2], spatial modulation (SM) is proposed as a multiple antenna transmission technique that avoids inter-channel interference and inter-antenna synchronization. According to SM, information bits are mapped into a constellation point in the 2-D signal domain, and a constellation point in the spatial domain such that the antenna index is employed to convey information. More specifically, at each transmission instant, only one transmit antenna is activated while the other antennas transmit zero power. At the receiver side, maximum receive ratio combining is used to estimate the active antenna index, and then the transmitted symbol is estimated.

Inspired by the underlying idea of SM, this paper exploits the subcarrier orthogonality in an innovative fashion to add a new dimension to the complex 2-D signal plan, which is referred to as subcarrier-index dimension. The proposed SIM transmission technique employs the subcarrier-index to convey information in an on-off keying (OOK) fashion. SIM OFDM aims at providing either BER performance enhancement or power-efficiency improvement over conventional OFDM by incorporating different power allocation policies.

The rest of the paper is organized as follows. Section II introduces the novel SIM idea. The analytical BERs of SIM OFDM under different power allocation policies are derived in section III. Section IV presents the simulation model and discusses the results. Finally, section V concludes the paper.

II. SUBCARRIER-INDEX MODULATION OFDM SYSTEM MODEL

The main concept of SIM OFDM is explained using the exemplary system depicted in Fig. 1. According to the basic OFDM system illustrated in Fig. 1(a), an arbitrary binary bit-stream B of length $(N_{\text{FFT}} \cdot \log_2(M))$ bits is transmitted using all N_{FFT} subcarriers, where N_{FFT} and M represent the FFT size and the signal constellation size, respectively. In the example, a square 4-QAM technique is used, $N_{\text{FFT}} = 16$, and the block size is 32. Please note that all the available subcarriers are active and the indices of the modulated subcarriers are labeled using italic numbers in Fig. 1(a). Unlike traditional OFDM depicted in Fig. 1(a), the SIM OFDM technique splits the serial bit-stream B into two bit-substreams of the same length as in this example. As depicted in Fig. 1(b), the first bit-substream B_{OOK} is on the right side of the splitting point while the second bit-substream B_{QAM} is on the left side. In general, the number of bits in the first bit-substream B_{OOK} is equal to the FFT size. Also, it is assumed that all subcarriers are dedicated for data transmission. Compared to the conventional OFDM system in Fig. 1(a), SIM OFDM has an additional module named subcarrier-index modulator.

The functionality of this module can be summarized in two main functions. Firstly, based on the bit-value of each bit in B_{OOK}, the subcarrier-index modulator forms two subsets from B_{OOK} (ones and zeroes). By comparing the cardinality of these subsets, the type of the majority bit-value can be determined. Secondly, the location of each bit in B_{OOK} is associated with the index of each subcarrier. Then, the group of subcarriers associated with the subset of the majority bit-value (ones in this example) are selected to be modulated by the second bit-substream B_{QAM} while the remaining subcarriers are turned-off (suppressed before the signal modulation). In other words, the bit-substream B_{OOK} is used in an OOK fashion to activate those subcarriers whose indices correspond to the majority bit-value. The type of the majority bit-value (one or zero) can be estimated using the Hamming weight of B_{OOK} (the Hamming weight of a binary bit stream is the number of ones). The number of bits of the majority bit-value N_{maj} can be formulated as follows:

$$N_{\text{maj}} = \max\{N_{\text{ones}}^{B_{\text{OOK}}}, (N_{\text{FFT}} - N_{\text{ones}}^{B_{\text{OOK}}})\} \qquad (1)$$

where $N_{\text{ones}}^{B_{\text{OOK}}}$ is Hamming weight of B_{OOK}. Clearly, if $N_{\text{ones}}^{B_{\text{OOK}}} \geq N_{\text{FFT}}/2$ then ones are majority, otherwise zeroes are majority. In the serial-to-parallel (S/P) module, the bit-substream B_{QAM} is multiplexed to modulate the activate subcarriers whose indices are labeled using italic magnified-numbers in Fig. 1(b).
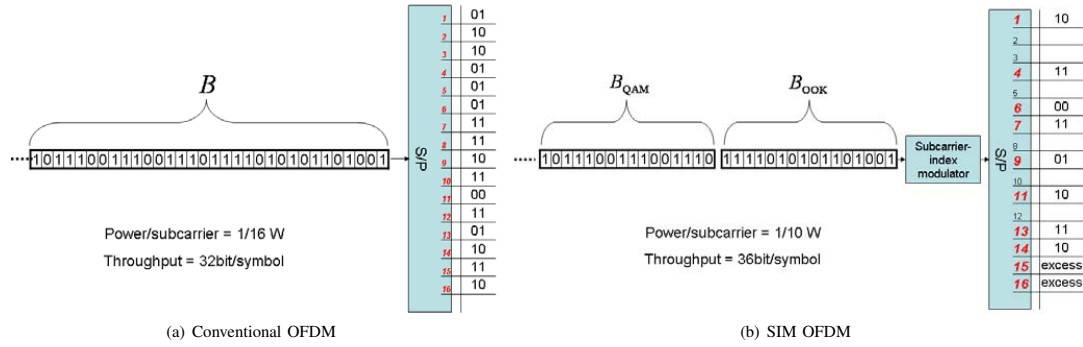
(a) Conventional OFDM

(b) SIM OFDM

Fig. 1.   OFDM sytem with the following parameters: FFT size: 16 subcarriers, modulation type: 4QAM (each subcarrier is loaded by 2 bits), and symbol transmit power: 1 W.
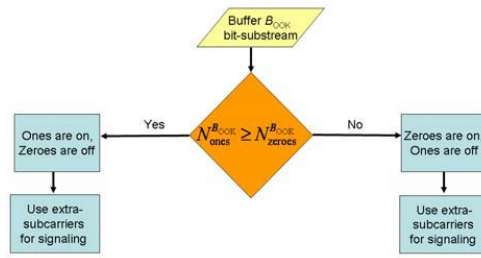

Fig. 2.   Exemplary algorithm for the majority bit-value signalling.

Fig. 3.   Comparison of the Euclidean distance of conventional OFDM against SIM OFDM for different power allocation policies.

A. Majority Bit-Value Signalling

As in the example illustrated in Fig. 1, the size of B_{QAM} is equal to $N_{\mathrm{FFT}}/2 < N_{\mathrm{maj}}$, hence, the number of excess subcarriers can be formulated as follows:

$$N_{\mathrm{ex}} = N_{\mathrm{maj}} - \frac{N_{\mathrm{FFT}}}{2} \qquad (2)$$

In this example, $N_{\mathrm{ex}} = 2$ subcarriers are used as control subcarriers to explicitly signal the type of the majority bit-value to the receiver, see Fig. 1(b). This approach is followed throughout this paper to signal the type of the majority bit-value in order to de-map B_{OOK} at the receiver side. A flowchart illustration of this algorithm is depicted in Fig. 2. According to Fig. 2, the bit-value of the majority bit-value is equal to one when $N_{\mathrm{ex}} = 0$. Therefore, no signalling is needed since this case is assumed to be predefined in the system. Alternatively, signalling the type of the majority bit-value can be avoided, and all excess subcarriers can be used for data transmission which results in better spectral efficiency. In order to estimate the status of each received subcarrier, a coherent OOK detector is used at the receiver side [1]. However, the receiver can only detect the combination of N_{maj} active subcarriers and $N_{\mathrm{FFT}} - N_{\mathrm{maj}}$ inactive subcarriers. Afterwards, the receiver uses the two possibilities of the majority bit-value (1 or 0) to construct two possible hypotheses of B_{OOK}.
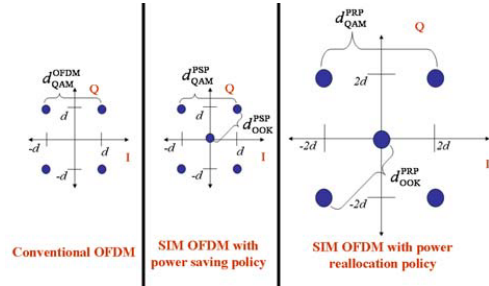
Then, each of the two hypotheses is attached to the estimated B_{QAM} to form two different versions of the original bit-stream B. Finally, forward error control techniques can be used to determine which version of B has less errors to be selected.

B. Power Allocation Policies

There are two possible policies to deal with the power originally allocated to the inactive subcarriers, namely, the power reallocation policy (PRP) and the power saving policy (PSP). In PRP, the power originally allocated to the inactive subcarriers is equally redistributed among the active ones. Thus, the power allocated to each active subcarrier is increased compared to conventional OFDM. This results in a better BER performance as will be shown later in the results section.

On the one hand, the average signal-to-noise-ratio (SNR) of an active subcarrier under PRP $\bar{\gamma}_{\mathrm{sc}}^{\mathrm{PRP}}$ can be written as follows:

$$\bar{\gamma}_{\mathrm{sc}}^{\mathrm{PRP}} = 10 \log_{10}\left(\frac{P_{\mathrm{Tx}}}{E[N_{\mathrm{maj}}]}\right) - 10 \log_{10}(n), \quad \mathrm{dB} \qquad (3)$$

where P_{Tx} is the total transmit power allocated to the OFDM symbol, $E[N_{\mathrm{maj}}]$ is the average number of majority bit-value, and n is the per-subcarrier average additive white Gaussian noise (AWGN) power. It is important to note that for an

uncoded bits-stream, i.e. a sequence of independent bits, the number of the majority bits is binomially distributed random variable, and $E[N_{\text{maj}}] \approx \frac{N_{\text{FFT}}}{2}$ for the case of equiprobable bits. As it can be seen from the example in Fig. 1, the power of each active subcarrier is increased by $\frac{1}{10} - \frac{1}{16} = \frac{3}{80}$ W. Moreover, a gain of 4 bits per OFDM symbols ($N_{\text{ex}} = 2$ multiplied by $\log_2(M = 4) = 2$) can be achieved according to the example. This gain in the symbol throughput is further discussed in section II-C. It is important to remember that, in this paper, the excess subcarriers are used to explicitly signal the bit-value of the majority bits to the receiver.

On the other hand, PSP completely suppresses the power originally allocated to the inactive subcarriers, which results in a better power efficiency. Hence, the average SNR of an active subcarrier under PSP $\bar{\gamma}_{\text{sc}}^{\text{PSP}}$ can be written as follows:

$$\bar{\gamma}_{\text{sc}}^{\text{PSP}} = 10 \log_{10}\left(\frac{P_{\text{Tx}}}{N_{\text{FFT}}}\right) - 10 \log_{10}(n), \quad \text{dB} \quad (4)$$

Assuming that $N_{\text{ex}} = 0$, Fig. 3 shows the influence of both PRP and PSP on the Euclidian distance compared to the case when conventional OFDM is used. In Fig. 3 $d_{\text{QAM}}^{\text{PSP}}, d_{\text{OOK}}^{\text{PSP}}, d_{\text{QAM}}^{\text{PRP}}, d_{\text{OOK}}^{\text{PRP}}$ and $d_{\text{QAM}}^{\text{OFDM}}$ denote the Euclidean distance between two adjacent symbols of the following: SIM OFDM QAM with PSP, SIM OFDM OOK with PSP, SIM OFDM QAM with PRP, SIM OFDM OOK with PRP, and conventional OFDM QAM, respectively.

C. Spectral Efficiency

Assuming all active subcarriers are used for data transmission, the spectral efficiency of SIM OFDM and conventional OFDM can be formulated as follows, respectively:

$$T^{\text{SIM-OFDM}} = 1 + \frac{E[N_{\text{maj}}]}{N_{\text{FFT}}} \log_2(M) \quad [\text{bits/s/Hz}] \quad (5)$$

$$T^{\text{OFDM}} = \log_2(M) \quad [\text{bits/s/Hz}] \quad (6)$$

As for the case of uncoded data with 4-QAM, $E[N_{\text{maj}}]$ is approximately equal to $\frac{N_{\text{FFT}}}{2}$ for equiprobable bits (as highlighted in section II-B). Therefore, a marginal improvement in the spectral efficiency over conventional OFDM is anticipated. However, the average N_{maj} can be increased by manipulating the bit probabilities, which is subject to future investigation.

III. ANALYTICAL BER CALCULATION FOR SIM OFDM

The computation of the analytical bit error performance of SIM OFDM involves analyzing two consecutive estimation processes. The first process is to estimate the status of all N_{FFT} subcarriers (active or inactive) in order to estimate the first bit-substream B_{OOK} using coherent OOK detector. The second estimation process is related to the conventional OFDM-based system, which transmits the second bit-substream B_{QAM} using M-ary APM symbols on only the active subcarriers. As explained in II-B, the power allocation policy has an impact on the average SNR of each active subcarrier. In what follows, B_{OOK} and B_{QAM} are assumed to be of equal lengths, and the excess subcarriers (if any) are used to signal the bit-value of the majority bit-value as highlighted earlier. In this paper, the excess subcarriers are not used for data transmission in order to maintain the same

OFDM symbol throughput compared to conventional OFDM which makes the BER comparison fair.

Throughout the computations, the two estimation processes are assumed to be independent to simplify the calculations. The considered APM for the second process is a square 4-QAM. The bit-stream B is correctly estimated if and only if both estimation processes are correct. Let A_1 and A_2 represent the first and the second estimation processes, respectively. Since B_{OOK} and B_{QAM} are of equal length, the respective probabilities are $P(A_1) = P(A_2) = \frac{1}{2}$. Now, let $P_{\text{sc}}(E)$ be the error probability for A_1 (the subcarrier activity) and $P_q(E)$ be the error probability for A_2 (the 4-QAM symbol recovery) at the receiver side. The overall probability $P_e(E)$ can be formulated using the law of total probability as follows:

$$\begin{aligned} P_e(E) &= P_e(E \mid A_1)P(A_1) + P_e(E \mid A_2)P(A_2) \\ &= \frac{1}{2}P_{\text{sc}}(E) + \frac{1}{2}P_q(E) \end{aligned} \quad (7)$$

In what follows, the error probability of each estimation process is considered separately using both PRP and PSP.

A. Analytical Bit Error Probability of Estimating B_{OOK} (P_{sc})

The estimation process of the subcarrier activity using coherent OOK detector is similar to multiple amplitude shift keying (M-ASK) detection [1]. For the binary case (on or off) the symbol error ratio (SER) expression over a Rayleigh fading channel can be written as follows [4]:

$$P_s = \frac{1}{2}\left(1 - \sqrt{\frac{\bar{\gamma}_s}{1 + \bar{\gamma}_s}}\right) \quad (8)$$

where $\bar{\gamma}_s \triangleq \overline{\alpha^2} \frac{\bar{E}_s}{N_o^{\text{sc}}}$ denotes the average SNR per symbol, and α and $\bar{E}_s$ are the fading amplitude and the average symbol energy, respectively. $\bar{E}_s$ can be calculated by dividing the total transmit power allocated to the OFDM symbol P_{Tx} by the number of the subcarriers considered by the estimation process. The power reallocation policy results in having $\bar{E}_s$ unchanged. This is because P_{Tx} and the number of considered subcarriers are still the same compared to the case where all subcarriers are active. In other words, the effective average SNR during the OOK detection using PRP $\bar{\gamma}_s^{\text{OOK-PRP}}$ is equal to $\bar{\gamma}_s$. The power saving policy uses half P_{Tx} while OOK applies to all subcarriers. Therefore, $\bar{E}_s$ is halved. Hence, the effective average SNR during the OOK detection using PSP $\bar{\gamma}_s^{\text{OOK-PSP}}$ is equal to $\frac{\bar{\gamma}_s}{2}$. Note that for binary ASK, the BER P_b and SER P_s are equal [1], hence, two versions of P_{sc} can be formulated for both PRP and PSP, respectively.

$$P_{\text{sc}}^{\text{PRP}} = \frac{1}{2}\left(1 - \sqrt{\frac{\bar{\gamma}_s}{1 + \bar{\gamma}_s}}\right) \quad (9)$$

$$P_{\text{sc}}^{\text{PRP}} = \frac{1}{2}\left(1 - \sqrt{\frac{0.5\bar{\gamma}_s}{1 + 0.5\bar{\gamma}_s}}\right) \quad (10)$$

B. Analytical Bit Error Probability of Estimating B_{QAM} (P_q)

According to [4], SER expression for M-ary QAM over a Rayleigh fading channel is:

$$\begin{aligned} P_s &= 2\left(\frac{\sqrt{M}-1}{\sqrt{M}}\right)\left(1 - \sqrt{\frac{1.5\bar{\gamma}_s}{M-1+1.5\bar{\gamma}_s}}\right) - \left(\frac{\sqrt{M}-1}{\sqrt{M}}\right)^2 \quad (11) \\ &\times \left[1 - \sqrt{\frac{1.5\bar{\gamma}_s}{M-1+1.5\bar{\gamma}_s}}\left(\frac{4}{\pi}\tan^{-1}\sqrt{\frac{M-1+1.5\bar{\gamma}_s}{1.5\bar{\gamma}_s}}\right)\right] \end{aligned}$$

Note that $\bar{\gamma_s} \triangleq \bar{\gamma} \log_2(M)$, where $\bar{\gamma}$ denotes the average SNR per bit. Also, note that for uncoded data the average BER can be approximated as $P_{\mathrm{b}} = \frac{P_s}{\log_2 M}$ [4], which becomes $P_{\mathrm{b}} = \frac{P_s}{2}$ for $M = 4$. Hence, P_q for square 4-QAM can be written as follows:

$$P_{\mathrm{q}} = -\frac{1}{8} - \frac{1}{2}\sqrt{\frac{\bar{\gamma_s}}{2+\bar{\gamma_s}}} + \frac{1}{2\pi}\sqrt{\frac{\bar{\gamma_s}}{2+\bar{\gamma_s}}}\tan^{-1}\sqrt{\frac{2+\bar{\gamma_s}}{\bar{\gamma_s}}} \tag{12}$$

The impact of both PRP and PSP on $\bar{E}_s$ can be analyzed in the same way as in III-A. Particularly, $\bar{E}_s$ is doubled when PSP is used. This is due to the fact that the 4-QAM estimator considers only the active subcarrier ($\simeq \frac{N_{\mathrm{FFT}}}{2}$), where P_{Tx} is equally redistributed among them at the transmitter. Therefore, the effective average SNR during the 4-QAM detection using PRP $\bar{\gamma}_s^{\mathrm{QAM-PRP}}$ is equal to $2\bar{\gamma}_s$. For the power saving policy, half P_{Tx} is redistributed among the active subcarriers, which leaves $\bar{E}_s$ unchanged. Hence, the effective average SNR during the 4QAM detection using PSP $\bar{\gamma}_s^{\mathrm{QAM-PSP}}$ is equal to $\bar{\gamma}_s$. The influence of both PRP and PSP on $\bar{E}_s$ can be inferred from the variation in the Euclidean distance as depicted in Fig. 3. The two versions of P_{q} associated with PRP and PSP can be written as follows, respectively:

$$P_{\mathrm{q}}^{\mathrm{PRP}} = -\frac{1}{8} - \frac{1}{2}\sqrt{\frac{2\bar{\gamma_s}}{2+2\bar{\gamma_s}}} + \frac{1}{2\pi}\sqrt{\frac{2\bar{\gamma_s}}{2+2\bar{\gamma_s}}}\tan^{-1}\sqrt{\frac{2+2\bar{\gamma_s}}{2\bar{\gamma_s}}} \tag{13}$$

$$P_{\mathrm{q}}^{\mathrm{PSP}} = -\frac{1}{8} - \frac{1}{2}\sqrt{\frac{\bar{\gamma_s}}{2+\bar{\gamma_s}}} + \frac{1}{2\pi}\sqrt{\frac{\bar{\gamma_s}}{2+\bar{\gamma_s}}}\tan^{-1}\sqrt{\frac{2+\bar{\gamma_s}}{\bar{\gamma_s}}} \tag{14}$$

C. Analytical Bit Error Probability of Estimating B (P_{e})

By substituting (9), (10), (13), and (14) into (7), the overall bit error probability using both PRP and PSP can be formulated as in (15) and (16), respectively.

IV. Simulation Model And Results

In the simulation, a single cell scenario with 500 m radius is assumed, and users are uniformly distributed in the cell. Table I. shows the system parameters considered for the simulation. The multipath time-varying channel coefficients are generated

TABLE I
SIMULATION PARAMETERS

Parameters	Values
Carrier frequency	5 GHz
System Bandwidth	100 MHz
Sampling Interval	10 ns
FFT length	1024
Constellation size	4
Speed	60 km/h

using Monte Carlo method. The channel is slow time-varying such that it is assumed to be constant for one OFDM symbol duration. In the simulation results, the BER performance (analytical and simulated) of estimating the bit-stream B using SIM OFDM for different power allocation policies is compared against and the case of using conventional OFDM. In order to assess the performance improvement resulted from using the coherent OOK detection, the BER performance of estimating B_{OOK} is obtained (SIM OOK curves).

A. Uncoded Data with Power Reallocation Policy

Compared to conventional OFDM, Fig. 4(a) shows that using SIM OFDM approximately results in a SNR gain of 26-22=4 dB for a BER of 10^{-3}. Also, it can be noticed that this gain is almost the same when increasing SNR. The reasons are twofold: First, the increment in the activated subcarrier power, quantified in (3), improves the detection quality of the signal constellation symbols. Second, the inherent high error rate performance of the coherent OOK detector, used to estimate the subcarrier activity, enhances the overall BER performance.

B. Uncoded Data with Power Saving Policy

Compared to conventional OFDM, Fig. 4(b) shows that using SIM OFDM approximately results in a SNR gain of 26-25=1 dB for a BER of 10^{-3}. Since there is no increment in the activated subcarrier SNR as illustrated in (4), this marginal gain can be attributed to the inherent high BER performance of the coherent OOK detector used to estimate the first bit-substream. Most importantly, however, there is a 3-dB enhancement in the power efficiency compared to conventional OFDM since, on average, only half transmit power is used.

C. Coded Data with Power Reallocation Policy

Fig. 5 shows the results for coded data using a convolutional encoder with $\frac{3}{4}$ rate. By comparing the BER of SIM OFDM against conventional OFDM, it can be seen that the SNR gain is about 36-32=4 dB for a BER of 10^{-6} and it slightly decreases with increasing SNR. This observation affirms the results obtained in Fig. 4(a), where the significant enhancement in the BER curves compared to the uncoded data case is solely due to the channel coding gain.

In all the results, it is clearly shown that both analytical and simulation results match closely. However, since the current analytical BER does not consider the error probability of estimating the type of the majority bit-value, a mismatch in the results can be noticed at the low SNR regime.

$$P_{\mathrm{e}}^{\mathrm{PRP}} = \frac{1}{2}\left[\frac{1}{2}\left(1 - \sqrt{\frac{\bar{\gamma_s}}{1+\bar{\gamma_s}}}\right)\right] + \frac{1}{2}\left[-\frac{1}{8} - \frac{1}{2}\sqrt{\frac{2\bar{\gamma_s}}{2+2\bar{\gamma_s}}} + \frac{1}{2\pi}\sqrt{\frac{2\bar{\gamma_s}}{2+2\bar{\gamma_s}}}\tan^{-1}\sqrt{\frac{2+2\bar{\gamma_s}}{2\bar{\gamma_s}}}\right] \tag{15}$$

$$P_{\mathrm{e}}^{\mathrm{PSP}} = \frac{1}{2}\left[\frac{1}{2}\left(1 - \sqrt{\frac{0.5\bar{\gamma_s}}{1+0.5\bar{\gamma_s}}}\right)\right] + \frac{1}{2}\left[-\frac{1}{8} - \frac{1}{2}\sqrt{\frac{\bar{\gamma_s}}{2+\bar{\gamma_s}}} + \frac{1}{2\pi}\sqrt{\frac{\bar{\gamma_s}}{2+\bar{\gamma_s}}}\tan^{-1}\sqrt{\frac{2+\bar{\gamma_s}}{\bar{\gamma_s}}}\right] \tag{16}$$

(a) Under power reallocation policy
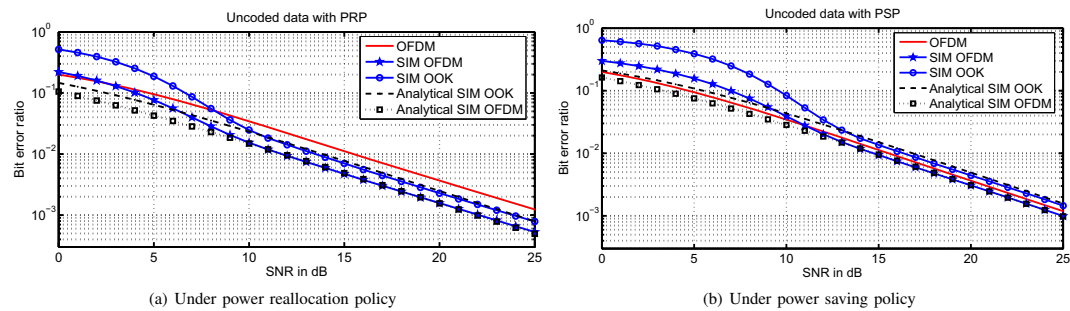
(b) Under power saving policy

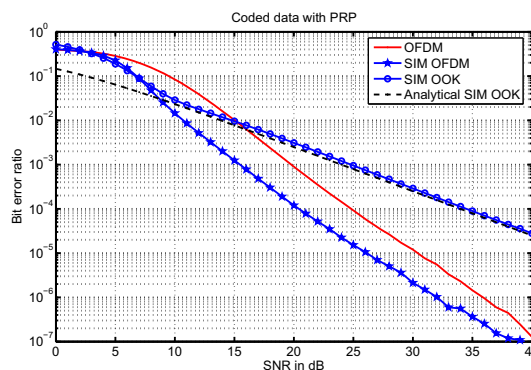Fig. 4. Comparison of bit error ratio between SIM OFDM and OFDM for uncoded data.

Fig. 5. Comparison of bit error ratio between SIM OFDM and OFDM for coded data.

V. SUMMARY AND CONCLUSIONS

A novel power-efficient an spectral-efficient multi-carrier modulation scheme has been presented. The new SIM scheme maps a stream of bits into the indices of the available subcarriers in an on-off keying fashion. In this paper, the subcarrier-index modulator activates a subset of subcarriers whose indices are associated with those bits of the majority bit-value to guarantee no degradation in the throughput compared to 4-QAM OFDM. Moreover, the subcarrier-index detection involves negligible complexity at the receiver. In order to support the simulation results, a closed form expression of the error probability of SIM OFDM using different power allocation policies has been derived. The analytical and simulation results of the error probability match closely for different power allocation policies. Two algorithms are proposed to detect the type of the majority bit-value at the receiver. The first detection algorithm (which is used to obtain the simulation results) relies on explicit signalling where the excess subcarriers are used to convey this control information. The second detection algorithm (which is to be implemented in future work) can be classified as a non-coherent detection approach since signalling is no longer required. The actual

benefits the second detection algorithm are difficult to evaluate at this point and require further investigation, but the potential for the spectral efficiency enhancement is obvious. SIM OFDM always provides performance improvement, but power efficiency can be traded-off against BER performance compared to pure OFDM.

The key advantages of SIM OFDM are:

- Exploit the orthogonality of the multi-carrier dimension in a radically different approach for information transmission.
- Per subcarrier allocated transmit power increases when PRP is used, which results in improved error rate performance compared to conventional OFDM.
- PSP makes SIM OFDM a potential candidate for power efficient systems and green radio applications.
- Reduction in the inter-subcarrier-interference and more robustness in frequency selective fading channels. Note that this feature is subject to future assessment since ideal synchronization is assumed throughout this paper.
- Excess subcarriers provide potential gain in the spectral efficiency.
- Simple subcarrier status detection using existing technology (coherent OOK detection).

In the future, one of the main goals is to study the influence of different interleaving and/or channel coding methods on the distribution of the excess subcarriers, and to investigate the involved trade-off between spectral efficiency and BER performance. In an attempt to further exploit the gain in the subcarrier SNR, future research directions will involve adaptive power/modulation techniques as potential candidates to be integrated with the SIM concept.

REFERENCES

[1] J. G. Proakis, *Digital Communications*. McGraw–Hill, 1995.
[2] R. Mesleh, H. Haas, S. Sinanović, C. W. Ahn, and S. Yun, "Spatial Modulation," *IEEE Transactions on Vehicular Technology*, vol. 57, no. 4, pp. 2228 – 2241, Jul. 2008.
[3] R. Mesleh, I. Stefan, H. Haas, and P. Grant, "On the Performance of Trellis Coded Spatial Modulation," in *ITG International Workshop on Smart Antennas (WSA09)*, Berlin, Germany, Feb. 16–19 2009. [Online]. Available: http://www.mk.tu-berlin.de/wsa2009/
[4] M.-S. Alouini and A. Goldsmith, "A Unified Approach for Calculating Error Rates Of Linearly Modulated Signals over Generalized Fading Channels," *IEEE Transactions on Communications*, vol. 47, no. 9, pp. 1324–1334, 1999.

References

[1] R. C. Hansen, *Microwave Scanning Antennass*. Academic Press, New York, 1964.

[2] E. Bruce, "Developments in short-wave directive antennas," *Proc. of the institute of radio engineers (IRE)*, vol. 19, pp. 1406–1433, Aug. 1931.

[3] G. Marconi, "Directive Antenna," in *Proc. of royal society, London*, p. 4131, 1906.

[4] H. Friis, "A new directional receiving system," *Proc. of the institute of radio engineers (IRE)*, vol. 13, pp. 685–707, Dec. 1925.

[5] E. Bruce and A. Beck, "Experiments with directivity steering for fading reduction," *Proc. of the institute of radio engineers (IRE)*, vol. 23, pp. 357–371, Apr. 1935.

[6] C. Shannon, "A Mathematical Theory of Communication," *Bell System Technical Journal*, vol. 27, pp. 379–423 & 623–656, July & Oct. 1948.

[7] H. Nyquist, "Certain Topics in Telegraph Transmission Theory," *Transactions of theAmerican Institute of Electrical Engineers,*, vol. 47, pp. 617–644, Apr. 1928.

[8] ITU-R, "Framework and Overall Objectives of the Future Development of IMT-2000 and Systems Beyond IMT-2000," Tech. Rep. ITU-R M.1645, ITU, Retrieved Jan. 12, 2009 from http://www.itu.int/rec/R-REC-M.1645/e, 2003.

[9] J. D. Gibson, *The Mobile Communications Handbook*. Springer/IEEE Press/CRC Press, June 1996.

[10] T. S. Rappaport, *Wireless Communications: Principles and Practice*. Prentice Hall, ISBN: 0130422320, 2 ed., Dec. 2001.

[11] K. Feher, *Wireless Digital Communications*. Prentice Hall, ISBN: 8120314727, Seventh Indian Reprint, 2003 ed., 1995.

[12] GSM World, "History: Brief History of GSM & the GSMA." Retrieved Mar. 2008, from http://www.gsmworld.com/about-us/history.htm.

[13] E. Dahlman, S. Parkvall, J. Sköld, and P. Beming, *3G Evolution: HSPA and LTE for Mobile Broadband*. Academic Press, 2 ed., 2008.

[14] UMTS World, "3G and UMTS Technology," Retrieved June 15, 2008 from http://www.umtsworld.com/technology/technology.htm.

[15] 3rd Generation Partnership Project (3GPP), Technical Specification Group Radio Access Network;, "High Speed Downlink Packet Access (HSDPA) – Overall Description, Stage 2 (Release 6)." 3GPP TS 25.308 V6.2.0 (2004-09), Sept. 2004.

[16] 3rd Generation Partnership Project (3GPP), Technical Specification Group Radio Access Network, "Summary of MIMO Schemes for EUTRA."

[17] 3rd Generation Partnership Project (3GPP), Technical Specification Group Radio Access Network, "Evolved Universal Terrestrial Radio Access (E-UTRA); Physical Channels and Modulation (Release 8)." 3GPP TS 36.211 V8.2.0, Mar. 2008.

[18] S. Sesia, I. Toufik, and M. Baker, *LTE - The UMTS Long Term Evolution: From Theory to Practice*. Wiley, 1 ed., 2009.

[19] WiMAX Forum, "Mobile WiMAX – Part I: A Technical Overview and Performance Evaluation." Retrieved Sept. 30, 2008, from www.wimaxforum.org/news/downloads/, Aug. 2006.

[20] J.-P. Rissen, "Mapping the Wireless Technology Migration Path: The Evolution to 4G Systems," tech. rep., Alcatel-Lucent, Retrieved Aug. 24, 2009, from http://www.alcatel-lucent.com/enrich/v2i12008/article_c4a4.html, 2008.

[21] C. Gallen, "In 2014 Monthly Mobile Data Traffic Will Exceed 2008 Total," tech. rep., New York, Retrieved Aug.11 2009, from http://www.abiresearch.com/press/1466-In+2014+Monthly+Mobile+Data+Traffic+Will+Exceed+2008+Total, 2009.

[22] Ericsson, "Long Term Evolution (LTE): An Introduction," white paper 284 23-3124 Uen, Ericsson, Retrieved Feb. 19, 2009, from www.ericsson.com/technology/whitepapers,Oct. 2007.

[23] Motorola Inc., "Long Term Evolution (LTE): A Technical Overview," white paper, Motorola Inc., Retrieved Jan. 12, 2009, from business.motorola.com/experiencelte/pdf/LTETechnicalOverview.pdf, 2007.

[24] E. Seidel, "Progress on "LTE Advanced" – the New 4G Standard," newsletter, NOMOR, Münich, Germany, July 24, 2008.

[25] H. Haas and S. McLaughlin, eds., *Next Generation Mobile Access Technologies: Implementing TDD*. Cambridge University Press, ISBN: 13:9780521826228, Jan. 2008.

[26] E. Telatar, "Capacity of Multi-Antenna Gaussian Channels," *European Transaction on Telecommunication*, vol. 10, pp. 585–595, Nov. / Dec. 1999.

[27] G. J. Foschini and M. J. Gans, "On Limits of Wireless Communications in a Fading Environment when Using Multiple Antennas," *Wireless Personal Communications*, vol. 6, no. 6, pp. 311–335, 1998.

[28] S. H. Ali, K.-D. Lee, and V. C. M. Leung, "Dynamic Resource Allocation in OFDMA Wireless Metropolitan Area Networks," *IEEE Wireless Communications*, vol. 14, pp. 6–13, Feb. 2007.

[29] D. Gesbert, S. G. Kiani, A. Gjendemsj, and G. E. ien, "Adaptation, Coordination, and Distributed Resource Allocation in Interference-Limited Wireless Networks," *Proc. of the 7th IEEE International Symposium on Wireless Communication Systems*, vol. 95, no. 12, pp. 2393–2409, 2007.

[30] C. Koutsimanis and G. Fodor, "A Dynamic Resource Allocation Scheme for Guaranteed Bit Rate Services in OFDMA Networks," in *Proc. of the IEEE International Conference on Communications (ICC 08)*, pp. 2524 – 2530, 19–23 May 2008.

[31] D. Love, R. Heath, and T. Strohmer, "Grassmannian Beamforming for Multiple-Input Multiple-Output Wireless Systems," in *Proc.of the International Conference on Communications (ICC 03)*, vol. 4, (Anchorage, Alaska), pp. 2618–2622, IEEE, 11–15 May 2003.

[32] K. Mukkavilli, A. Sabharwal, B. Aazhang, and E. Erkip, "Performance Limits on Beamforming with Finite Rate Feedback for Multiple Antenna Systems," in *Proc. of the 36th Asilomar Conference on Signals, Systems and Computers*, vol. 1, (Pacific Grove, California), pp. 536–540, 3-6 Nov. 2002.

[33] D. Love and R. Heath, "Limited Feedback Unitary Precoding for Spatial Multiplexing Systems," *IEEE Transactions on Information Theory*, vol. 51, no. 8, pp. 2967–2976, 2005.

[34] S. Zhou, Z. Wang, and G. Giannakis, "Quantifying the Power Loss When Transmit Beamforming Relies on Finite-Rate Feedback," *IEEE Transactions on Wireless Communications*, vol. 4, no. 4, pp. 1948–1957, 2005.

[35] K. Mukkavilli, A. Sabharwal, E. Erkip, and B. Aazhang, "On Beamforming with Finite Rate Feedback in Multiple-Antenna Systems," *IEEE Transactions on Information Theory*, vol. 49, pp. 2562–2579, Oct. 2003.

[36] S. T. Chung, A. Lozano, and H. Huang, "Approaching Eigenmode BLAST Channel Capacity Using V-BLAST With Rate and Power Feedback," in *Proc. of the 54th Vehicular Technology Conference (VTC 01)*, vol. 2, (Atlantic City, New Jersey), pp. 915–919, 7–11 Oct. 2001.

[37] H. Zhuang, L. Dai, S. Zhou, and Y. Yao, "Low Complexity Per-Antenna Rate and Power Control Approach for Closed-Loop V-BLAST," *IEEE Transactions on Communications*, vol. 51, pp. 1783–1787, Nov. 2003.

[38] Z. Zhou and B. Vucetic, "MIMO Systems with Adaptive Modulation," in *Proc. of the 59th Vehicular Technology Conference (VTC 04)*, vol. 2, (Milan, Italy), pp. 765–769, 17–19 May 2004.

[39] S. T. Chung, A. Lozano, and H. Huang, "Low Complexity Algorithm for Rate and Power Quantization in Extended V-BLAST," in *Proc. of the 2001 IEEE 53rd Vehicular Technology Conference*, vol. 2, (Atlantic City, New Jersey), pp. 910–914, 7-11 Oct. 2001.

[40] S. Catreux, P. Driessen, and L. Greenstein, "Data Throughputs Using Multiple-Input Multiple-Output (MIMO) Techniques in a Noise-Limited Cellular Environment," *IEEE Transactions on Wireless Communications*, vol. 1, pp. 226–235, Apr. 2002.

[41] A. Gorokhov, D. Gore, and A. Paulraj, "Receive Antenna Selection for MIMO Flat-Fading Channels: Theory and Algorithms," *IEEE Transactions on Information Theory*, vol. 49, pp. 2687–2696, Oct. 2003.

[42] D. Gore, R. Heath, and A. Paulraj, "Statistical Antenna Selection for Spatial Multiplexing Systems," in *Proc. of the International Conference on Communications (ICC 02)*, vol. 1, (New York, USA), pp. 450–454, 28 Apr.–2 May 2002.

[43] D. Gore and A. Paulraj, "MIMO Antenna Subset Selection with Space-Time Coding," *IEEE Transactions on Signal Processing*, vol. 50, pp. 2580–2588, Oct 2002.

[44] A. Molisch, M. Win, and J. Winters, "Capacity of MIMO Systems with Antenna Selection," in *Proc. of the International Conference on Communications (ICC 01)*, vol. 2, (Helsinki, Finland), pp. 570–574, 11–14 June 2001.

[45] Z. Zhou, Y. Dong, X. Zhang, W. Wang, and Y. Zhang, "A Novel Antenna Selection Scheme in MIMO Systems," in *International Conference on Communications, Circuits and Systems (ICCCAS 04)*, vol. 1, (Chengdu, China), pp. 190–194, 27–29 June 2004.

[46] A. Molisch, M. Win, and J. Winters, "Reduced-Complexity Transmit/Receive-Diversity Systems," *IEEE Transactions on Signal Processing*, vol. 51, pp. 2729–2738, Nov. 2003.

[47] R. Heath and A. Paulraj, "Antenna Selection for Spatial Multiplexing Systems Based on Minimum Error Rate," in *Proc. of the International Conference on Communications (ICC 01)*, vol. 7, (Helsinki, Finland), pp. 2276–2280, 11-14 June 2001.

[48] A. Ghrayeb and T. Duman, "Performance analysis of MIMO Systems with Antenna Selection Over Quasi-Static Fading Channels," pp. 333–337, June 2002.

[49] I. Bahceci, T. Duman, and Y. Altunbasak, "Antenna Selection for Multiple-Antenna Transmission Systems: Performance Analysis and Code Construction," *IEEE Transactions on Information Theory*, vol. 49, pp. 2669–2681, Oct. 2003.

[50] P. Viswanath, D. Tse, and R. Laroia, "Opportunistic Beamforming Using Dumb Antennas," in *Proc. of the International Symposium on Information Theory*, (Lausanne , Switzerland), p. 449, IEEE, June 30–July 5 2002.

[51] W. Choi, A. Forenza, J. G. Andrews, and R. W. Heath Jr., "Capacity of Opportunistic Space Division Multiple Access with Beam Selection," in *Proc. of the Global Telecommunications Conference (GLOBECOM 06)*, (San Francisco, USA), pp. 1–5, IEEE, 27 Nov.–1 Dec. 2006.

[52] K.-K. Wong, R. Murch, and K. Letaief, "A Joint-Channel Diagonalization for Multiuser MIMO Antenna Systems," *IEEE Transactions on Wireless Communications*, vol. 2, pp. 773–786, July 2003.

[53] H. Dai, A. Molisch, and H. Poor, "Downlink Capacity of Interference-Limited MIMO Systems with Joint Detection," *IEEE Transactions on Wireless Communications*, vol. 3, pp. 442–453, March 2004.

[54] C. Wang and R. Murch, "Adaptive Cross-Layer Resource Allocation for Downlink Multi-User MIMO Wireless System," in *Proc. of the 61st Vehicular Technology Conference (VTC 05)*, vol. 3, (Stockholm, Sweden), pp. 1628–1632, 30 May–1 June 2005.

[55] M. Costa, "Writing on Dirty Paper," *IEEE Transactions on Information Theory*, vol. 29, pp. 439–441, May 1983.

[56] H. Weingarten, Y. Steinberg, and S. Shamai, "The Capacity Region of the Gaussian MIMO Broadcast Channel," in *Proc. of the International Symposium on Information Theory (ISIT 04)*, (Chicago, USA), pp. 174–182, 27 June–2 July 2004.

[57] A. Goldsmith, S. Jafar, N. Jindal, and S. Vishwanath, "Capacity Limits of MIMO Channels," *IEEE Journal on Selected Areas in Communication*, vol. 21, pp. 684–702, June 2003.

[58] S. Vishwanath, N. Jindal, and A. Goldsmith, "Duality, Achievable Rates, and Sum-Rate Capacity of Gaussian MIMO Broadcast Channels," *IEEE Transactions on Information Theory*, vol. 49, pp. 2658–2668, Oct. 2003.

[59] C. Windpassinger, R. Fischer, T. Vencel, and J. Huber, "Precoding in Multiantenna and Multiuser Communications," *IEEE Transactions on Wireless Communications*, vol. 3, pp. 1305–1316, July 2004.

[60] B. Hochwald, C. Peel, and A. Swindlehurst, "A Vector-Perturbation Technique for Near-Capacity Multiantenna Multiuser Communication. part II: Perturbation," *IEEE Transactions on Communications*, vol. 53, pp. 537–544, March 2005.

[61] M. Airy, S. Bhadra, R. Heath, and S. Shakkottai, "Transmit Precoding for the Multiple Antenna Broadcast Channel," in *Proc. of the 63rd Vehicular Technology Conference (VTC 06)*, vol. 3, (Melbourne, Australia), pp. 1396–1400, IEEE, 7–10 May 2006.

[62] Z. Pan, K.-K. Wong, and T.-S. Ng, "Generalized Multiuser Orthogonal Space-Division Multiplexing," *IEEE Transactions on Wireless Communications*, vol. 3, pp. 1969–1973, Nov. 2004.

[63] Z. Shen, R. Chen, J. Andrews, R. Heath, and B. Evans, "Low Complexity User Selection Algorithms for Multiuser MIMO Systems with Block Diagonalization," in *Proc. of the 39th Asilomar Conference on Signals, Systems and Computers.*, pp. 628–632, Oct. 2005.

[64] C.-B. Chae, D. Mazzarese, and R. W. Heath, "Coordinated Beamforming for Multiuser MIMO Systems with Limited Feedforward," *Fortieth Asilomar Conference on Signals, Systems and Computers (ACSSC)*, pp. 1511–1515, Oct.-Nov. 2006.

[65] S. Shi, M. Schubert, and H. Boche, "Downlink MMSE Transceiver Optimization for Multiuser MIMO Systems: MMSE Balancing," *IEEE Transactions on Signal Processing*, vol. 56, pp. 3702–3712, Aug. 2008.

[66] M. Schubert and H. Boche, "Solution of the Multiuser Downlink Beamforming Problem with Individual SINR Constraints," *IEEE Transactions on Vehicular Technology*, vol. 53, pp. 18–28, Jan. 2004.

[67] L.-U. Choi and R. Murch, "A Transmit Preprocessing Technique for Multiuser MIMO Systems Using a Decomposition Approach," *IEEE Transactions on Wireless Communications*, vol. 3, pp. 20–24, Jan. 2004.

[68] Q. Spencer, A. Swindlehurst, and M. Haardt, "Zero-Forcing Methods for Downlink Spatial Multiplexing in Multiuser MIMO Channels," *IEEE Transactions on Signal Processing*, vol. 52, pp. 461–471, Feb. 2004.

[69] R. Chen, R. W. Heath, and J. G. Andrews, "Transmit Selection Diversity for Unitary Precoded Multiuser Spatial Multiplexing Systems With Linear Receivers," *IEEE Transactions on Signal Processing*, vol. 55, pp. 1159–1171, March 2007.

[70] D. J. Love, R. W. Heath Jr., W. Santipach, M. L. Honig, "What is the Value of Limited Feedback for MIMO Channels," *IEEE Communications Magazine*, Oct. 2004.

[71] 3rd Generation Partnership Project (3GPP), Technical Specification Group Radio Access Network, "Uplink sounding for obtaining mimo channel information at nodeb in eutra," 2006.

[72] 3rd Generation Partnership Project (3GPP), Technical Specification Group Radio Access Network, "Physical channels and modulation (release 8)."

[73] R. Blum, "MIMO Capacity with Interference," *IEEE Journal on Selected Areas in Communications*, vol. 21, pp. 793–801, June 2003.

[74] R. Abualhiga and H. Haas, "Implicit Pilot-Borne Interference Feedback for Multiuser MIMO TDD Systems," in *Proc. of the International Symposium on Spread Spectrum Techniques and Applications (ISSSTA)*, (Bologna, Italy), pp. 334–338, IEEE, Aug. 25–28, 2008.

[75] R. Mesleh, H. Haas, S. Sinanović, C. W. Ahn, and S. Yun, "Spatial Modulation," *IEEE Transactions on Vehicular Technology*, vol. 57, pp. 2228 – 2241, July 2008.

[76] R. Mesleh, I. Stefan, H. Haas, and P. Grant, "On the Performance of Trellis Coded Spatial Modulation," in *ITG International Workshop on Smart Antennas (WSA09)*, (Berlin, Germany), Feb. 16–19 2009.

[77] J. Jeganathan, A. Ghrayeb, and L. Szczecinski, "Generalized space shift keying modulation for MIMO channels," in *Proc. IEEE 19th International Symposium on Personal, Indoor and Mobile Radio Communications PIMRC 2008*, pp. 1–5, 15–18 Sept. 2008.

[78] J. Jeganathan, A. Ghrayeb, L. Szczecinski, and A. Ceron, "Space Shift Keying Modulation for MIMO Channels," *IEEE Transaction on Wireless Communications*, vol. 8, pp. 3692–3703, July 2009.

[79] R. Mesleh, H. Haas, C. W. Ahn, and S. Yun, "Spatial Modulation – OFDM," in *Proc. of the International OFDM Workshop*, (Hamburg, Germany), Aug. 30–31, 2006.

[80] J. Heiskala and J. Terry, *OFDM Wireless LANs: A Theoretical and Practical Guide.* Sams Publishing, ISBN: 0672321572, 2002.

[81] European Broadcasting Union, "Radio Broadcasting Systems; Digital Audio Broadcasting (DAB) to Mobile, Portable and Fixed Receivers," 2006. Retreived Jan. 30, 2007 from http://webapp.etsi.org/action/OP/OP20060526/en-300401v010401o.pdf.

[82] ETSI EN 300 744 v1.5.1 (2004-06), "Digital Video Broadcasting (DVB): Framing Structure, Channel Coding and Modulation for Digital Terrestrial Television," June 2004.

[83] H. Liu and G. Li, *OFDM-Based Broadband Wireless Networks : Design and Optimization.* JOHN WILEY & SONS INC., 2005.

[84] H. Schulze and C. Lüders, *Theory and Applications of OFDM and CDMA.* John Wiley & Sons Ltd., 2005.

[85] W. Jun and Y. Chenyang, "The influence of analog device on OFDM system," in *Proc. International Conference on Communication Technology (ICCT)*, vol. 2, (Beijing, China), pp. 1060–1062, Apr. 9–11 2003.

[86] J. G. Proakis, *Digital Communications.* McGraw–Hill, 1995.

[87] T. Keller and L. Hanzo, "Adaptive Modulation Techniques for Duplex OFDM Transmission," *IEEE Transactions on Vehicular Technology*, vol. 49, pp. 1893–1906, Sept. 2000.

[88] C. Fragouli, N. Al-Dhahir, and W. Turin, "Training-Based Channel Estimation for Multiple-Antenna Broadband Transmissions," *IEEE Transactions on Wireless Communications*, vol. 2, pp. 384–391, Mar. 2003.

[89] B. Popovic, "Generalized chirp-like polyphase sequences with optimal correlation properties," *IEEE Transactions on Information Theory*, vol. 38, pp. 1406–1409, July 1992.

[90] S. Geirhofer and O. Oyman, "Client-centric Fractional Frequency Reuse Based on User Cooperation in OFDMA Networks," in *Proc. of the Annual Conference on Information Sciences and Systems (CISS)*, (Princeton, NJ, USA), pp. 95–100, IEEE, Mar. 19–21, 2008.

[91] H. Lei, L. Zhang, X. Zhang, and D. Yang, "A Novel Multi-Cell OFDMA System Structure Using Fractional Frequency Reuse," in *Proc. of the International Symposium on Personal, Indoor and Mobile Radio Communications (PIMRC)*, (Athens, Greece), pp. 1–5, IEEE, Sept. 3–7, 2007.

[92] B. Fan, Y. Qian, K. Zheng, and W. Wang, "A Dynamic Resource Allocation Scheme Based on Soft Frequency Reuse for OFDMA Systems," in *Proc. of the International Symposium on Microwave, Antenna, Propagation and EMC Technologies for Wireless Communications (MAPE)*, (Hangzhou, China), pp. 1–4, IEEE, Aug. 14–16, 2007.

[93] R. Giuliano, C. Monti, and P. Loreti, "WiMAX Fractional Frequency Reuse for Rural Environments," *IEEE Wireless Communications*, vol. 15, pp. 60–65, June 2008.

[94] T. S. Rappaport, *Wireless Communications: Principles and Practice.* Prentice Hall PTR, 2 ed., 2002.

[95] G. Pottie, "System Design Choices in Personal Communications," *IEEE Personal Communications*, vol. 2, pp. 50–67, Oct. 1995.

[96] M. Pätzold, *Mobile Fading Channels*. John Wiley & Sons, Ltd., 2002.

[97] P. Höher, "A Statistical Discrete-Time Model for the WSSUS Multipath Channel," *IEEE Transactions on Vehicular Technology*, vol. 41, pp. 461–468, Nov. 1992.

[98] J. G. Proakis and D. K. Manolakis, *Digital Signal Processing: Principles, Algorithms and Application*. Prentice Hall, 4 ed., Apr. 2006.

[99] A. Paulraj, R. Nabar, and D. Gore, *Introduction to Space-Time Wireless Communications*. U.K.: Cambridge University Press, 2003.

[100] K. Yu and B. Ottersten, "Models for MIMO Propagation Channels, A Review," *Special Issue on Adaptive Antennas and MIMO Systems, Wiley Journal on Wireless Communications and Mobile Computing*, vol. 2, no. 7, pp. 653–666, 2002.

[101] J. Zander and M. Frodigh, "Capacity allocation and channel assignment in cellular radio systems using reuse partitioning," *Electronics Letters*, vol. 28, pp. 438–440, Feb. 27, 1992.

[102] Z. J. Haas, J. H. Winter, and D. S. Johnson, "Simulation results of the capacity of cellular systems," *IEEE Transactions on Vehicular Technology*, vol. 46, pp. 805–817, Nov. 1997.

[103] V. K. Garg and J. E. Wilkes, *Wireless and Personal Communications Systems*. Prentice Hall, ISBN: 0132346265, 1996.

[104] A. Viterbi, *Principles of Spread Spectrum Communication*. Addison–Wesley, 1995.

[105] K. S. Gilhousen, I. M. Jacobs, R. Padovani, A. J. Viterbi, L. A. J. Weaver, and C. E. I. Wheatley, "On The Capacity of a Cellular CDMA System," *IEEE Transactions on Vehicular Technology*, vol. 40, pp. 303–312, May 1991.

[106] G. E. Corazza, G. D. Maio, and F. Vatalaro, "CDMA cellular systems performance with fading, shadowing, and imperfect power control," *IEEE Transactions on Vehicular Technology*, vol. 47, pp. 450–459, May 1998.

[107] A. J. Viterbi, "Wireless Digital Communication: A View Based on Three Lessons Learned," *IEEE Communications Magazine*, vol. 29, pp. 33–36, Sept. 1991.

[108] J. H. Winters, "Smart antennas for wireless systems," *IEEE [see also IEEE Wireless Communications] Personal Communications*, vol. 5, pp. 23–27, Feb. 1998.

[109] GSM Europe, "History of GSM." http://www.gsmworld.com, Oct. 2000.

[110] A. Furuskar, S. Mazur, F. Muller, and H. Olofsson, "EDGE: Enhanced Data Rates for GSM and TDMA/136 Evolution," *IEEE Personal Communications*, vol. 6, pp. 56–66, June 1999.

[111] T. Halonen, J. Romero, and J. Melero, *GSM, GPRS and EDGE Performance*. John Wiley & Sons Ltd.; Second Edition, 2003.

[112] H. Holma and A. Toskala, *WCDMA for UMTS*. John Wiley and Sons Inc, 2000.

[113] E. Dahlman, P. Beming, J. Knutsson, F. Ovesjo, M. Persson, and C. Roobol, "WCDMA-the radio interface for future mobile multimedia communications," *IEEE Transactions on Vehicular Technology*, vol. 47, pp. 1105–1118, Nov. 1998.

[114] M. Frodigh, S. Parkvall, C. Roobol, P. Johansson, and P. Larsson, "Future-generation wireless networks," *Personal Communications, IEEE [see also IEEE Wireless Communications]*, vol. 8, pp. 10–17, Oct. 2001.

[115] E. Dahlman, B. Gudmundson, M. Nilsson, and A. Skold, "UMTS/IMT-2000 based on wideband CDMA," *IEEE Communications Magazine*, vol. 36, pp. 70–80, Sept. 1998.

[116] P. Vandenameele, L. V. D. Perre, M. G. E. Engels, B. Gyselinckx, and H. J. D. Man, "A combined OFDM/SDMA approach," *IEEE Journal on Selected Areas in Communications*, vol. 18, pp. 2312–2321, Nov. 2000.

[117] Motorola Inc., "The Drivers to LTE," solution paper, Motorola Inc., Retrieved Jan. 12, 2009, from http://www.motorola.com, 2007.

[118] Motorola Inc., "Driving 4G: WiMAX & LTE," positioning paper, Motorola Inc., Retrieved Feb. 19, 2009, from http://www.motorola.com, 2007.

[119] 3rd Generation Partnership Project (3GPP), Technical Specification Group Radio Access Network, "Eutra downlink pilot requirements and design," 2005.

[120] B. Hassibi and B. M. Hochwald, "How Much Training is Needed in Multiple-Antenna Wireless Links?," *IEEE Transactions on Information Theory*, vol. 49, pp. 951–963, 2003.

[121] A. Goldsmith, *Wireless Communications*. Cambridge University Press, 2005.

[122] V. Kühn, *Wireless Communications over MIMO Channels*. John Wiley & Sons Ltd., 2006.

[123] D. Piazza and U. Spagnolini, "Random beamforming for spatial multiplexing in downlink multiuser MIMO systems," in *Proc. of the 16th International Symposium on Personal, Indoor and Mobile Radio Communications PIMRC*, vol. 4, (Berlin, Germany), pp. 2161–2165, Sept. 2005.

[124] U. Vornefeld, C. Walke, and B. Walke, "SDMA techniques for wireless ATM," *IEEE Communications Magazine*, vol. 37, pp. 52–57, Nov. 1999.

[125] S. M. Alamouti, "A Simple Transmit Diversity Technique for Wireless Communications," *IEEE Journal on Selected Areas in Communications*, vol. 16, pp. 1451–1458, Oct. 1998.

[126] G. J. Foschini, "Layered Space-Time Architecture for Wireless Communication in a Fading Environment when Using Multi-Element Antennas," *Bell Labs Technical Journal*, vol. 1, pp. 41–59, Sept. 1996.

[127] R. Learned, A. Willsky, and D. Boroson, "Low complexity optimal joint detection for oversaturated multiple access communications," *IEEE Transactions on Signal Processing*, vol. 45, pp. 113–123, Jan. 1997.

[128] S. Borst and P. Whiting, "Dynamic channel-sensitive scheduling algorithms for wireless data throughput optimization," *IEEE Transactions on Vehicular Technology*, vol. 52, pp. 569–586, May 2003.

[129] E.F. Chaponniere, P.J. Black, J.M. Holtzman, D.N.C. Tse, "Transmitter Directed Code Division Multiple Access System Using Path Diversity to Equitably Maximize Throughput," *US Patent 6449490*, 2002.

[130] T. Bonald, "A Score-Based Opportunistic Scheduler for Fading Radio Channels," in *Proc. of the European Wireless Conference (EWC)*, (Barcelona, Spain), Feb.24–27 2004.

[131] R. Jain, D. Chiu, and W. Hawe., "A Quantitative Measure of Fairness and Discrimination for Resource Allocation in Shared Computer Systems," Tech. Rep. 301, DEC Technical Report, 1984.

[132] M. Kazantzidis, L. Wang, and M. Gerla, "On Fairness and Efficiency of Adaptive Audio Application Layers for Multihop Wireless Networks," in *Proc. of the Workshop on Mobile Multimedia Communications (MoMuC 99)*, (San Diego, USA), pp. 357–362, IEEE, 15–17 Nov. 1999.

[133] A. Pandey, S. Emeott, J. Pautler, and K. Rohani, "Application of MIMO and Proportional Fair Scheduling to CDMA Downlink Packet Data Channels," in *Proc. of the 56th Vehicular Technology Conference (VTC 02)*, vol. 2, (Vancouver, Canada), pp. 1046–1050, IEEE, Sept. 24–28, 2002.

[134] R. W. Chang, "Synthesis of Band-Limited Orthogonal Signals for Multichannel Data Transmission," *Bell Systems Technical Journal*, vol. 45, pp. 1775–1796, Dec. 1966.

[135] S. Weinstein and P. Ebert, "Data Transmission by Frequency-Division Multiplexing Using the Discrete Fourier Transform," *IEEE Transactions on Communication Technology*, vol. 19, pp. 628–634, Oct. 1971.

[136] A. Peled and A. Ruiz, "Frequency Domain Data Transmission Using Reduced Computational Complexity Algorithms," in *Proc. of the IEEE International Conference on Acoustics, Speech and Signal Processing (ICASSP)*, vol. 5, (Denver, USA), pp. 964–967, Apr. 9–11 1980.

[137] J. Armstrong, "OFDM for Optical Communications," *Journal of Lightwave Technology*, vol. 27, no. 3, pp. 189–204, 2009.

[138] E. Costa and S. Pupolin, "M-QAM-OFDM System Performance in the Presence of a Nonlinear Amplifier and Phase Noise," *IEEE Transactions on Communications*, vol. 50, pp. 462–472, Mar. 2002.

[139] R. Abualhiga and H. Haas, "Subcarrier-Index Modulation OFDM," in *Proc. of the International Symposium on Personal, Indoor and Mobile Radio Communications (PIMRC)*, (Tokyo, Japan), Sept. 13–16, 2009.

[140] M.-S. Alouini and A. Goldsmith, "A Unified Approach for Calculating Error Rates Of Linearly Modulated Signals over Generalized Fading Channels," *IEEE Transactions on Communications*, vol. 47, no. 9, pp. 1324–1334, 1999.

[141] M. Bossert, *Channel Coding for Telecommunications*. John Wiley and Sons Ltd., 1999.

[142] H. Sirisena, A. Haider, M. Hassan, and K. Fawlikowski, "Transient Fairness of Optimized End-to-End Window Control," in *Proc. of the Global Telecommunications Conference (GLOBECOM)*, vol. 7, (San Francisco, USA), pp. 3979–3983, IEEE, Dec. 1–5, 2003.